MAÍRA REIS DE ASSIS

MECHANICAL AND PHYSICAL PROPERTIES OF *Eucalyptus* CHARCOAL FROM PYROLYSIS UNDER DIFFERENT CONDITIONS

LAVRAS – MG

2016

MAÍRA REIS DE ASSIS

MECHANICAL AND PHYSICAL PROPERTIES OF *Eucalyptus* CHARCOAL FROM PYROLYSIS UNDER DIFFERENT CONDITIONS

Tese apresentada à Universidade Federal de Lavras, como parte das exigências do Programa de Pós-Graduação em Ciência e Tecnologia da Madeira, área de concentração em Processamento e Utilização da Madeira, para a obtenção do título de Doutor.

Orientador

Dr. Alfredo Napoli

Coorientadores

Dr. Loïc Brancheriau

Dr. Paulo Fernando Trugilho

LAVRAS - MG

2016

Ficha catalográfica elaborada pelo Sistema de Geração de Ficha Catalográfica da Biblioteca Universitária da UFLA, com dados informados pelo(a) próprio(a) autor(a).

Assis, Maíra Reis de.
Mechanical and physical properties of *Eucalyptus* charcoal from pyrolysis under different conditions / Maíra Reis de Assis. – Lavras : UFLA, 2016.
153 p. : il.

Tese (doutorado) – Universidade Federal de Lavras, 2016.
Orientador(a): Alfredo Napoli.
Bibliografia.

1. Bulk compression. 2. Mechanical strength. 3. Carbonization temperature. 4. Ultrasounds. 5. Juvenile wood. I. Universidade Federal de Lavras. II. Título.

MAÍRA REIS DE ASSIS

MECHANICAL AND PHYSICAL PROPERTIES OF *Eucalyptus* CHARCOAL FROM PYROLYSIS UNDER DIFFERENT CONDITIONS

Tese apresentada à Universidade Federal de Lavras, como parte das exigências do programa de Pós-Graduação em Ciência e Tecnologia da Madeira, área de concentração em Processamento e Utilização da Madeira, para obtenção do título de Doutor.

APROVADA em 03 de junho de 2016.

Dr. Paulo Fernando Trugilho	UFLA
Dr. Loïc Brancheriau	CIRAD
Dr. Paulo Ricardo Gherardi Hein	UFLA
Dr. José Otávio Brito	ESALQ/USP

Dr. Alfredo Napoli (CIRAD)

Orientador

LAVRAS – MG

2016

Aos meus pais, Maurílio e Selma, pelo amor e proteção incondicional.

Dedico

AGRADECIMENTOS

À Deus, razão da minha existência. À Maria Santíssima, pelo acalento e intercessão constantes.

À Universidade Federal de Lavras, pelo suporte durante todo esse processo de formação profissional.

Aos professores do Programa de Pós-graduação em Ciência e Tecnologia da Madeira, em especial, ao orientador e amigo professor Dr. Paulo Fernando Trugilho, pelo constante incentivo durante toda minha pós-graduação; ao orientador professor Dr. Alfredo Napoli, pela confiança e por ter proporcionado a ampliação da minha formação acadêmica, cultural e pessoal, com a oportunidade de um doutorado sanduíche Brasil/França.

Ao programa de doutorado francês *Doctorants du Sud*, pela concessão da bolsa de estudo europeia, possibilitando a execução deste trabalho. À equipe do CIRAD-UR BioWooEB. Ao Mr. Loïc Brancheriau, pela orientação e pelos valiosos ensinamentos, amizade, sempre disponível e competente nas discussões deste trabalho durante os períodos no CIRAD/França e UFLA/Brasil; ao Mr. Silvan Lotte, Mr. Daniel Guibal e Mrs. Nabila Boutahar, pela amizade e auxílio na preparação dos corpos de prova e nos ensaios laboratoriais; Mr. Sebastien Paradis, pela amizade e por me acolher tão generosamente em sua sala; e à Mrs. Isabelle Chalon, pela constante disponibilidade e atenção: je vous remercie à tous!

Aos amigos do Laboratório de Biomateriais e demais colegas do programa de Pós-graduação em Ciência e Tecnologia da Madeira, pela amizade e companheirismo.

Às professoras e amigas Jamile Khalil, por ter me ajudado a vencer o grande desafio de me expressar em francês e Samira Spiller, pelo apoio e carinho durante a escrita da tese.

Aos amigos de jornada, pelo companheirismo, amizade e pelos bons momentos de convívio nesse período de aprendizagem e amadurecimento profissional e pessoal.

À minha querida família, agradeço de todo meu coração, meus amados pais, Maurílio e Selma, por todo amor e incentivo constantes desde meus primeiros anos de vida; ao meu amado irmão Maurício, pela amizade e companheirismo fraternal.

Às instituições de financiamento à pesquisa e desenvolvimento CNPq, CAPES e Fapemig, que viabilizaram a execução deste trabalho.

REMERCIEMENTS

A Dieu, la raison de mon existence. A Sainte Marie, pour l'appui et l'intercession constants.

Je remercie l'Université Fédérale de Lavras pour le soutien tout au long de ce processus de formation.

Les professeurs du programme d'études supérieures en Sciences et Technologie du Bois, en particulier, l'encadrant, professeur et ami Dr. Paul Fernando Trugilho pour l'encouragement constant tout au long de mon enseignement post-universitaire; l'encadrant et ami Dr. Alfredo Napoli pour la confiance et pour avoir permis l'agrandissement de ma formation académique, culturelle et personnelle avec la possibilité d'un doctorat sandwich Brésil / France.

Le programme de doctorat français Doctorants du Sud pour l'octroi de la bourse européenne, permettant l'exécution de ce travail; à toute l'équipe CIRAD-UR BioWooEB, en particulier, Dr. Loïc Brancheriau pour les conseils, les enseignements précieux, l'amitié, toujours disponible et compétent dans les discussions de ce travail à CIRAD / France et UFLA / Brésil; M. Sylvain Lotte, M. Daniel Guibal e Mlle. Nabila Boutahar, pour l'amitié et l'aide dans la préparation des échantillons et les tests de laboratoire; M. Sébastien Paradis, pour l'amitié et pour m'accueillir si généreusement dans son bureau; et Mme Isabelle Chalon, pour la disponibilité et l'attention constants: je vous remercie tous!

Les amis du Laboratoire de Biomatériaux et d'autres collègues dans le programme d'études supérieures en Sciences et Technologie du Bois, pour l'amitié et la camaraderie.

Les professeurs et amies Jamile Khalil, pour m'aider à surmonter le défi de m'exprimer en français et Samira Spiller pour son soutien au cours de la rédaction de la thèse.

Les amis du Brésil et de France pour la camaraderie, l'amitié et les bons moments de convivialité durant cette période d'apprentissage et de croissance professionnelle et personnelle.

Ma chère famille, je vous remercie de tout mon cœur: mes parents aimés Maurílio et Selma, pour tout l'amour et l'encouragement constant depuis mes premières années au monde ; mon bien-aimé frère Maurício Luiz, pour l'amitié et la communion fraternelle.

Les institutions brésiliennes de financement à la recherche et au développement CNPq, CAPES et FAPEMIG, qui ont rendu possible l'exécution de ce travail.

RESUMO

Com a realização do presente estudo procurou-se compreender, experimentalmente, o comportamento mecânico de um leito fixo a carvão vegetal de *Eucalyptus* produzido em diferentes condições de carbonização. Para isso, o trabalho foi dividido em duas fases: (i) caracterização destrutiva e não destrutiva da madeira e do carvão vegetal; (ii) análise do comportamento mecânico de leitos de carvão. Foram realizadas análises das propriedades físicas (densidade básica e aparente, contrações radial e tangencial e ponto de saturação de fibras) e estimativas de propriedades mecânicas (módulo de elasticidade em flexão e compressão, módulo de cisalhamento) da madeira. A madeira foi carbonizada a temperaturas finais de 500 °C e 900 °C. Determinou-se a densidade aparente, módulo de elasticidade e módulo de cisalhamento do carvão vegetal. A resistência ao esmagamento do carvão vegetal foi obtida convencionalmente por um teste estático nas três direções (radial, tangencial e longitudinal). Num segundo momento, leitos de carvão foram ensaiados em um dispositivo que consiste em um cilindro de aço e um êmbolo empurrado por uma máquina universal de teste. Os experimentos consistiram na realização de testes repetidos de compressão de carvão obtido a 500 °C e 900 °C, de tamanho controlado (granulometrias de 10 e 20 mm) e temperaturas de compressão de 20 °C e 300 °C. Uma distribuição de tamanho de partículas após os ensaios é obtida como uma função da carga aplicada, sendo classificada quantitativamente por peneiramento e pesagem. Verificou-se que: (a) O módulo de elasticidade e a densidade do carvão aumentaram com a temperatura final de pirólise, mas o efeito da temperatura foi menos significativo para a densidade do carvão. (b) O módulo de elasticidade e a densidade do carvão vegetal apresentaram maiores valores nas amostras provenientes da região próxima à casca, mas a temperatura de carbonização elevada parece reduzir o efeito da posição radial. (c) Independentemente da temperatura final de carbonização, o carvão vegetal é de fato intimamente correlacionado com a madeira de origem. (d) O melhor preditor para estimar a resistência à compressão do carvão vegetal foi a densidade aparente da madeira somada à interação da temperatura de carbonização e a direção da compressão. (e) A partir da PCA foi possível separar quatro grupos de acordo com as temperaturas de carbonização e tamanhos de partícula. O efeito da temperatura de compressão dos leitos de carvão não foi significativo, uma vez que a temperatura não é um efeito cumulativo. (f) A dimensão dos fragmentos parece estar correlacionada com a temperatura de carbonização da madeira. (g) Leitos de carvão expostos à temperatura mais elevada de compressão apresentaram menos fragmentos na categoria > 8 mm.

Palavras-chave: Compressão de meio granular. Mecânica do carvão vegetal. Temperatura de carbonização. Ultrasom. Madeira juvenil.

ABSTRACT

This research aimed to understand, experimentally, the mechanical behavior of a fixed bed of *Eucalyptus* charcoal blast furnace under different carbonization conditions. To attend the main goal, this study was divided into two phases: (i) destructive and non-destructive characterization of wood and charcoal produced at different carbonization temperatures. (ii) mechanical behavior of charcoal beds. Modulus of elasticity (flexion and compression), shear modulus, basic and apparent density, radial and tangential shrinkage and fiber saturation point were determined to evaluate wood properties. In a second step, wood samples were pyrolized at 500 °C and 900 °C. Apparent density, modulus of elasticity and shear modulus of charcoal samples were measured. Finally, the crushing strength was conventionally obtained by a static test in the three directions (longitudinal, radial and tangential). In a second phase, taking into account the procedures for the obtention of charcoal (500 and 900 °C), different granulometries (10 and 20 mm) and temperatures of compression bed tests (20 and 300 °C), a total of eight charcoal layers were made to evaluate the mechanical behavior of the granular medium. An apparatus consisting of a tube and a piston that is pushed by a universal test machine was prepared. The experiments consisted in carrying out repeated compression tests of controlled-sized charcoal with the apparatus. A particle size distribution is obtained as a function of the applied load, which is then classified by screening and weighing. Based on that, the particle size distribution is analyzed quantitatively. It was found that: (a) The charcoal MOE and apparent density increased with the final pyrolysis temperature, but the temperature effect was less significant for density. (b) Charcoal properties were higher for samples cut near the bark, but a high carbonization temperature seemed to reduce this phenomenon. (c) Charcoal is indeed, mechanical and physically, closely related with origin wood, independently of the final carbonization temperature. (d) The best predictor to estimate charcoal crushing strength was wood apparent density associated carbonization temperature and direction of compression. (e) The PCA indicated four groups, identified by different carbonization temperatures and particle sizes. However, the temperature effect of charcoal bed assays is not significant, since temperature is not a cumulative effect. (f) The dimension of fragments seems to be correlated with wood carbonization temperature. (g) Charcoal beds exposed to the highest compression temperature generally show less fragments in the > 8mm category.

Keywords: Bulk compression. Mechanical strength. Carbonization temperature. Ultrasounds. Juvenile wood.

LIST OF FIGURES

LIST OF TABLES

LIST OF NOTATIONS

Anisot	Anisotropy coefficient
BING	Beam Identification by Non-destructive Grading®
D12 / ρ12	Apparent density of wood
D / ρ	Basic density of wood
FSP	Fiber Saturation Point
G	Shear modulus
G_{LR}	Shear modulus in the longitudinal-radial
G_{RT}	Shear modulus in the radial-tangential direction
G_{TL}	Shear modulus in the tangential-longitudinal direction
MOE	Modulus of elasticity
MOE BING	Flexural modulus of elasticity by BING
MOE US	Modulus of elasticity in compression by ultrasounds
MOE US Long	Modulus of elasticity in compression in the cubes by ultrasounds in the longitudinal direction
MOE US Rad	Modulus of elasticity in compression in the cubes by ultrasounds in the radial direction
MOE US Tang	Modulus of elasticity in compression in the cubes by ultrasounds in the tangential direction
US	Ultrasounds
Ychar	gravimetric yield in charcoal
δ	Shrinkage tangential (Tg) or radial (Rd)

SUMÁRIO

1 INTRODUCTION

1.1 Context

The world steel industry is based on the use of virgin raw materials, such as iron ore and coking coal, mainly in the blast furnace (BF) iron-making process. The core of the process is to convert iron oxides into hot metal, which is done by using carbon and hydrogen-based reducing agents. The metallurgical coke in the blast furnace performs three functions: It acts as a reducing agent, provides energy to the process and serves as a support medium for the burden material (GUPTA, 2003). The use of biofuels and bio-reducing agents, in the iron-making process, helps reduce the issue of global warming, but also reduce the dependence on conventional fuels when facing power shortage and high costs of fossil fuel.

Charcoal is a highly carbonized product, often compared with coke, and is a promising bio-reducer when used as a partial replacement for top coke in BF's (SUOPAJÄRVI; PONGRÁCZ; FABRITIUS, 2013). The total renewable CO_2 balance is favorable when using charcoal, since all the carbon in charcoal is generated from CO_2 of the atmosphere and recycled as CO_2 in the BF process. Besides the positive environmental effect, the use of charcoal will also provide economic advantages, since the pig iron produced with charcoal has a better quality and possibility of higher productivity (BABICH; SENK; FERNANDEZ, 2010).

Charcoal is the main solid product generated from carbonization of biomass, a slow pyrolysis (maximum of 10 °C.min^{-1}) that occurs in the absence or controlled presence of oxygen. The properties of charcoal are controlled by the manufacturing process and the raw material used. Such manufacturing process comprises the following steps:

• The drying phase, together with the onset of thermal decomposition of some biomass components, occurs preferentially until 200 °C. The water

contained in wood evaporates because of the heat, thus taking away a part of volatile products present in the material;

• Between 200 and 280 °C, the endothermic reaction predominates, producing acetic and formic acids, methanol, water and carbon dioxide;

• The exothermic reactions occur between 280 and 500 °C, releasing carbon monoxide, methane and tars. In this phase, there is an important mass loss, accompanied by the decrease in mechanical properties (compression strength and friability);

• Above 500 °C, stable charcoal is found, releasing only hydrogen; there is an improvement in the mechanical properties of charcoal, due to the increase in concentration and structural rearrangement of carbon with the crossing of graphite beams, and a smaller mass loss is observed in this phase (BLANKENHORN; KLINE; BEALL, 1973; BRIANE; DOAT, 1985; MOORE et al., 1974; OLIVEIRA; GOMES; ALMEIDA, 1982; TRUGILHO; SILVA, 2001). The final charcoal is a product rich in carbon, generally superior to 75 %, depending on the final carbonization temperature.

Besides carbon, charcoal consists of up to 25% volatile material and 1% ashes, which consists of inorganic material (BRITO, 1990). Most of the specifications involved on the quality control of charcoal are dictated by the steel industry or chemical industry. Such quality criteria are important in the international market. The quality of charcoal is defined by several characteristics which, although related among themselves in a certain magnitude, are measured and assessed separately. The most important properties of charcoal for the steel mill are the chemical composition, density, moisture content, granulometry (particle size distribution) and mechanical resistance (compression strength) (Table 1). Charcoal presents low density, high reactivity, high friability, low ash content (almost sulfur and phosphorus free), high carbon–ash ratio, relatively few and un-reactive inorganic impurities, stable pore structure with high

porosity (BABICH; SENK; FERNANDEZ, 2010). However, coke presents a higher mechanical resistance than charcoal. Coke better supports the load of ore deposited alternately within the BF.

Table 1 Properties of charcoal compared to coke used for blast furnace steelmaking

Properties	**Charcoal**	**Steel quality charcoal**	**Coke**	**Steel quality coke**
Moisture content (%)	8-20	<7	~3	1-6
Fixed carbon (%)	72-78	74-77	88-92	85- 88
Density (dry) $kg.m^{-3}$	220-270	>250	400-500	-
Volatile matter (%)	25-35	22-25	7.8-11	1-3
Ash (%)	<1	1-1.5	> 9	0.1-0.5
Size (mm)	10-100	40-50 / Uniform	50-80	-
Resistance to compression ($kg.cm^{-2}$)	10-80	50-100	130-160	100-200

Source: (MEYERS; JENNINGS, 1979; ROUSSET et al., 2011)

Among the properties of charcoal that are directly related to its behavior and performance in the furnace, mechanical resistance stands out as one of the most important and considered the main bottlenecks of using charcoal in the BF. The mechanical resistance of charcoal is important in the production chain of steel, since the manufacturing, transport, storage, sifting and within the BF, where its layer must support those of iron ore, not damaging the permeability of the channel. There is a problem with the total replacement of lump coke in a large BF with charcoal since it has much lower strength than coke. However, the requirement of compression strength for charcoal particles in small-scale BF's (useful volume < 300 m^3) is much lower than in large scale BF's (CHATTERJEE, 2010).

Due to its low mechanical resistance, charcoal is classified as a friable material. Friability may be defined as the property of charcoal to produce fines

(particles between 9 and 12 mm), when subjected to abrasion, friction or fall (GOMES; OLIVEIRA, 1980). Due to such high friability, charcoal produces between 25 and 30 % of fines between the manufacturing process and use in iron reduction furnaces. Low mechanical resistance generates a great extent of fines when submitted to a gradient of temperature, as well as to the action of abrasion within the furnace (OLIVEIRA; GOMES; ALMEIDA, 1982). Fines generated from charcoal may be used mainly in the cement industry and in ore sintering (OLIVEIRA; GOMES; ALMEIDA, 1982). They also may be injected in the furnace and reduce the usage of granular coal up to a certain limit (ASSIS; MARTINS; VIEIRA, 2003; BABICH; SENK; FERNANDEZ, 2010). Granulometry is a physical property responsible for the permeability of the load inside the furnace. It is known that charcoal presents difficulties in maintaining a uniform granulometry because of its high friability; however, even with such difficulties, the granulometry of charcoal is one characteristic that may be relatively controlled in order to attain the properties required for its use as a thermoreducer. The practice of sifting charcoal before its introduction in the furnace has been adopted, and clear definitions regarding the limits of tolerance are required for such characteristic. A norm by Associação Brasileira de Normas Técnicas to determine granulometry is in effect (ASSOCIAÇÃO BRASILEIRA DE NORMAS TÉCNICAS - ABNT, 1982).

Although charcoal represents a raw material of great potential in the BF, there are few standards regarding the mechanical evaluation of the reducer at the present. In the 1980s, Oliveira, Gomes and Almeida (1982) have already commented on the importance to establish a new standard for essays with coke, once it is indispensable to correlate its properties to the performance in the furnace. It should also have been considered for charcoal test standards; however, until the present day, such norms are incipient. The drum test is used with the objective to determine the resistance of charcoal to the combined action of abrasion and fall

(Method of drum essay NBR 8740-85 (ABNT, 1985). This test determines the friability index, production of fines during handling and transport. The test for the determination of the fall index also determines the friability index, which was standardized by NBR7416-84 (ABNT, 1984). The fall test consists of measuring the fragmentation index of a material when submitted to freefall. The use of non-destructive tests on charcoal can also be an important tool to help determine the mechanical resistance of this complex material (ANDRADE, 2009; VIEIRA, 2009).

Strength modulus (which is an expression of the brittleness of charcoal), like any modulus, relates charcoal contraction to the compressive force exerted on it. If strength modulus is low, charcoal is less rigid during compression. It is noteworthy that compression is never reversible; therefore, it is not an elastic phenomenon. Vieira (2009) performed destructive testing using the universal machine EMIC DL 30000 on charcoal from *Eucalyptus* sp. (Table 2). It was observed that the mechanical properties evaluated (compression strength modulus at compression parallel to the fibers and crushing strength modulus at dynamic flexion) increased with the increase in carbonization temperature from 350 to 900 °C. Considering the radial position, the mechanical resistance improved from the center (pith) to the periphery (cambium).

Table 2 Maximum stress, called compression strength modulus of hybrid charcoal clones from *Eucalyptus* sp.

Mechanical test of charcoal	Radial position	Carbonization temperature (°C)			
		350	450	550	900
Compression strength modulus – static compression (MPa)	Periphery (cambium)	544	576	681	1197
	Center (pith)	371	494	679	897

Source: (VIEIRA, 2009).

Chrzazvez et al. (2014) characterized the mechanical properties of common species in temperate and Mediterranean Europe. They presented typical behavior of the static compression test parallel to the fibers in charcoal specimen of *Betula* produced at 500 °C (Figure 1). The typical test curve comprises three main phases. The pressure is applied and, after the initial contact, a gradual rise occurs, which corresponds to setting up the compression test. Posterior, a linear rise in stress occurs until the peak, called the crushing strength, which corresponds to the crushing of the whole sample. This step is directly linked to the maximum force (pressure) that can be applied to a piece of charcoal before complete destruction. Finally, a more or less continued decrease in stress, possibly with non-negligible drag strain, corresponds to the destruction of the charcoal structure. It was found that charcoal is resistant to pressure up to 22.5 MPa (CHRZAZVEZ et al., 2014).

Figure 1 Typical stress-strain curve of the compression test in *Betula* charcoal

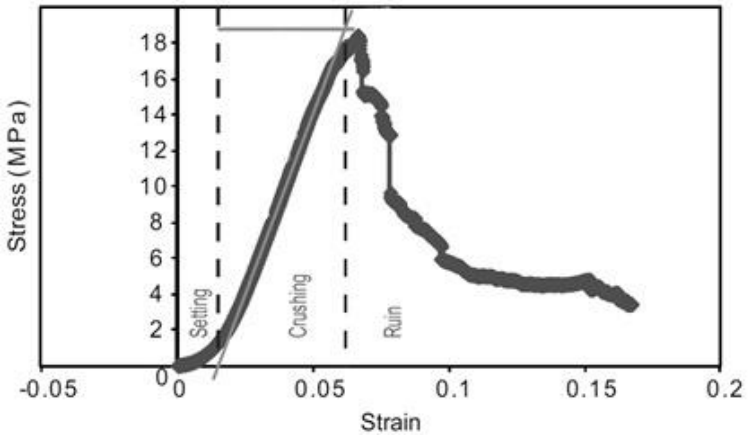

Source: (CHRZAZVEZ et al., 2014)

Little is known of the mechanical properties of such bio-thermoreducer, related to the performance in the BF. Therefore, while trying to deal with problems of charcoal production to support the steel mill in expansion, it is

necessary to provide a basic scientific knowledge which may contribute to lessen the problems related to this limiting structural factor. In this review, the knowledge of the mechanical properties of charcoal is summarized. It starts with a discussion of the key properties of the raw material, followed by carbonization process parameters which determine the properties of mechanical charcoal.

1.2 Objectives and scientific approach

The iron and steel industry is among the most energy intensive industrial sectors in the world and due to the fact that the dominating iron and steelmaking processes are still mainly coal-based, substantial amounts of fossil carbon dioxide emissions are released, which gives it a position as the largest contributor to emissions in iron and steel production, globally (BROWN et al., 2012). This industry contributed with around 2.3 Gt, or 30%, of direct industrial CO_2 emissions in 2007. Much research has been devoted to finding potential ways to increase efficiency and to decrease the use of fossil reductants and the rate of emissions of these processes (HELLE et al., 2010; HELLE; HELLE; SAXÉN, 2011; TOBIESEN; SVENDSEN; MEJDELL, 2007; TRUGILHO et al., 2001; TSUPARI et al., 2013; UEDA; ARIYAMA, 2008). Charcoal, a renewable and less pollutant energy source than coke coal, is a promising alternative to fossil energy, being used in small-scale blast furnaces instead of coke, as a reducer, fuel, and in some blast furnaces in Brazil. Approximately 25% of the steel produced in the country is from charcoal and 75% is coke; there are hybrid furnaces that use both charcoal and coke, or even industries working with smaller furnaces powered only by charcoal and industries that use larger furnaces, powered only by coke. More than 75% of energy wood is destined to steel and almost all the coke is used to steel. The largest steel producers work with both coke and charcoal, mainly not to be totally dependent on coal, a raw

material imported by Brazil (SINDICATO DA INDÚSTRIA DE FERRO NO ESTADO DE MINAS GERAIS - SINDIFER, 2014).

The increasing interest of metallurgists towards the use of wood charcoal for ironmaking has brought about a need to better understand its properties (chemical, physical, mechanical, electrical and structural). Charcoal is the most expensive raw material that is part of the load in blast furnaces (NORGATE; LANGBERG, 2009). Its physical properties influence the performance of the blast furnace, while the chemical composition is more related to the amount of charcoal needed to produce a ton of iron and the composition of pig iron and steel produced. The ability to access the quality of the charcoal obtained by the carbonization of wood is a challenge facing the steel industry. In general, the quality of charcoal can be represented by a number of properties. They concern, in particular, moisture content, calorific value, elementar composition, apparent and true densities, porosity and pore volume distribution, surface area, electrical resistivity, reactivity, hardness (abrasion resistance) and compressive strength (ANTAL; GRØNLI, 2003). Although it has some advantages over coke in terms of higher reactivity and lower ash contents, charcoal is mechanically unstable compared to coke; it has inherently lower mechanical strength and higher friability, imposing difficulties to its transportation, handling and use in processes.

An increasing number of studies have highlighted the advantages of using charcoal instead of coke in blast furnaces in view of energy and environmental problems associated with the use of fossil fuels (CHEREMISINOFF, 1980; DEMIRBAS, 2001; DIBLASI et al., 1999; GAUR; REED, 1995; RAVEENDRAN; GANESH; KHILAR, 1995). However, while the mechanical properties of coal/coke have been studied on a large scale by various workers (PATRICK; STACEY, 1978; RAGAN; GRINT; MARSH, 1981; SINHA et al., 1982; TSAI et al., 1984), many questions concerning

mechanical properties of charcoal, the methods of their measurement, and the analyses made from them remain open problems. In past decades, some researchers studied physical and structural characteristics of charcoals (BLANKENHORN; JENKINS; KLINE, 1972; BLANKENHORN; KLINE; BEALL, 1973; KUMAR; GUPTA, 1993; KUMAR; VERMA; GUPTA, 1999; KWON et al., 2009; OLIVEIRA; GOMES; ALMEIDA, 1982).

A steel blast furnace operates in countercurrent, hot gases upwards and load downwards. Permeability, which is the passage of gases through the load, is strongly affected by particle size distribution. The low mechanical strength of charcoal affects the load size distribution in the furnace as a result of greater generation of fines on handling and under load weight, thus hindering the contact of the gas with the metal charge due to the formation of preferential paths within the blast furnace, changing ore reduction reactions (RAAD; MELO, 2014). Charcoal mechanical strength determines the effective height, the internal volume and, consequently, the capacity and performance of the blast furnace (RAAD; MELO, 2014). The research issue is to improve properties of compressive strength and fragmentation of charcoal, without losing the quality of the remaining properties. The control of the carbonization process allows narrowing the fixed carbon range of charcoal and control the mechanical strength. The narrow carbon range and higher mechanical strength strongly influence the operational stability of the blast furnace (RAAD; MELO, 2014).

There is no approved method for evaluating the mechanical strength of charcoal. In studies conducted in large steel companies, mainly integrated, no correlation was found in the experimental results that could provide benefits to normalize a methodology (RAAD; MELO, 2014). The existing methods used in other studies consist in using prepared specimens and compressing them in the direction of the fibers (DOAT; PETROFF, 1975; KUMAR; VERMA; GUPTA, 1999; OLIVEIRA; GOMES; ALMEIDA, 1982; VIEIRA, 2009).

The mechanical strength of charcoal beds in the Brazilian context of iron and steel furnaces is very important and contributes for reducing the specific consumption of industrial units. As charcoal is irregular shaped, granular and anisotropic, compression tests in the axial direction using prepared specimens may not reveal the behavior of a charcoal bed, as a whole, when undergoing compressive loads. This may not relate to industrial conditions, where the load on charcoal is not exclusively applied on the direction of the fibers, but is randomly applied instead. This thesis proposes an approach to quantify the effects of applying load on randomly distributed bulk charcoal. This represents an attempt of simulating conditions similar to what is expected in the industrial practice, such as in a blast furnace. From the result, it is possible to describe the behavior of charcoal through breakage index and its particle size distribution. This type of information can provide parameters for operational improvement and projects involving charcoal blast furnaces. This research aimed to understand, experimentally, the mechanical behavior of a fixed bed of *Eucalyptus* charcoal blast furnace under different carbonization conditions.

To attend the main goal of this study, a series of questions is raised:

a) What is the relationship between properties of wood and charcoal obtained?
b) What are the effects of pyrolysis conditions on charcoal properties?
c) What are the effects of temperature and particle size on fragmentation in uniaxial compression?
d) What is the relationship between charcoal bed properties and its fragmentation in uniaxial compression?

To attend these purposes, this study falls into two parts. The first consisted in destructive and non-destructive wood characterization and charcoal produced at different carbonization temperatures and the second in

the mechanical behavior of charcoal beds at different temperatures and particle sizes.

The results should allow us to assess:

i. Provide information about the relation between mechanical properties of wood and *Eucalyptus* charcoal;

ii. Predicting the mechanical properties of charcoal from wood properties and under different carbonization conditions;

iii. Experimental understanding of the mechanical behavior of a fixed bed of *Eucalyptus* charcoal blast furnace obtained under different carbonization conditions.

2 LITERATURE REVIEW

2.1 Influence of wood material properties on mechanics of charcoal

2.1.1 Basic density

Wood basic density (ratio of dry mass to saturated volume) is positively correlated to the charcoal density (ANTAL; GRØNLI, 2003; BRITO; BARRICHELO, 1980; PEREIRA et al., 2000; TRUGILHO et al., 1997). Charring tends to regulate density differences between species; however, charcoal density remains globally proportional to the initial wood density (CHRZAZVEZ et al., 2014). Doat and Petroff (1975) stated that denser woods produce a denser and less friable charcoal. Therefore, it is expected that charcoals produced with dense woods present a higher mechanical resistance (ANTAL; MOK, 1990; CHRZAZVEZ et al., 2014). The higher the density of charcoal, the greater is its resistance to parallel compression of charcoal fibers, its strength modulus and gravimetric yield (MOUTINHO, 2013). Moutinho (2013) also stated that wood density is the physical property which is mostly correlated to the charcoal density, the elastic modulus, resistance to the parallel compression of charcoal fibers, gravimetric yield, radial, axial and tangential linear degradation. This strong correlation of basic density of the wood with the charcoal density has important implication on the reducing process, since the furnaces will present a higher productivity with the use of denser charcoal with the same volume being occupied by a larger mass. Although it is generally true that charcoal density is positively correlated to dry wood density, the results of Lancelotti et al. (2010) showed that, after the wood was subjected to charring denser species, it tended to be less resistant to compressive forces than less compact woods. Changes in density strongly depend on the species involved in carbonization (LANCELOTTI et al., 2010), between hardwood and softwood,

for example (RECORD, 1914). Density loss markedly increases with temperature from 400 to 750 °C. Average density loss is 40%, with variations from 33 to 50%, according to the species (CHRZAZVEZ et al., 2014).

2.1.2 Moisture content

Friability is linked to wood drying before carbonization. A high moisture content (10% or more) of wood causes a great propensity for internal and/or external cracks in charcoal, since the pressure of the steam formed when the wood is heated weakens and/or fragments the resulting charcoal. Laboratory tests demonstrate that the humidity of charcoal considerably influences the production of fines in drum tests (ROUSSET et al., 2011). Prior and Alvin (1986) investigated the relationship between the moisture content of *Dichrostachys* wood and the damage caused by charring. Air-dried (moisture contents of approximately 8-13%) and saturated cubes of fully developed wood of *Dichrostachys cinerea* (*Leguminosae*) were charred for 60 minutes at 400°C. The authors used SEM techniques to elucidate the anatomical differences of the charcoal structure (Figure 2). It was observed that the charring of saturated *Dichrostachys* cubes results in the formation of large radial splits associated with the wood rays, together with anatomical changes in the fibrous tissue.

Figure 2 Pictures of Scanning Electron Microscopy (SEM) - *Dichrostachys cinerea*. - A: Tangential longitudinal fracture of specimen charred dry showing radial openings typically confined to the wood rays and confined within their height; - B: Similar view of specimen charred saturated; note wide openings not restricted to the height of wood rays.

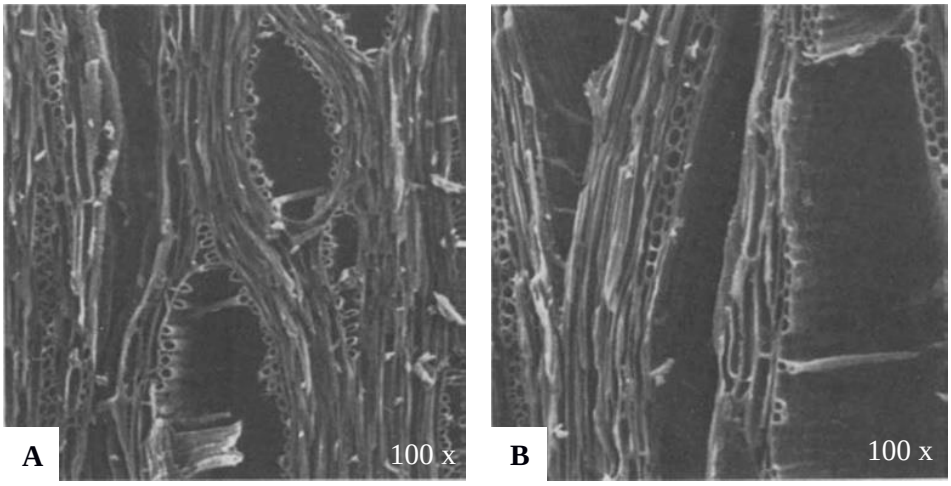

Source: (PRIOR; ALVIN, 1986).

2.1.3 Dimensions of wood pieces

The dimensions of pieces for carbonization are also correlated to the friability of charcoal. When carbonized, larger diameters will suffer more negative impacts during piece drying, that is, it will have more difficulty in drying and displace the carbonization front throughout the piece, since it follows towards the center of the piece (JUVILLAR, 1979). Coutinho and Ferraz (1988) observed a considerable increase in the production of fines in charcoals originated from wood having a larger diameter. The capacity of water circulation from one fiber to another depends, among other factors, on the age of the tissue where they are located. When a piece is put in a carbonization furnace, the sapwood dries quickly and the humidity of heartwood is hardly removed. Cracks

and internal clefts of charcoal are tension concentration zones and the source of such tensions may be attributed to the high impermeability of the heartwood of the wood pieces. It is common to find fissures in carbonized pieces with representative heartwood areas, while sapwood does not present such behavior. Any procedure that delays the formation of heartwood will reduce the amount of fissures during carbonization (OLIVEIRA; ALMEIDA, 1980). This fact will reduce the tendency to form fines when handling charcoal. The only way to control the formation of heartwood is using younger trees, that is, reducing the cutting cycle. On the other hand, due to the amounts of lignin and extractives, heartwood has a higher resistance to thermal degradation than sapwood (SILVA; TRUGILHO, 2003). Basic density is positively affected by the extractive content, which indirectly reflects on the mechanical properties of wood. Therefore, smaller heartwood dimensions generally tend to decrease friability problems of charcoal. The carbonizing state will change from the external to the internal part of the wood. Carbonizing shrinkage at temperatures above 300°C (also at high levels in the longitudinal direction) will show crack-inducing gradients, both parallel and transverse to the fiber. Smaller dimensions can limit the temperature gradient within the wood. The increase in the generation of fines is also related to density gradients between the regions of the bark and the pith of the trees, besides anatomical factors.

2.1.4 Chemical composition

Wood is an organic material which consists of carbon, hydrogen, oxygen, nitrogen and a small part of mineral elements. The main components of wood are cellulose, hemicelluloses and lignin. During carbonization, the production of condensable and non-condensable gases occurs, besides the solid fraction, charcoal. Properties of the solid material are related to the interaction of

these precursors. Therefore, the amount of each component and the way they are organized influence directly the mechanical properties of wood and, consequently, the quality of the charcoal obtained after carbonization (JUVILLAR, 1979). The main component that acts on the formation of charcoal is lignin, since it is technically more stable than the carbohydrates of wood. According to Bartkowiak and Zakrzewski (2004), mass losses for lignin do not surpass 60% at temperatures above 600 °C. Mass losses related to hemicelluloses and cellulose are large and occur in a temperature range from 270 to 380 °C (BEALL; BLANKENHORN; MOORE, 1974; KHEZAMI et al., 2005; PEREIRA et al., 2013). After thermogravimetric analysis (TG) and differential thermic analysis (DTA) of charcoal of *Eucalyptus grandis* x *Eucalyptus urophylla* hybrids, Soares (2011) found that the thermal degradation of charcoal occurs in only one step. She noticed the absence of a phase corresponding to the degradation of hemicelluloses, which indicates the occurrence of thermic degradation of cellulose components of wood during pyrolysis. The beginning of the mass loss of charcoal occurs from approximately 310 °C, corresponding to the beginning of the second phase of wood degradation, characterizing the supremacy of cellulose and lignin derivatives. Blankenhorn, Jenkins and Kline (1972) suggest that the thermal degradation of wood, especially of lignin, is similar to the formation of glassy carbon of phenolic resins. In temperatures below 500 °C, lignin dehydrates, while at higher temperatures there is the formation of several aromatic compounds (VELDEN et al., 2010). Materials constituted in their essence by carbon atoms, have the characteristic to bind indefinitely with themselves; thus, they can assume variable structures, acquiring distinct properties according to the handling of the raw material and the production process used (JENKINS; KAWAMURA, 1976). A high content of substances of aromatic nature such as

extractives and lignin generates a charcoal with a higher density and greater mechanical resistance (BLANKENHORN; KLINE; BEALL, 1973).

2.1.5 Anatomy

The amount and arrangement of the anatomical components, as well as the proportions of heartwood and sapwood, the proportion of early and late wood in the rings and the variability along the radius, influence the formation of charcoal and also its mechanical properties (CHRZAZVEZ et al., 2014; MOREIRA, 1999). For example, it is known that the juvenile wood has a lower density, shorter fibers and more parenchyma (TRUGILHO; LIMA; MENDES, 1996), thus producing a less resistant charcoal. Observing the microstructure of charcoal, it was observed that, independently of the temperature, the wood structure keeps integer, although there are different levels of concentrations in the different elements that constitute the wood structure (BLANKENHORN; JENKINS; KLINE, 1972). Klar (1925) accented that charcoal retains the form and structure of the biomass from which it is produced to such an extent that the appearance of the charcoal can be used to identify its origin. The porosity of charcoal is closely associated to the carbonization temperature, wood density from which it had originated and the speed of carbonization (BLANKENHORN et al., 1978; CHRZAZVEZ et al., 2014; KUMAR; GUPTA, 1993; OLIVEIRA; GOMES; ALMEIDA, 1982; WENZL, 1970). Blankenhorn et al. (1978) indicate that, for the wood of Black Cherry (*Prunus serotina* Ehrh), the total porosity increased with the increase in temperature of up to 600 °C and then decrease with carbonization temperatures of up to 900 ºC. Kumar and Gupta (1993) concluded from their experiments with wood chars produced from *Acacia* and *Eucalyptus* and under slow carbonization (about 4 $^{o}C.min^{-1}$) that the porosity increases with the carbonization temperature up to 1000 ºC and after, its value is

nearly constant. According to Chrzazvez et al. (2014), the presence of spiral thickenings (in hardwood genres, such as *Corylus*, *Carpinus* and *Acer*), which are preserved after charring, is linked to a higher crushing strength, although the density of these species is not higher than that of *Fraxinus*, for example. The low value of crushing strength is either linked to high porosity of charcoal, or to its low density. Fragmentation intensity is related to charcoal porosity. Marked porous zones with large vessels or radial pore files are prone to fragmentation. Conversely, more homogeneous porous wood (with small isolated diffuse vessels or homoxylates) tends to be less fragmented (CHRZAZVEZ et al., 2014). The total number of fragments after compression depends mainly on the species, regardless of carbonization temperature (CHRZAZVEZ et al., 2014). Mechanical resistance to compression is higher when compression is applied lengthwise to the cross-section (LANCELLOTI et al., 2010). At higher temperatures, more volatile matter is forced out of charcoal, which results in an overall opening of the structure. Manabe et al. (2007) found an increase in the total volume of micropores (less than 2 nm of diameter) and specific surface area of Hinoki charcoal (Cypress, *Chamaecyparis obtusa*) with increases in carbonization temperature up to 1000 °C, with a less pronounced improvement between 800 and 1000 °C. Oliveira, Gomes and Almeida (1982) evaluated the structure in carbonizations between 300 and 700 °C through of optical microscopy in charcoal. They found clean vessels at 300 °C due to the higher loss of volatile compounds through hemicelluloses and, at 500 °C, the fiber cavities were also cleaned. Between 300 and 500 °C, a decrease in vessel diameter was observed and this diameter was increased between 500 and 700 °C. The morphology of *Quercus variabilis* charcoals was investigated by scanning electron microscopy (SEM) by Kwon, Kim and Cha (2009). Figure 3 shows the changes of vessel diameter in the cross section of wood carbonized at 500 °C. The vessel shrinkage of the tangential direction was about 7.6 times

higher than that of the radial direction at carbonization temperatures around 350 – 500 °C. The difference might be due to the presence of rays that constrain the radial dimensional change. The vessels in wood samples carbonized at 500 °C showed cracks along the tangential direction (Figure 3).

Figure 3 Severe cracks in the tangential direction during the charring process at 500 °C.

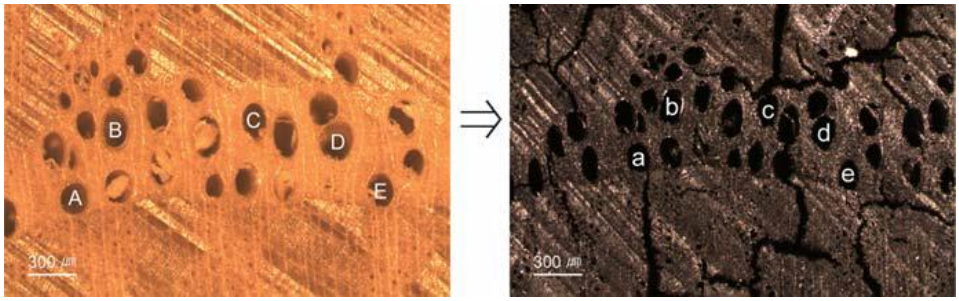

Source: (KWON; KIM; CHA, 2009).

2.2 Influence of the carbonization process on mechanics of charcoal

2.2.1 Temperature

Blankenhorn et al. (1978) observed, when carbonizing black cherry, that the density decreased until 600 °C, and then it increased with the increase in temperature until 900 °C. Moore et al. (1974) performed mechanical tests on carbonized wood from *Betula* trees at temperatures between 200 and 700 °C. They concluded that the strength modulus of the charcoal decreases at approximately 450 °C. Mass loss and the retraction accompanied the decreasing trend of the strength modulus. Treatments above approximately 500 °C resulted in a substantially smaller reduction in mass and retraction, but resulted in an increase in the elastic modulus of the carbonized *Betula* wood (Figure 4).

Figure 4 Variation in the dynamic elastic modulus of carbonized *Betula* as a function of carbonization temperature.

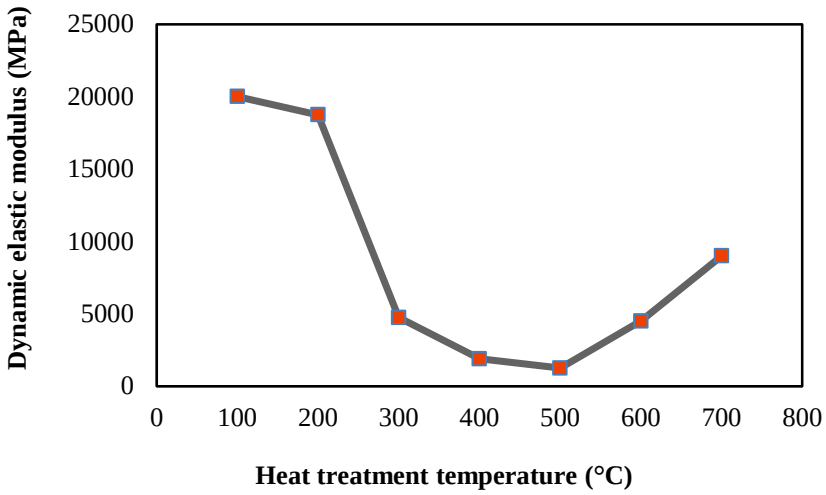

Source: (MOORE et al., 1974).

Results of studies developed by Oliveira, Gomes and Almeida (1982) showed the influence of the carbonization temperature on the compression strength in charcoal. The authors observed an increase in the resistance to compression with the increase in temperature from 300 to 900 °C in eight-year-old *Eucalyptus grandis*. At 900 °C, the resistance to compression is higher than at 500 °C; corresponding to the temperature usually used in charcoal manufacturing (OLIVEIRA; GOMES; ALMEIDA, 1982). The increase in resistance as a function of temperature may be related to the increase in the amount of fiber per unit of area (OLIVEIRA; GOMES; ALMEIDA, 1982). Andrade and Della Lucia (1995) related the decrease in resistance to compression up to 500 °C to an increase in the porosity of charcoal due to the higher extraction of volatiles. In this carbonization range, charcoal does not suffer significant shrinkage and number of fibers per unit of area, which suggests a lower mechanical resistance. Baileys and Blankenhorn (1982) related

an increase in total porosity with the increase in peak temperature until 500 °C. The carbonization temperature had a remarkable influence over pore volume in charcoal and, consequently, over its resistance to compression. The increase in mechanical resistance above 500 °C may be related to factors like the decrease in volume observed during carbonization, even above 500 °C (BAILEYS; BLANKENHORN, 1982), changes in size, shape and distribution of the porosity of the material at high temperatures (>500-600ºC) and a possible structural rearrangement of charcoal components, especially carbon. The higher the temperature, the more resistant is the charcoal structure (BLANKENHORN; JENKINS; KLINE, 1972; BLANKENHORN; KLINE; BEALL, 1973; BEALL; BLANKENHORN; MOORE, 1974; MOORE et al., 1974; OLIVEIRA; ALMEIDA, 1980; OLIVEIRA; GOMES; ALMEIDA, 1982). According to Oliveira, Gomes and Almeida (1982) this structural rearrangement is accompanied by the increase in the charcoal density. On the other hand, Chrzazvez et al. (2014) observed that an increase in the temperature of carbonization induces a decrease in charcoal resistance, regardless of species. This decrease is partly due to the reduction in charcoal density, which is most pronounced between 500 and 750 °C. More recently, a study of the mechanical properties of species from the north of India showed that resistance to compression and the dimensions of the ensuing fragments is correlated positively to formation temperatures of charcoal (LANCELOTTI et al., 2010). Charring temperature greatly affects the structure of charcoal. Kim and Hanna (2006) examined the charcoal morphology of *Quercus variabilis* prepared in an electric furnace under nitrogen gas atmosphere at 400, 600, 800 and 1000 °C (Figure 5). In charcoal prepared at 400 °C, most of the morphological characteristics remained relatively unchanged, with the exception of the cell-wall layering. The cell walls appeared homogenous and glass-like. Above 400 °C, there was an increase in cell-wall thinning and volumetric shrinkage, with an

increase in charring temperature. These two factors were responsible for most of the observed changes in the structure. Fracture surfaces became increasingly rough and disrupted. Vessel elements were increasingly distorted and tyloses disintegrated with increases in temperature (Figure 5).

Figure 5 Transverse surfaces of charcoal prepared at 400 °C (A), 600 °C (B), 800 °C (C) and 1000 °C (D).

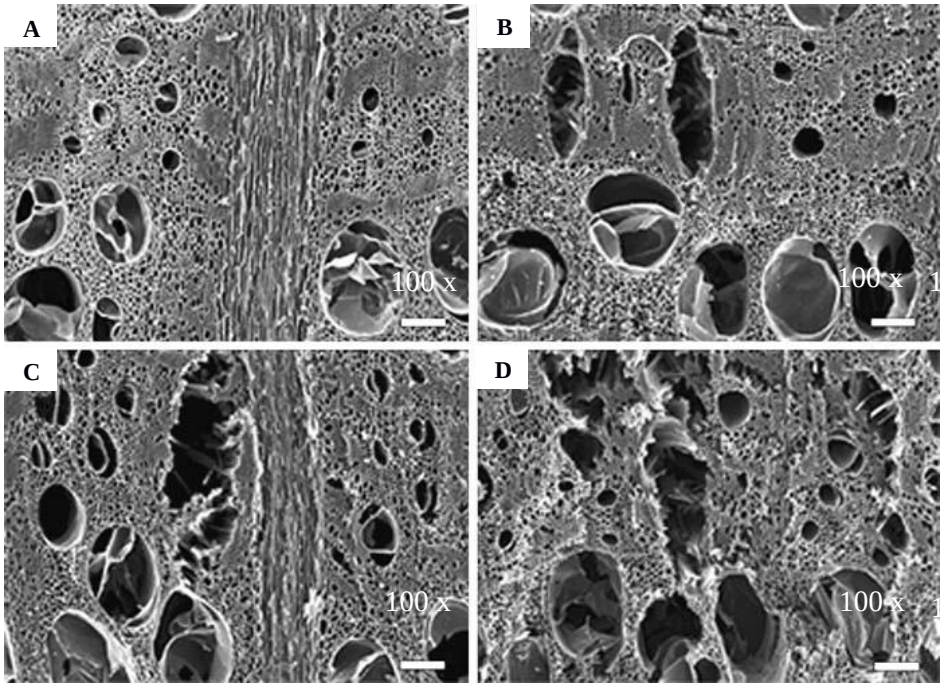

Source: (KIM; HANNA, 2006).

The structure of solids formed by carbon is directly related to the type of binding or hybridization with which carbon combines with other carbon or other element. The carbonized wood presents graphite-type crystallites, despite being considered a non-graphitic material (EMMERICH et al., 1987). The maximum of structural disorder is observed in carbonaceous materials called isotropics, whose stacking structure of carbon hexagon layers presents a bidirectional

ordination, independently of the temperature of the thermal treatment; therefore, they are classified as non-graphtizable (FERRARI; REZENDE, 1998). Raman spectroscopy is a technique that has been widely used for the structural characterization of different carbonaceous materials, identifying the types of bindings and providing information on the degree of disorder of the crystalline net (LOBO et al., 2005; OCARIS, 2014). Hinoki charcoal (Cypress, *Chamaecyparis obtusa*) carbonized at 400 °C, 600 °C, 800 °C and 1000 °C was analyzed through Raman spectroscopy in order to investigate the effect of the carbonization temperature over the structure of charcoal (MANABE et al., 2007). The band at 1580 cm^{-1} is assigned to the graphite (band G) originated from the crystalline carbon of graphite, and the band at 1350 cm^{-1} is assigned to the disorder originating from defects in the carbon structure with pending bindings (band D). It is found that the intensity ratio of the D-band to the G-band (I(D)/I(G)) increases with increasing carbonization temperatures. It is assumed, therefore, that the generation of gases such as CO_2 proceeds to the formation of many dangling bonds in the C-C structure by carbonization. The authors verified that, with the increase in temperature, there was a change in the position of band G for a superior band and band D changed for an inferior band. Since the peak shift relates changes of the molecular vibration mode, these results suggest changes in the chemical bond state in charcoal. It is suggested that the C=C bond formed in the pyranose ring in charcoal changed into the C-C bond between 600 °C and 800 °C, which is the starting point to the formation of the macromolecule. A better organization of the structure of the material occurs with the increase in temperature, thus increasing the mechanical strength of charcoal (MANABE et al., 2007). McGinnes, Kandeel and Szopa (1971) compared X-ray diffraction patterns of graphite, activated charcoal and conventional charcoal carbonized in a static atmosphere. The diffraction patterns indicated a high degree of crystallinity in wood carbonized in a static

atmosphere. The change from "amorphous" (disordered) to "crystalline" (ordered) structure was apparent. The results of studies with techniques of analyses for chemical and structural characterization recently performed, like solid-state ^{13}C NMR (Nuclear Magnetic Resonance spectroscopy) (MCBEATH et al., 2011; SUN et al., 2012), FTIR absorbance spectra (Fourier-transform infrared spectroscopy), X-ray diffraction, solid-state ^{13}C NMR (WU et al., 2012), in biochar of different sources of biomass showed that the increase in the final temperature (from 400 to 600 °C, in most cases) results in an increase in the proportion of aromatics C and/or the size of the aromatic C agglomerate. Ultrasonic velocities in a parallel (axial direction - *v*ax) and perpendicular (radial direction - *v*rad) to plant fiber directions were measured for yucca, before and after carbonization (KRZESIŃSKA; ZACHARIASZ, 2007). As it can be seen from Figure 6 (A), the ultrasonic velocity in raw yucca rapidly decreased after the heating of the sample at 300 °C, due to the higher bulk porosity of the carbonized material. Further heating up to 750 °C increased the velocity value. At this temperature, *v*ax achieved the same value as that of raw yucca, while *v*rad was found to be higher. It is a result of the substantial increase in rigidity of the carbonized yucca structure. Heating samples at higher temperatures produced less additional weight loss and reduction in dimensions, but formed much stiffer char than that obtained at lower temperatures. As it was shown in Figure 6 (B), the chars obtained at temperatures higher than ~330°C were characterized by more isotropic properties than raw yucca.

Figure 6 (A) Ultrasonic velocity of raw and carbonized yucca at the temperature range from 300°C to 950°C; (o) – axial direction, (●) – radial direction; (B) Elastic anisotropy of raw and carbonized yucca at different carbonization temperatures.

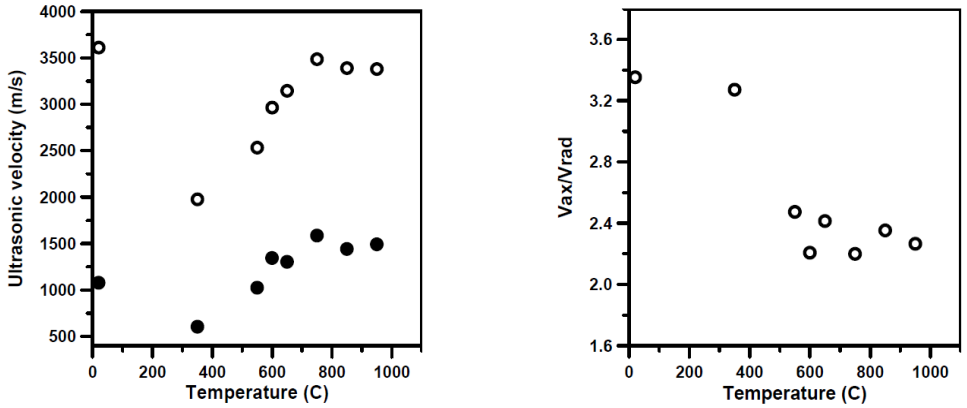

Source: (KRZESIŃSKA; ZACHARIASZ, 2007).

2.2.2 Heating rate

Heating rate has a great influence on product weight yields (dry wood basis) obtained by different wood pyrolysis modes. Fast and intermediate pyrolysis (occurs in a few seconds or less) favors the production of liquid. In the case of slow pyrolysis (10-60 min until days) it is possible to observe carbonization, gasification, combustion and torrefaction (BRIDGWATER, 2012). Violette (1853 cited by ANTAL; GRØNLI, 2003), related a greater friability of charcoal when the wood was quickly heated. Oliveira, Gomes and Almeida (1982) mentioned that lower heating rates may smooth the drying and the output of carbonization gases, thus reducing the defects and cracks in the carbonized samples. Kumar and Gupta (1993) found that wood samples carbonized slowly (about 4 $^{o}C.min^{-1}$) have a lower porosity than the ones fastly carbonized (20, 43, 80 and 174 $^{o}C.min^{-1}$). For charcoal produced by fast

carbonization, porosity increased progressively with temperature, due to two factors: the release of volatile matter and the formation of cracks and voids. Xie (2008) found that slow heating rates caused the formation and growth of graphene sheets in turbostratic crystallites, which had a positive significant influence on the Young's modulus of the carbonized wood. A reduction in the heating rate is beneficial with respect to carbon properties and the prevention of crack production during the manufacture of large monolithic carbon specimens from wood and wood-based materials (XIE, 2008). Grønli (1996) observed that the resistance of charcoal to compression decreased with the increase in the heating rate, and the charcoal of resinous species was more fragile than the charcoal obtained from broadleaved woods. Nisgoski et al. (2014) demonstrated that the heating rate, the difference in regimes (steady increase versus ramp heating) and the duration of the process are mainly related to the dimensional alterations of charcoal.

2.2.3 Pressure

When the carbonization process is conducted in reactors under high pressure, it is observed that there is a condensation of volatiles in the solid matrix. Secondary reactions between highly reactive substances rearrange to a more stable structure called secondary charcoal, resulting in an increase in gravimetric yield of solids and higher fixed carbon content (MANYÀ et al., 2014; NUMAZAWA, 2000; RICHARD; ANTAL, 1994; SYRED et al., 2006). High pressures improves heat transference within the reactor, thus producing a more uniform charcoal and reducing the time required for heating (ANTAL et al., 1996). Rousset et al. (2011), studying the effects of temperature (450 ºC and 600 °C), pressure (0, 5 and 10 bar) and humidity (0, 15 and 110%) in charcoal from *Eucalyptus grandis* wood, concluded that the best charcoal for steelmaking

was obtained in higher values of pressure and temperature (10 bar and 600 °C) with the wood completely dried. From Figure 7, it is possible to observe the increase in the content of the cell ray with the increase in pyrolysis pressure.

Figure 7 Photos by scanning electron microscopy (SEM) of tangential plan *Bagassa guianensis* charcoal produced at different pressures: (A) atmospheric pressure; (B) 2 bar; (C) 7.3 bar and (D) 10 bar

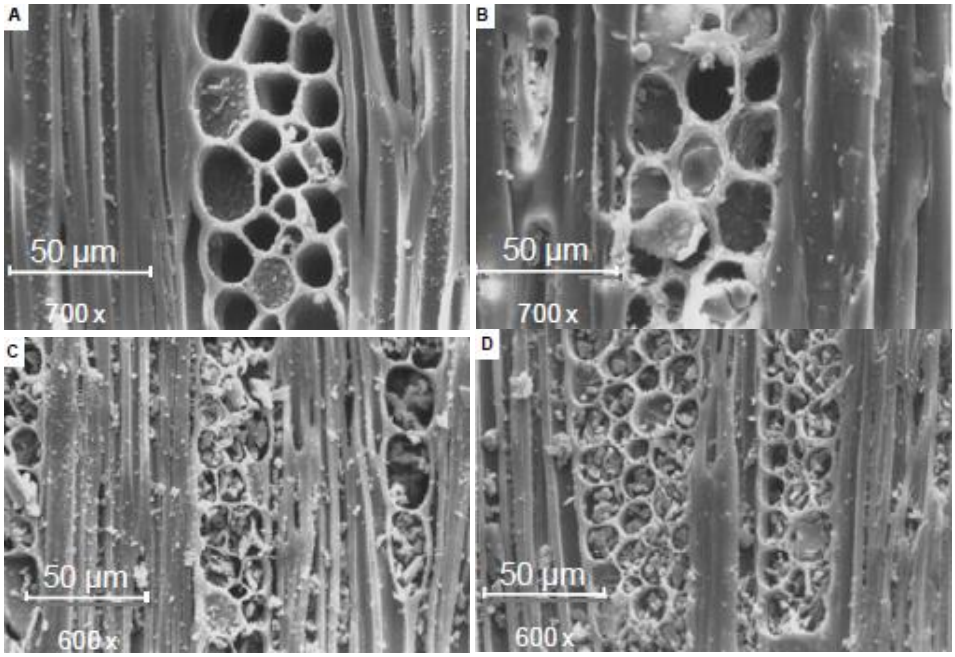

Source: (NUMAZAWA, 2000)

3 MATERIAL AND METHODS

3.1 Origin of the material

A total of 73 trees of one hybrid clone of *Eucalyptus urophylla* ST Blake with 6 years old were harvested. The trees came from a commercial plantation belonging to GERDAU S.A., and were located in the same plot at Santo Antônio do Amparo, Minas Gerais - Brazil (20°56'48'' S and 44°55'09'' O, alt 1000 m). The climate is subtropical humid (Cwa), according to the Köppen classification (PEEL; FINLAYSON ; MCMAHON, 2007), with an average annual temperature of 24 °C, average annual rainfall of 1300 mm, average annual humidity of 67% and a dry season from May to October. The plot was a dystrophic Oxisol A typical moderate (clayey), characterized by a flat soil, with quality ranging from average to high. The seedlings were planted in a randomized design, and plantation density was 1190 trees/ha (3.0 x 2.8 m spacing). The trees were sampled in a single installment to be considered as identical site conditions. With diameters at 1.30 m, total and commercial height were measured after harvest. Figure 8 shows the experimental planting of *Eucalyptus* sp. at time of specimen collection.

Figure 8 Experimental planting of *Eucalyptus* sp.: time of specimen collection

Source**:** personal image

3.2 Sample preparation

In each tree, logs with about 1 m in length were removed, starting from the base of the tree, between 0.3 m and 1.3 m height. The logs were deployed in central boards with 10 cm thick, 10 cm width and 40 cm in length. From the central boards, samples were made considering three radial positions from pith to bark, as internal, middle and external (Figure 9). The number of samples from each tree-sample was not the same. For diameters lower than 18 cm, only one sample was cut (identified as 'middle', N = 27). In the other case, for diameters larger than 18 cm, two samples were prepared (identified as 'internal', N = 45, and 'external', N = 46). A total of 118 wood specimens with nominal sizes of 30 x 30 x 200 mm (in R, T and L directions) were produced from 73 central boards and transported to the CIRAD in Montpellier, France. Figure 9 sums up the sampling strategy of the wood.

Figure 9 Strategy for preparing wood samples

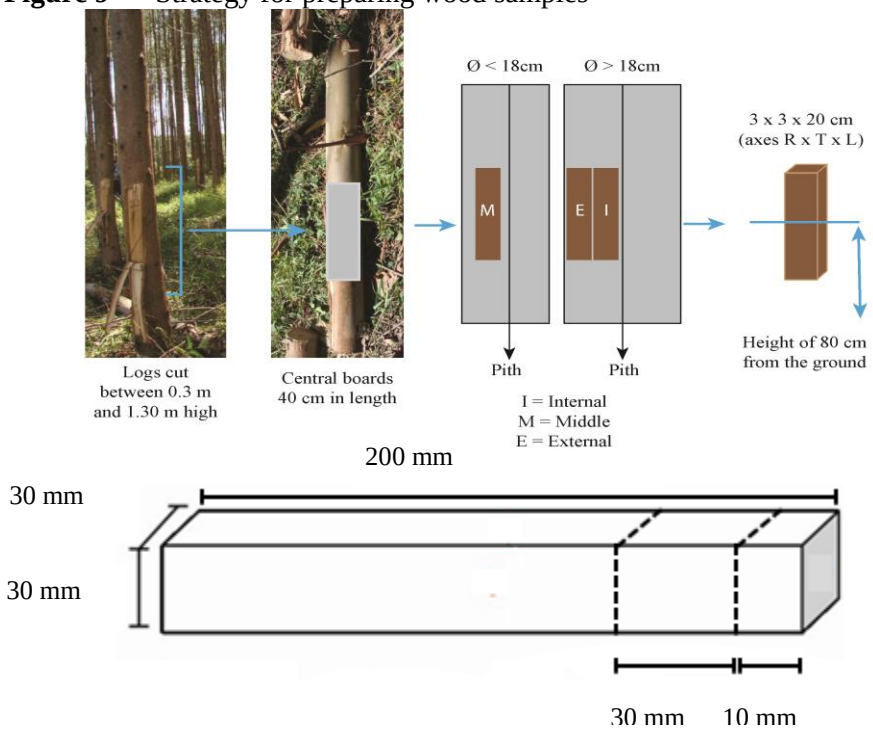

Longitudinal vibration tests and ultrasound measurements were performed on wood samples measuring 30 mm × 30 mm × 200 mm; after these measurements, beams were cut from them with nominal dimensions of 30 mm x 30 mm x 30 mm to determine the modulus of elasticity by ultrasonic measurements and modulus of shear in the three directions and wood samples with 30 mm x 30 mm x 10 mm for wood density and shrinkage measurements (Figure 9). Table 3 list the methods used to determine the wood properties and dimensions of wood samples.

The samples were kept in a conditioned room with 65±5% relative humidity and temperature of 20 °C before analysis. Under these conditions, the theoretical moisture content was 12%.

Table 3 Summary of physical and mechanical properties measured on wood and corresponding specimen dimensions

Wood properties	Dimensions
ρ12 (kg.m^{-3})	30 mm x 30 mm x 200 mm
MOE BING (MPa)	30 mm x 30 mm x 200 mm
MOE US (MPa)	30 mm x 30 mm x 200 mm
MOE US Longitudinal (MPa)	30 mm x 30 mm x 30 mm
MOE US Radial (MPa)	30 mm x 30 mm x 30 mm
MOE US Tangential (MPa)	30 mm x 30 mm x 30 mm
G_{LR} (MPa)	30 mm x 30 mm x 30 mm
G_{RT} (MPa)	30 mm x 30 mm x 30 mm
G_{TL} (MPa)	30 mm x 30 mm x 30 mm
ρ (kg.m^{-3})	30 mm x 30 mm x 10 mm
FSP (%)	30 mm x 30 mm x 10 mm
δ rd (%)	30 mm x 30 mm x 10 mm
δ tg (%)	30 mm x 30 mm x 10 mm

The cubic samples (30 mm in L, R and T directions) used in the determination of modulus of elasticity and shearing in wood were subsequently carbonized (N = 58). The sample population was previously divided into two batches: the samples were sorted according to wood density, and the even ranks were associated with a pyrolysis temperature of 500 °C (odd ranks with a temperature of 900 °C).

3.3 Experimental protocol

The various steps of the experimental protocol are presented in Figure 10.

Figure 10 Presentation of experimental tests performed

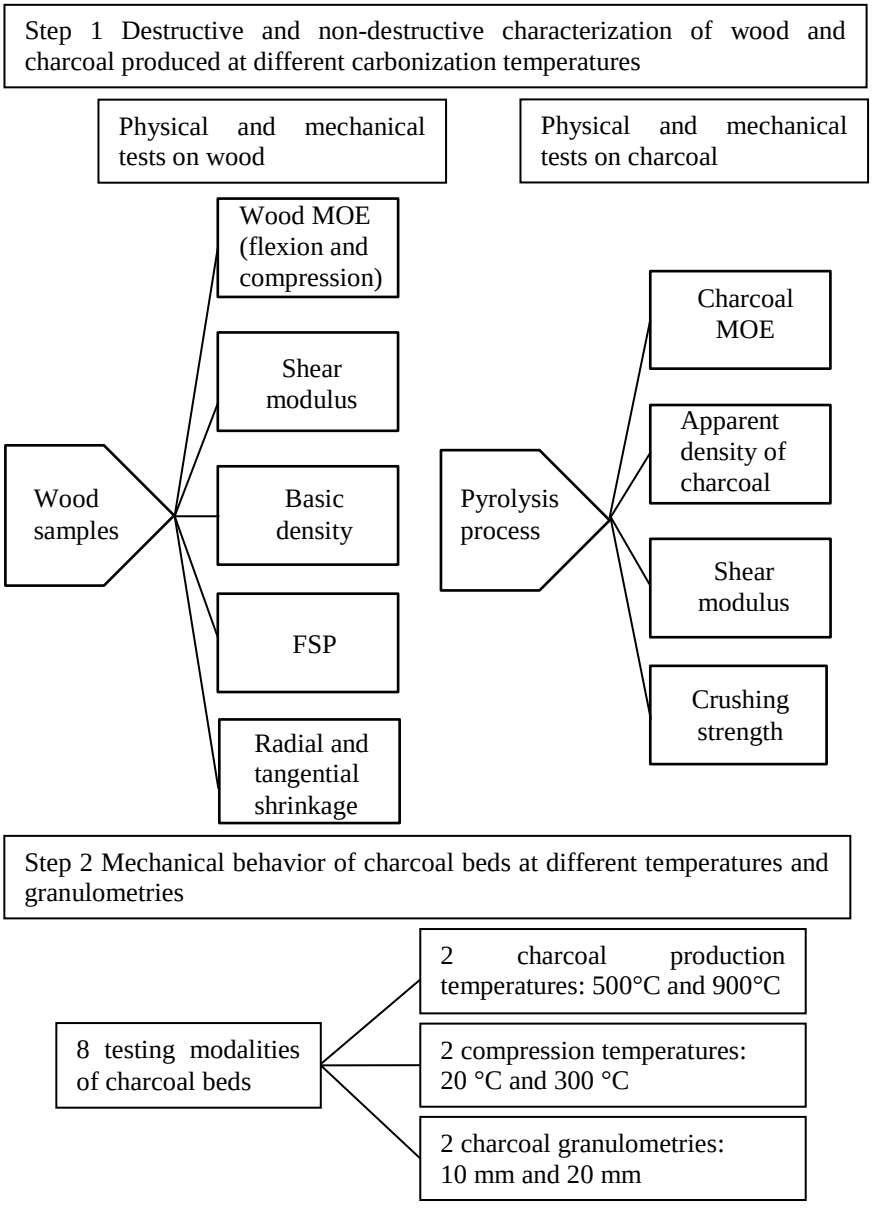

Apparent wood density (ρ12) was first determined. The modulus of elasticity (MOE), flexed by BING® vibration tests and compression by ultrasonic (US) measurements in the longitudinal direction were then assessed. Subsequently, the shear modulus (G) and the modulus of elasticity were obtained by ultrasound (MOE US) in longitudinal, radial and tangential directions. Therefore, radial (δ rd) and tangential compression (δ tg), basic density and fiber saturation point (FSP) were the physical parameters considered and determined in wood. In a second step, the cubic samples were pyrolized. The apparent density of charcoal samples was measured. The modulus of elasticity and shear modulus of charcoal samples was determined by ultrasounds. Finally the crushing strength was conventionally obtained by a static test in the three directions.

In a second phase, taking into account the procedures for the obtention of charcoal, different granulometries and temperatures of compression bed tests, a total of eight charcoal layers were made to evaluate the mechanical behavior of the granular medium.

3.3.1 Pyrolysis process

On a laboratory scale, carbonizations were performed in a specific eletric cylindrical reactor Macro-ATG (Figure 11), with a capacity of, approximately, 0.7 m^3 (30 cm internal diameter and 100 cm height). The reactor was developed by Cirad and set at Universidade Federal de Lavras.

Figure 11 Photo of Macro ATG prototype and its main components

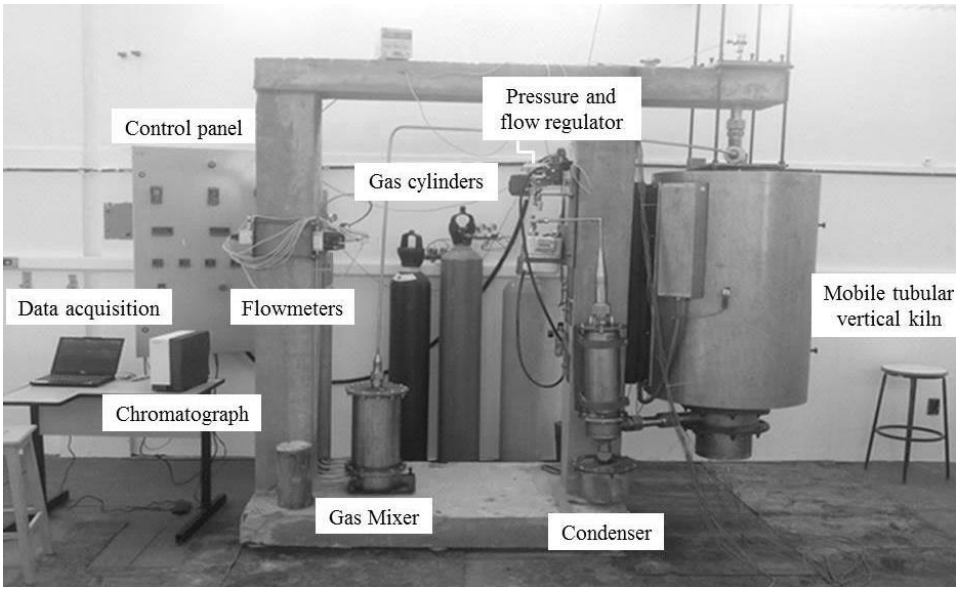

58 cubic wood samples were subjected to carbonization. Before the carbonization process, the samples were taken into an oven at 105±3 °C for the determination of wood dry mass. The samples were pyrolized at two final temperatures, 500°C and 900°C, using a heating rate of 1.0 °C/min. The carbonizations were conducted under an inert atmosphere (nitrogen) with gas flow of 10 Nl.min^{-1}, initial temperature of 40 °C and residence time of 1 (for final temperature of 500 °C) to 2 (for final temperature of 900 °C) hours.

The sample population was previously divided into two batches: the samples were sorted according to wood density, and the even ranks were associated with a pyrolysis temperature of 500 °C (odd ranks with a temperature of 900 °C). After removed, the samples were taken into an oven to constant weight, for the determination of wood dry mass and carbonization gravimetric yield.

The gravimetric yield in charcoal (GYC) was obtained for each sample by the ratio: $$GYC\ (\%) = \frac{CDM}{WDM}\ x\ 100 \quad (1)$$

Where: CDM is charcoal dry mass and WDM, wood dry mass.

The charcoals thus obtained were then examined for their apparent density and mechanical properties.

3.3.2 Density

The apparent density of wood samples was determined, and the volume was computed by measuring the dimensions with a digital caliper.

For the basic density of wood, samples (measuring 30 mm × 30 mm ×10 mm) were removed from the wood of the specimens used in vibration and ultrasonic tests. These wood samples were used for shrinkage (δrd and δtg) measurements, fiber saturation point (FSP) and basic density (ρ), which was determined by the ASTM D2395-07 (ASTM, 2007) procedures. The formula for calculating basic density is given as follows:

$$\rho = \frac{oven\text{ - }dried\ weight}{saturated\ volume} \qquad (2)$$

The saturated volume of a piece of wood was determined by water displacement, according to the principle of Archimedes. The samples were first soaked in water with the aid of an autoclave to ensure that water is not taken up during the immersion process. After determining the saturated volume, the samples were oven-dried at 103±2 °C.

The apparent density of charcoal samples was measured according to the ASTM D2395-07 (ASTM, 2007) (volume by water immersion). An experimental device was used for measuring the volume of charcoal samples. The samples were waterproofed with a very thin layer of grease before obtaining charcoal volume (Figure 12).

Figure 12 1) Scale setup; 2) Obtention of sample dry mass; 3) Tare; 4) Sample waterproofing; 5) Volume determination

Source: Personal image.

3.3.3 Ultrasonic testing (modulus of elasticity and shear modulus)

Elastic modulus (MOE US) and shear modulus (G) were estimated at the sample level for wood and charcoal. Two contact transducers were used in transmission mode. Each sample was placed between the piezoelectric transducers with honey for wood and grease silicon for charcoal, used as a coupling medium. The emission frequency was set to 1 MHz, and the received signal was digitized with a 12-bit resolution and a sampling period of 0.1 µs (the

average propagation time for wood is 6.4 μs). A computer algorithm calculated the propagation time by determining a threshold, based on an analysis of the statistical properties of the signal noise. This determination method was appropriate in this case, given that the signal-to-noise ratio was greater than 30 dB. The ultrasonic modulus of elasticity (MOE US) was determined by the conventional Equation 3, where ρ12 is the apparent density, L is the sample length, and τ is the propagation time. The mean of three measurements was used to determine the MOE value of each sample.

$$MOE = \rho 12\left(\frac{L}{\tau}\right)^2 \quad (3)$$

In order to estimate the dynamic shear modulus (G), the wood and charcoal samples were tested with an ultrasonic device designed by CIRAD (500 kHz transmission, detection by the first positive peak), in the three planes (Figure 13) longitudinal-radial (G_{LR}), radial-tangential (G_{RT}) and tangential-longitudinal (G_{TL}).

Figure 13 Ultrasonic shear test transmission (500 kHz)

Source: Personal image

3.3.4 Vibration test

Acoustic vibration measurements are made by placing the samples on elastic strings. The vibrations are generated by an impact at one end (throw of a metallic ball with 1 cm in diameter) and recorded by a laser at the other end (Figure 14). The analysis of the signal, the selection of the natural frequencies of vibration and the estimates of flexural MOE were performed using the software BING® (Beam Identification by Non Destructive Grading, CIRAD, Montpelier, France, version 9.1.3). The sampling frequency of the signal was 39 kHz for flexural vibration. The spectral acquisition was carried out by using 32,768 points for each test.

Figure 14 Device for estimating dynamic elastic properties of wood based on vibration tests

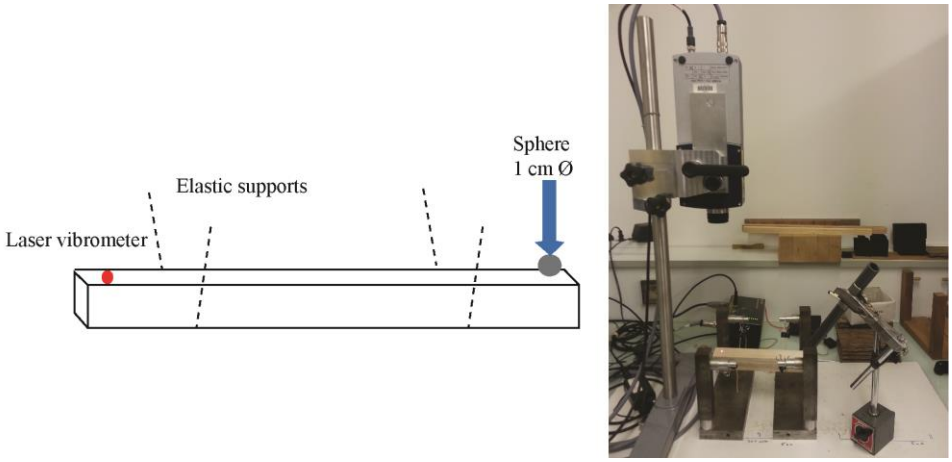

Source: Personal image

3.3.5 Determination of shrinkages and fiber saturation point

The dimensional stability of wood samples was measured. Radial and tangential shrinkages, as well as fiber saturation point (FSP), were determined simultaneously. Radial (δrd) and tangential (δtg) shrinkages were determined in

five conditions: from a full saturated condition to theoretical moisture steps of 18%, 12%, 6%, and then oven-dried (0%). The formula for calculating the shrinkage is given as follows:

$$\boldsymbol{\delta = \frac{initial\ length - final\ length}{initial\ length}\ x\ 100} \quad (4)$$

A digital dispositive was then used for precisely measuring sample dimensions of the saturated samples immediately after measuring the saturated volume (Figure 15).

Figure 15 Experimental device for measuring the saturated volume (A) and mass of the samples (B), sample dimensions (C) and obtention of the dry weight of the samples

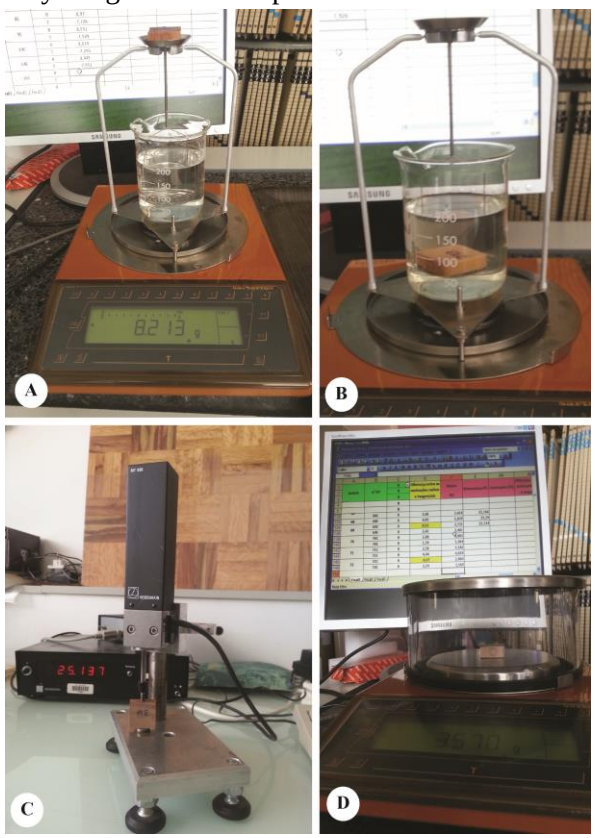

Source: Personal image

The anisotropy coefficient defined as the ratio between tangential and radial contraction was also calculated. Anisotropy coefficient values were obtained according to the following Equation 5:

$$\boldsymbol{Anisotropy\ coefficient} = \frac{\boldsymbol{Shrinkage\ Tangential}\ (\%)}{\boldsymbol{Shrinkage\ Radial}\ (\%)} \qquad (5)$$

The fiber saturation point (FSP) is the moisture value below which wood shrinkage is observed. According to the technological definition, the FSP is

given by drawing a linear regression line «y = a*x* + b» between the wood moisture and shrinkage. This value corresponds to the extrapolated moisture at which the contraction is zero (b = 0) (Figure 16).

Therefore, between the sample measurements in the saturated condition and the sample measurement in dry condition, three other measurement conditions were performed at three intermediate moistures: 18%, 12% and 6%. The samples were held in a climate chamber. In order to minimize errors, only the FSP in which the linear regression lines were obtained with an R^2 of 0.99 were considered.

The true stability moisture of each sample is then recalculated for each theoretical condition (18, 12 and 6%) (Hi), according to the mass to the considered moisture (MHi) and dry mass (M0) (Equation 6).

$$\boldsymbol{Hi} = \frac{(\boldsymbol{MHi} - \boldsymbol{M0})}{\boldsymbol{M0}} \qquad (6)$$

Figure 16 Example of determination of the FSP by regression: interception between wood moisture and shrinkage, this value corresponds to moisture extrapolated to which the shrinkage is null.

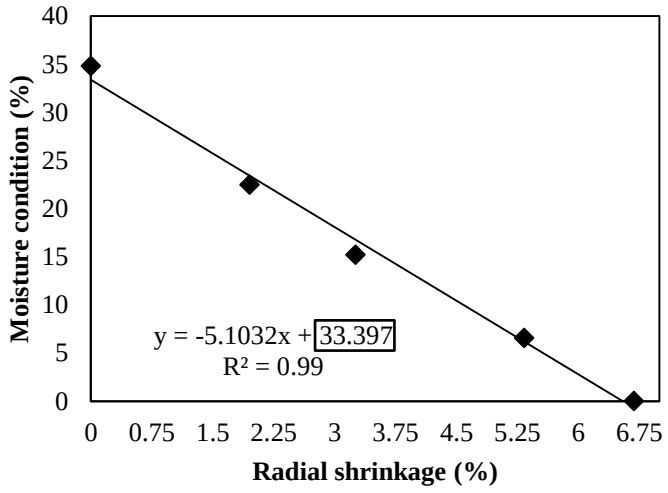

3.3.6 Static compression test

After dynamic tests, the charcoal specimens were tested using a universal testing machine. Static compression tests were performed to determine the maximum charcoal crushing strength. The important factors in crushing strength determination are that the specimens must have the maximum possible original, crack and void free, parallel and flat surfaces for applying load (KUMAR; VERMA; GUPTA, 1999). The surfaces of the charcoal samples were carefully sanded with 300-grit sandpaper to get surfaces as parallel as possible (to ensure their flatness and parallelism). The surfaces were then measured using image analysis (ImageJ). The charcoal specimens had variable dimensions. The percent change in volume caused by shrinkage during the carbonization of *Eucalyptus* wood depends, among other factors, on the final carbonization temperature.

A hydraulic traction-compression testing machine, equipped with a 10 kN sensor (ADAMEL Lhomargy DY 36 - DY36D MTS), was used for the compression experiments. A 10 kN static and uniform load (i.e. gradually imposed and evenly spread over the entire area) was applied to each sample, and the speed of compression was set at 0.005 mm/s and the test was conducted until material disruption. The charcoal specimen was placed between two rams and compression was applied in three different directions: parallel to the fibers (on transverse section) and perpendicular to the fibers (on radial and tangential section).

Figure 17 Resistance test to charcoal compression

Source: Personal image

The samples population (N = 58) was previously divided into six batches (Table 4), associated to pyrolysis temperature of 500 °C and 900 °C and sorted according to the wood density. The reported values of crushing strengths are the average of eight to eleven measurements (Table 4).

Table 4 Resume of number of samples used in compression tests according to the direction

Compression direction	500 °C	900 °C
	N	N
Longitudinal	10	11
Radial	10	10
Tangential	9	8
N	29	29

The pressure applied and the resulting decrease in the height of the sample (displacement of the tray), were recorded during the tests. These values allowed to plot the stress (MPa)/strain (%) curves, by dividing the force by the surface of the transversal side of the sample (stress), on one hand, and the displacement by the height of the sample (strain), on the other hand.

The crushing strengths of *Eucalyptus* charcoal was calculated by using the following formula:

$$\boldsymbol{\sigma} = \frac{\boldsymbol{W}}{\boldsymbol{S}} \qquad (7)$$

Where σ is the crushing strength in MPa; W is the load at fracture in N; and S is the surface of the cross-section of the sample in mm^2.

3.3.7 Specific compression test designed for charcoal beds

Charcoal bed compression tests are based on the break of an amount of a controlled size sample of charcoal by a compressive load and subsequent analysis of the size distribution of the sample.

This study was conducted at Cirad-BioWooEB/France, where a specific experimental device was designed to work at high temperatures. Compression tests were performed at two temperatures, 20 °C and 300 °C. The temperature of 300 °C was set due the flammability limit point of charcoal in the presence of oxygen (LULLIN, 1925). The charcoal bed compression test follows the recommendations of ASTM D143-94 standards (Standard Test Methods for Small Clear Specimens of Timber), with modifications (ASTM, 2009). A cell containing the charcoal bed is added to the device. This cell is a hollow cylinder closed by two elements, which provide a piston operation. The load is applied by a universal testing machine and transmitted to the sample by a transmission bar, which pushes a steel piston ring. All material is retained by the piston. The cylinder is 150 mm in internal diameter and has a 147 mm piston. A universal testing machine was used (ADAMEL Lhomargy DY 36 - DY36D MTS), with a maximum load of 100 kN.

Confined charcoal compression tests are carried out using a cylindrical steel tube and a compressive platen. The material is confined by the tools and compressed axially in a press. The force shall be applied at a constant speed of 0.02 mm/s, with a maximum force defined of 12 kN. Figure 18 shows a sketch of the experimental apparatus used to determine the compressive strength of charcoal beds.

Figure 18 Schematic drawing and photo of the experimental device and its main components.

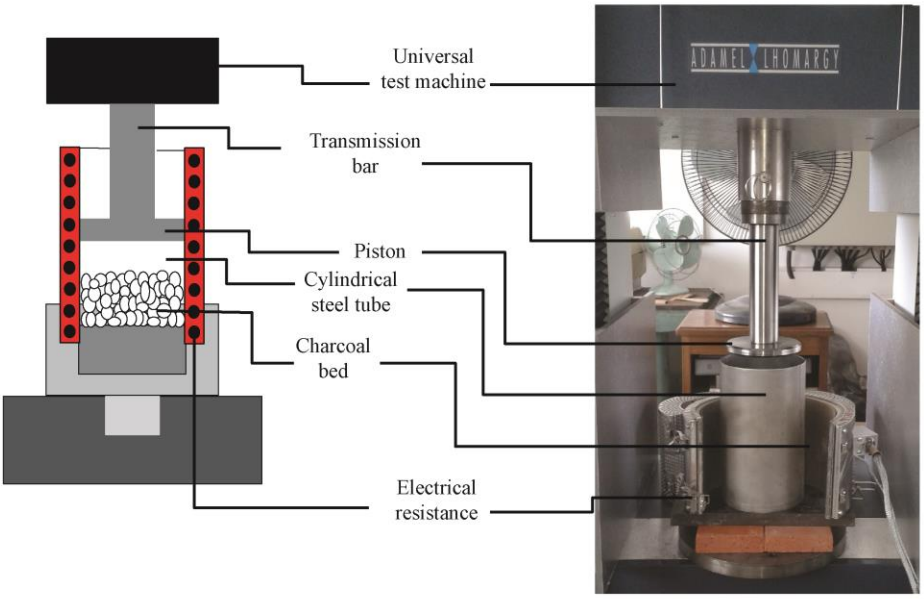

The production of charcoal at this stage was carried out from *Eucalyptus* sp. wood with dimensions of 30 x 30 x 200 mm, taken from the opposite side of the cord of the same log boards from which samples were removed for physical and mechanical characterization of the material. As for the sample level, two final temperatures were taken into account for charcoal production: 500 °C and 900 °C.

Packing density is a key feature of a granular medium (MIKSIC, 2008). Therefore, two granulometries were selected for the study: 10 and 20 mm. Breaking and screening were performed for the obtention of charcoal, in order to control charcoal size distribution before and after the application of compressive load. Granulometries of 10 and 20 mm were determined, using a set of 20- and 10-mm sieves. Regarding charcoal crushing, due to the small amount used in the tests, it was decided to perform the manual breaking of the material with the aid of a hammer. The crushed charcoal is screened and classified using 10- and 20-

mm sieves. Materials lower than 10 mm are considered fine for the purposes of this study. Each of the granulometries was stored separately.

The sample is randomly placed in the apparatus shown in Figure 19. The hydraulic system device was turned on and the scheduled force was applied to the charcoal bed through a die and plunger. The furnace was then turned on and heated, using a programmed PID controller. The heating cycle was: heating to 150 °C at 10 °C/min, heating from 150 °C to the experimental temperature at 300 °C, reside at the experimental temperature for the test and finally cool to room temperature. After compression, the apparatus and the sample were removed from the machine. Charcoal was recovered, weighed and classified.

The sample is weighed to control the amount of input and output material of the test and, subsequently, classified in sieves with openings of 8, 4 and 1.6 mm. The weight of different sizes is recorded, using an analytical scale to determine the granulometric distribution of charcoal after the test. The result is expressed as percentage of pieces that passed or not through sieves of different meshes.

Taking into account the procedures for the obtention of charcoal and compression temperatures, a total of 13 tests was conducted, using a column with 15 cm charcoal in each.

A support computer is provided with a program for which the experimental values are adjusted for each analysis and the acquired information is recorded. Data is collected in a spreadsheet with the respective values for time, applied force and displacement. The objective is to allow the modeling of cell transformation (deformation/pressure curve) at continuously increasing uniaxial deformation. The plasticity formalism applied to granular materials can be used.

Figure 19 Charcoal bed inside the confined compression test apparatus after one of the fracture tests. Some broken charcoals are visible in the steel tube.

3.4 Statistical analysis

The descriptive statistics, comparisons between means and analysis of covariance were performed using the R statistical software - version 3.1.3 (R DEVELOPMENT CORE TEAM - 2015). The parameters of each analysis are given in the corresponding Tables.

The comparison between averages was carried out by a nonparametric Wilcoxon test due to the low number of samples. The kernel density estimation method (KDE) was chosen to build the probability density function graphs. Analysis of covariance evaluated the influence of variables related to wood, carbonization process, direction of compression force and their interaction on the charcoal mechanical property.

The correlations between variables of physical and mechanical properties of wood and charcoal were estimated by Pearson coefficient (r). It was considered that two variables are associated with each other when the correlation coefficient was significant at 5% probability. However, only significant correlations considered high (greater than 0.65) were discussed in this research. The multivariate analyses of principal components (PCA) was performed in order to reduce the number of variables and identify those with the greatest contribution to the total variance contained in the original data and are uniquely defined by the eigenvectors of the correlation matrix of the original data (MANLY, 1986; WILKS, 2006).

In order to study the connections between the different qualitative variables of wood and charcoal taken together, varimax Rotated Principal Components Analysis (RPCA) was applied. When physical interpretation rather than data compression is the primary goal of PCA, it is often desirable to rotate a subset of the initial eigenvectors on the eigenvectors, which may lead to interpretation difficulties, especially for the second and subsequent PCs that

must be orthogonal to previously determined eigenvectors, regardless of the nature of the physical processes that have given rise to the data. A well known analytical algorithm to rotate the loadings is given by the varimax rotation method proposed by Kaiser (1985). The varimax method makes orthogonal rotation axes, keeping them mutually perpendicular in the principal component analysis, eigenvalue factors greater than one (1) were retained, as long as the accumulated variances explained more than 70% of the total variation.

PCA and RPCA were performed using the R statistical software version 3.1.3 (R DEVELOPMENT CORE TEAM - 2015).

4 RESULTS AND DISCUSSION

4.1 Growth traits

Diameters at 1.30 m height (or diameter at breast height – DBH), commercial (considered with a diameter minimum of 5 cm with bark) and total height, were measured after the trees were harvested. Table 5 shows the descriptive statistics of growth traits in a hybrid clone of *Eucalyptus urophylla* sample tree from a commercial energetic plantation established in Brazil.

Table 5 Descriptive statistics of growth traits for *E. urophylla*, including diameter at 1.3 meter height, commercial and total height (N=73).

Growth traits	Min	Max	Average	SD
Total height (m)	24.2	30.6	28.5	1.25
Commercial height (m)	15.1	22.3	19.7	1.32
Diameter at 1.30 m (cm) (DBH)	13.1	20.9	17.9	1.55

SD: standard deviation

The sample trees presented an average diameter of 17.9 cm at breast height, 28.5 meters of total height and 19.7 meters of commercial height. The growth traits of these trees were higher than those reported by Trugilho (2009), who evaluated 6-year-old *E. urophylla* from Avaré (Brazil), planted in a commercial spacing of 3 x 2 m, with an average diameter of approximately 10.8 cm at breast height, total height of about 15 meters and average commercial height of about 11.2 meters. Pereira et al. (2012) found average diameter levels of 15.15 cm at breast height and 23.3 meters of total height for two hybrid clones of *Eucalyptus urophylla* from a clonal test conducted with a spacing of 3.8 × 2.4 m, and the trees were harvested at the age of 7.5 years in Três Marias, Brazil.

E. urophylla trees from this clonal plantation presented a low variation range (CV %) in their growth traits: 4.4% for total height, 6.7% for commercial

height and 8.7% for diameter at breast height. This result was expected, since a clonal plantation has a low genetic variation, where the best offspring is vegetatively propagated and trees growing under optimal conditions produce biomass at high growth rates. The environment effect on the growth rate of the trees from the commercial plantation was not considered, since sample trees were collected in the same plot/site.

Figure 20 shows the histograms of absolute rate of sample trees for each diameter class, commercial height and total height. Absolute frequencies distributions of growth traits showed normal behavior.

Figure 20 Number of sample trees for each diameter class and relative frequencies for commercial and total height classes

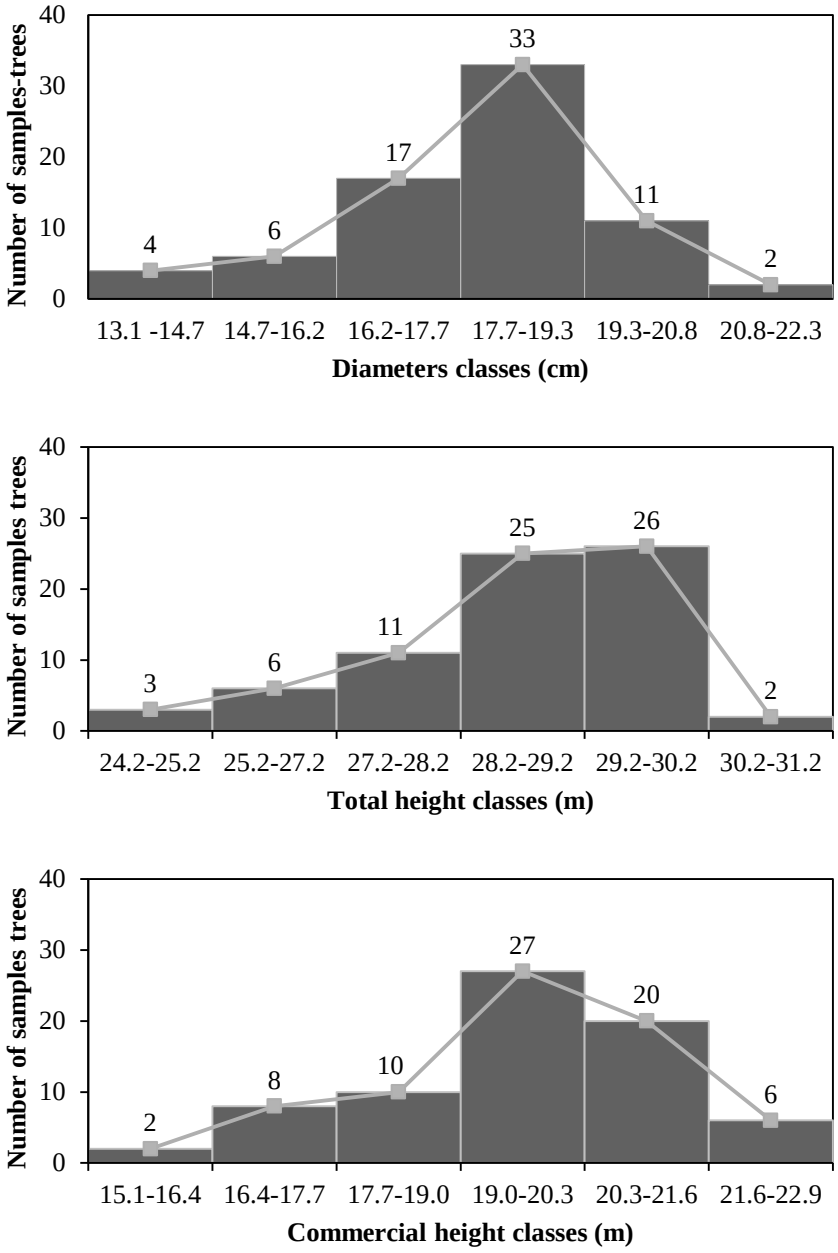

4.2 Influence of radial positions

4.2.1 Variation in wood properties according to radial position

From previous results obtained by the cited authors in theoretical reviews, it is known that charcoal density and compression strength are linked to wood density and rigidity. Furthermore, this link is a function of radial position and pyrolysis temperature. Therefore, a preliminary study was conducted in order to discover the influence of the radial position of the raw material and carbonization temperature on charcoal density and rigidity.

The sample population was divided into three groups in order to study the effect of radial position. For small diameters, only one cubic sample was cut in the middle of the radius. Density and longitudinal modulus of elasticity were measured on wood samples before and after pyrolysis, according to three radial positions and two final temperatures. The descriptive statistics of wood density and MOE according to radial position are summarized in Table 6.

Table 6 Descriptive statistics of wood density and MOE according to radial position.

Radial position	N	Wood density ($kg.m^{-3}$)				MOE (MPa)			
		Min	Max	Average	SD	Min.	Max.	Average	SD
Internal	22	473	610	518	40	8939	12546	10397	964
Middle	13	491	616	556	40	10347	17912	14315	2272
External	22	484	697	588	54	9765	17202	14116	1924

SD: standard deviation. N: Number of samples**.**

Figure 21 shows the associated probability density functions. Wood properties were found to be lower near the pith. Density values ranged from 473 $kg.m^{-3}$ near the pith to 697 $kg.m^{-3}$ near the bark, and from 8939 MPa to 17912 MPa for MOE. The variation density patterns were similar to those of MOE

(Figure 21). The 'middle' and 'external' curves were superimposed (average density of 556 kg.m^{-3} and 588 kg.m^{-3}, average MOE of 14315 MPa and 14116 MPa), and these curves were different from the 'internal' probability density function (average density of 518 kg.m^{-3}, average MOE of 10397 MPa). From this last observation, it was deduced that the sample population should be divided into two groups and not into three groups, prior to further analysis.

Figure 21 Probability density function of wood density and MOE according to radial position.

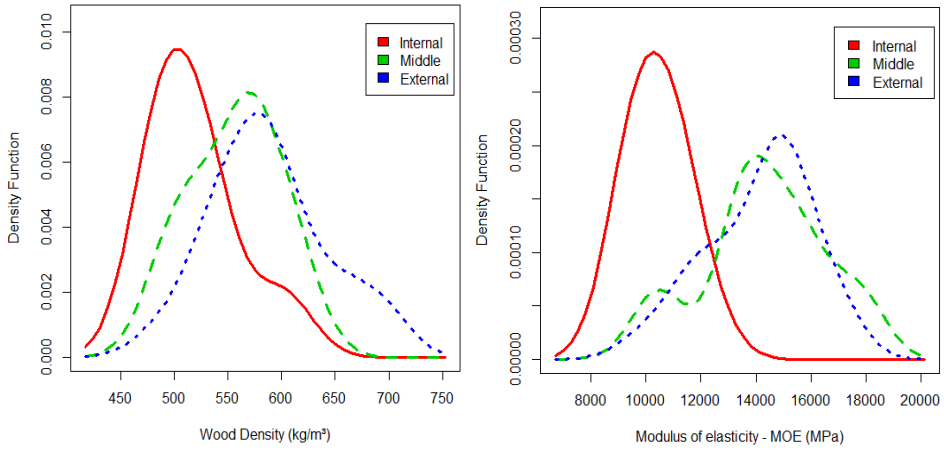

The probability distributions were tested using the Kolmogorov–Smirnov test, and the Wilcoxon test was used to compare means. These tests led to the same conclusion, and confirmed the existence of two groups, according to the radial positions. The Wilcoxon test results are presented in Table 7. The sample population was thus divided into two groups, identified as 'Internal' (N = 22) and 'Mid-Ext' (N = 35).

Table 7 Wilcoxon unpaired tests for wood density and MOE according to radial position.

Wood Properties	Wilcoxon *p* (bilateral)		
	Internal vs. Middle	Middle vs. External	Internal vs. External
Density (kg.m^{-3})	0.01*	0.12^{ns}	<0.001**
MOE (MPa)	<0.001**	0.84^{ns}	<0.001**

Significance levels: 0.0001 '***'; 0.001 '**'; 0.01 '*'; 0.05 '.'; Non-significant 'ns'.

The pertinence of the sampling location was a question during the study; this was solved by a statistical analysis, allowing to group locations with similar properties. Wood properties were lower near the pith. The radial variation observed for wood properties (density and MOE) was explained by the transition from juvenile to mature wood (BERDNT, 2002). One very important contributor to wood behavior is the effect of juvenile wood. Juvenile wood has physical and anatomical properties different from mature wood and transition wood (EVANS II; SENFT; GREEN, 2000). According to Trugilho et al. (2005), the radial variation may be determined primarily by the presence, ratio and physico-chemical characteristics of juvenile wood on the stem, where the juvenile area variation gradient decreases over time, influencing the final form of use of wood. According to Evans II, Senft and Green (2000), when measured outward from the pith, properties of juvenile wood make a gradual transition toward those of mature wood. The boundary of this zone, while dependent upon the property measured, occurs on the average at 5 to 20 rings from the pith (although there can be wide variations) (EVANS II; SENFT; GREEN, 2000). The age of transition from juvenile and adult wood of *E. grandis* could be identified through the radial variation of fibers and the microfibril angle, and took place between the 5th and the 11th year of growth (RAMOS et al., 2011).

Juvenile wood is characterized by a high cellulose microfibril angle in the S2 cell wall layer and a low density (short fibers with thin walls and low percentage of latewood in the annual rings). In hardwoods, the chemical composition shows little change from pith to bark, while softwoods have wood cores with lower cellulose and higher lignin contents. Juvenile wood in hardwoods occurs in a core and the characteristics for the most part make a gradual transition to some steady, mature state. There does not seem to be an exact demarcation where juvenile effects end and mature wood begins, but rather there is a property dependent on the transition zone (BENDTSEN, 1978; EVANS II; SENFT; GREEN, 2000).

Short rotation ages result in large proportions of juvenile wood. In large stems, old-growth timber, the proportion of juvenile wood is relatively small and its effects are confined to the material taken from the center of the tree (often largely contained within one piece). With large stems, one piece is a small portion of the total yield, and has little effect on the average behavior of the whole. With the advent of plantation-grown timber, and the increased harvesting of younger, smaller-diameter stems, the proportion of juvenile wood in the resource became greater (BRENDTSEN, 1978). *E. urophylla* showed a statistically significant difference for volumes, with and without bark, from the sixth to the seventh year of age. This fact indicates that *E. urophylla* is still booming at seven years of age (TRUGILHO, 2009).

Considering the radial position, the mechanical resistance increased from the pith to the bark (EVANS II; SENFT; GREEN, 2000). Strength can be reduced up to 50 percent by the presence of juvenile wood (EVANS II; SENFT; GREEN, 2000); here, 36% was the difference in the value of internal to the external MOE. The radial variation of mechanical properties and basic density of wood in *E. urophylla* clones at 5.5 years of age was determined by Cruz, Lima and Muniz (2003). Basic density and mechanical properties of the clones

increased from the pith outwards. The authors found values of 466 kg.m^{-3} in the inner radial position of the stem, 509 kg.m^{-3} in the intermediate position and 551 kg.m^{-3} in the position near the bark. On the other hand, for the modulus of elasticity at a compression parallel to the fibers (tests performed by static assays), the authors found values of 7176 MPa near the pith, 7535 MPa in the intermediate radial position and 8225 MPa in the external position of the stem.

4.2.2 Effect of radial position and carbonization temperature on charcoal properties

The descriptive statistics of charcoal density and MOE according to radial position and carbonization temperature are presented in Table 8. Wilcoxon tests were used to study the influence of the two factors (Table 9).

Table 8 Descriptive statistics of charcoal density and MOE according to radial position and carbonization temperature

Charcoal density (kg.m^{-3})										
Radial position	500°C					900°C				
	N	Min	Max	Average	SD	N	Min	Max	Average	SD
Internal	11	224	328	250	27.8	11	251	334	291	23.2
Mid-Ext	18	246	369	309	35.4	18	259	484	341	58.2
MOE charcoal (MPa)										
Radial position	500°C					900°C				
	N	Min	Max	Average	SD	N	Min	Max	Average	SD
Internal	11	985	1346	1052	100.5	11	2962	4237	3379	387.1
Mid-Ext	18	1089	1592	1372	137.3	18	2880	6153	4047	850.5

SD: standard deviation.

Radial position and carbonization temperature had significant effects on density and the elastic modulus. The MOE increased with the final pyrolysis temperature, from 1052 MPa to 3379 MPa for the internal position, and from 1372 MPa to 4047 MPa for the Mid-Ext position (charcoal was 3 times more rigid at 900 °C than at 500 °C). This effect was less pronounced for density, from 250 $kg.m^{-3}$ to 291 $kg.m^{-3}$ for the internal position, and from 309 $kg.m^{-3}$ to 341 $kg.m^{-3}$ for the Mid-Ext position (density was 1.13 times greater at 900 °C than at 500 °C). The difference between 309 $kg.m^{-3}$ and 341 $kg.m^{-3}$ was non-significant (p=0.106) with the Wilcoxon test (Table 9). The charcoal MOE and density were found to be higher for the Mid-Ext position than for the internal position. The relative difference between the radial positions was reduced to 900 °C. The density ratio (Mid-Ext/Internal) was 1.24 at 500 °C and 1.17 at 900 °C; the MOE ratio was 1.30 at 500 °C and 1.20 at 900°C (this observation was shown at Figure 22, the curves were overlapped at 900 °C). Thus, a high carbonization temperature seemed to soften the effect of radial position.

Trugilho, Lima and Mendes (1996) showed that juvenile wood produced a less resistant charcoal than mature wood. Couto et al. (2015) evaluated the effect of radial position and final carbonization temperature on the properties of charcoal from wood of *Eucalyptus urophylla* hybrid clones at seven years old. The pattern of radial variation of the apparent density of charcoal observed by Couto et al. (2015) is similar to that found in this study. The average apparent density of charcoal clones ranged from 276 $kg.m^{-3}$ to 389 $kg.m^{-3}$, from pith to bark.

Table 9 Wilcoxon unpaired tests for charcoal density and MOE according to radial position and carbonization temperature.

Charcoal properties	Combination of factors	Wilcoxon *p* (bilateral)
Density ($kg.m^{-3}$)	Internal and 500°C / 900°C	0.002*
	Mid-Ext and 500°C / 900°C	0.106^{ns}
	500°C and Internal / Mid-Ext	<0.001**
	900°C and Internal / Mid-Ext	0.016*
MOE char (MPa)	Internal and 500°C / 900°C	<0.001**
	Mid-Ext and 500°C / 900°C	<0.001**
	500°C and Internal / Mid-Ext	<0.001**
	900°C and Internal / Mid-Ext	0.016*

Significance levels: 0.0001 '***'; 0.001 '**'; 0.01 '*'; 0.05 '.'; Non-significant 'ns'

Figure 22 Probability density function of charcoal density and MOE according to radial position (Internal, Mid-Ext) and carbonization temperature (T500, T900).

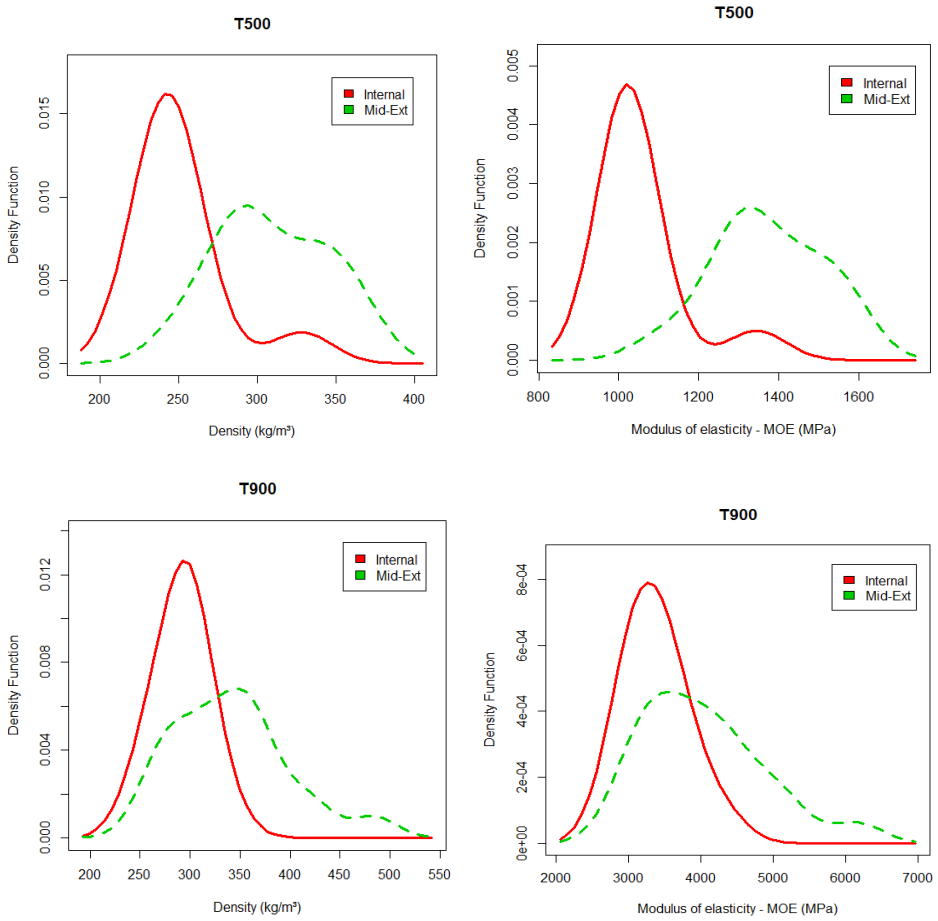

4.3 Description and link between wood and charcoal properties

4.3.1 Wood properties

Table 10 shows the statistical summary of the mechanical and physical properties of wood, including average, minimum (Min) and maximum (Max), as well as standard deviation (SD) values of the results.

Table 10 Descriptive statistics of 6-year-old *Eucalyptus urophylla* wood (N = 118).

	Min	Max	Average	SD
Apparent density (kg.m^{-3})	469	697	555	53
Basic density (kg.m^{-3})	372	533	428	33
MOE BING (MPa)	6873	22964	14152	3536
MOE US (MPa)	10776	24639	16306	3315
MOE US Long (MPa)	8939	19777	13079	2559
MOE US Rad (MPa)	673	3138	1552	413
MOE US Tang (MPa)	387	1786	793	237
G_{LR} (MPa)	546	1655	1011	166
G_{RT} (MPa)	109	1178	215	101
G_{TL} (MPa)	185	903	688	108
FSP (%)	24.6	44.7	34.4	2.7
Rd (%)	2.9	10.0	5.9	1.3
Tg (%)	4.0	12.3	9.3	1.7
Anisotropy coefficient (%)	0.5	2.5	1.7	0.4

Abbreviations: Flexural modulus of elasticity by BING = MOE BING, modulus of elasticity in compression by ultrasounds (US) = MOE US, modulus of elasticity in the cubes, in the longitudinal direction = MOE US Long, modulus of elasticity in compression in the cubes in the radial direction = MOE US Rad, modulus of elasticity in compression in the cubes in the tangential direction = MOE US Tang, shear modulus in three directions = G_{LR}, G_{RT} and G_{TL}, fiber saturation point = FSP, radial shrinkage = Rd, tangential shrinkage = Tg.

The patterns of these wood traits are in accordance with those reported in similar studies on *Eucalyptus* genus, i.e., in general, the shrinkage in the tangential direction is two times greater than the shrinkage in the radial direction (GLASS; ZELINKA, 2010). The high range patterns were found for properties, due to the difference between the studied radial positions (section 4.2.1). Wood samples shrinked 9.3% (tangentially) and 5.9% (radially) from the fiber saturation point condition to the oven-dried condition resulting in an anisotropy coefficient of 1.7. Hein, Silva and Brancheriau (2013) reported similar shrinkage anisotropy values for wood samples, of about 1.6% (7.8% tangentially and 4.8% radially), from 6-year-old *Eucalyptus grandis* x *Eucalyptus urophylla* trees. The difference between radial and tangential shrinkage is explained by a restraining influence of the wood rays in the radial direction in hardwoods (KOLLMANN; CÔTÉ, 1968). Donaldson (2008) stated that the microfibril angle (MFA) is one of the dominant parameters affecting shrinkage. As water bound to cellulose and hemicelloses moves out of the cell wall during timber drying, these molecules move closer to each other and the wall shrinks (BARNETT; BONHAM, 2004). As a result, cell walls with very low MFA tend to have greater tangential shrinkage, while cell walls with very high MFA tend to have greater longitudinal shrinkage (DONALDSON, 2008). The radial-tangential shrinkage ratio (anisotropy) is an important parameter to infer the dimensional stability of the wood. The lower the values of the anisotropies, the higher the stability inferred for the wood. In the case of wood carbonization, the lowest anisotropy coefficient value may result in fewer cracks during drying and consequently, in fewer cracks in charcoal, producing a more resistant charcoal (GALVÃO; JANKOWSKY, 1985).

Basic density is regarded as a reference quality index, since it affects wood properties and, consequently, those of its derivatives (PANSHIN; ZEEUW, 1980; PEREIRA et al., 2012). Among the physical characteristics of wood,

density has the greatest influence on the quality of charcoal (TRUGILHO; SILVA, 2001). Couto et al. (2015) evaluated the wood of two hybrid clones of seven-year-old *Eucalyptus urophylla*, and found mean values of basic density of 503 $kg.m^{-3}$ for clone VM04 and 471 $kg.m^{-3}$ for clone MN463. Castro et al. (2013), studying clones of 7-year-old *E. urophylla*, reported woods with an average basic density of 557 $kg.m^{-3}$. In this study, the average basic density was 428 $kg.m^{-3}$ ranging from 372 $kg.m^{-3}$ to 533 $kg.m^{-3}$, with a coefficient of variation of 7.7%.

Dynamic elastic modulus on flexural vibration test by BING® and dynamic elastic modulus on longitudinal test by ultrasound on specimens measuring 30 mm x 30 mm x 200 mm ranged from 6873 MPa to 22964 MPa and from 10776 MPa to 24639 MPa, respectively. The average value of MOE US (16306 MPa) was higher than MOE BING (14152 MPa). The average value of MOE US (16306 MPa) was higher than MOE US Long (13079 MPa). Longitudinal vibration is affected by the Poisson effect when the length to thickness ratio of the beams is small (RAYLEIGH, 1877), coupled to the viscoelastic effect (more pronounced at high frequencies in the case of longitudinal vibration) (HAINES; LEBAN; HERBE, 1996). The length to thickness ratios of the beams and cube specimens were 6.7 and 1, respectively.

Modulus of elasticity values in all three planes have respective averages of 13079 MPa (8939-19777 MPa) in longitudinal; 1552 MPa (673-3138 MPa) in radial; and 793 MPa (387-1786 MPa) in tangential. Values for strength and stiffness along the grain versus across the grain may vary by a factor of 20 or even more. In addition, transverse properties radially and tangentially also differ (ZINK-SHARP, 2009). All modulus obtained are neighbors of the tendencies of the longitudinal (12700 MPa), radial (1710 MPa) and tangential (1020 MPa) modulus according to the apparent density (581 $kg.m^{-3}$) (adjustments for hardwoods) (GUITARD, 1987). Gonçalves, Trinca and Pellis (2014) presented the results of six elastic constants of wood

- three modulus of elasticity (E_L, E_R, and E_T) and three shear modulus (G_{LR}, G_{LT}, and G_{RT}), of *Eucalyptus saligna* using ultrasound tests. They found E_L = 14538 MPa, E_R = 3568 MPa, E_T = 2034 MPa, G_{LR} = 2115 MPa, G_{LT} = 1149 MPa and G_{RT} = 848 MPa. The values obtained in this study (Table 10) were much lower than these ones found by Gonçalves, Trinca and Pellis (2014).

Shear modulus values in all three planes have respective averages of 215 MPa (109-1178 MPa) in RT; 688 MPa (185-903 MPa) in TL; and 1011 MPa (546-1655 MPa) in LR. According to Guitard (1987), for model hardwoods (average density of the tested samples of 556 $kg.m^{-3}$), values close to 178 MPa at RT, 577 MPa TL and 749 MPa at LR, are expected. Hein et al. (2012), studied hybrid clones of *Eucalyptus grandis* x *urophylla* (average density of 518 $kg.m^{-3}$), and found a value of 694 MPa in LR. The values obtained in this study (Table 10) were consistent with the expected values for wood ($G_{LR} > G_{TL} > G_{RT}$) and are of the same order of magnitude as those obtained in the literature, except for the LR plane, where the average value is higher. The ratios of anisotropy between modules (G LR/TL = 1.5; G LR/RT = 4.9), however, remain consistent, with the same order of magnitude as those deduced from hardwood (G LR/TL = 1.3; G LR/RT = 4.2). Astley, Stol and Harrington (1998), during the study of the elastic properties of coniferous wood, showed that the values of G_{RL} and G_{TL} are highly influenced by the orientation of the angles of the microfibrils. This observation must be verified in the particular case of this study.

Table 11 presents the statistical summary of the bivariate correlation matrix, based on 14 characteristic parameters. The analysis showed correlations of high magnitude between them. A principal component analysis was then performed. This analysis resulted in a new set of parameters (principal components).

Table 11 Simple correlation of mechanical and physical properties of *Eucalyptus* wood (N = 118)

	ρ12 (kg.m^{-3})	MOE BING (MPa)	MOE US (MPa)	MOE US Long (MPa)	MOE US Rad (MPa)	MOE US Tang (MPa)	GLR (MPa)	GRT (MPa)	GTL (MPa)	D (kg.m^{-3})	FSP (%)	Rd (%)	Tg (%)
MOE BING (MPa)	0.58												
MOE US (MPa)	**0.78**[(1)]	**0.83**											
MOE US Long (MPa)	**0.73**	**0.80**	**0.88**										
MOE US Rad (MPa)	0.16	-0.37	-0.24	-0.30									
MOE US Tang (MPa)	-0.07	-0.54	-0.42	-0.43	0.43								
G_{LR} (MPa)	0.29	-0.33	-0.16	-0.31	**0.66**	0.41							
G_{RT} (MPa)	0.20	-0.03	0.05	0.01	0.16	0.27	0.24						
G_{TL} (MPa)	0.16	-0.14	-0.02	-0.17	0.01	0.43	0.34	0.26					
D (kg.m^{-3})	**0.90**	0.48	**0.65**	0.59	0.28	0.13	0.33	0.25	0.20				
FSP (%)	0.17	0.33	0.26	0.22	-0.39	-0.40	-0.13	-0.05	0.13	0.03			
Rd (%)	0.24	0.45	0.42	0.49	-0.60	-0.15	-0.42	0.08	0.14	0.23	0.40		
Tg (%)	**0.65**	**0.73**	**0.75**	**0.69**	-0.13	-0.60	-0.07	-0.06	-0.14	0.47	0.44	0.11	
Anisot	0.15	0.01	0.05	-0.04	0.50	-0.23	0.34	-0.11	-0.24	0.07	-0.10	**-0.80**	0.46

[(1)] Values in bold refer to significant correlations (minimum value considered 0.65).

Basic density was correlated significantly and positively only with apparent density and MOE US in the bars. In addition, apparent density showed a positive and significant correlation with the MOE BING, MOE US Long and tangential shrinkage. Similar correlations occurred between the MOE BING and the same characteristics (MOE US, MOE US Long and tangential contraction). According to Record (1914), density is one of the major factors affecting the mechanical properties of wood and, in particular, seems to be directly correlated with strength. In general, density is most likely the best single predictor of mechanical properties of clear, straight-grained defect-free wood (ZINK-SHARP, 2009). Ilic (2001) tested small samples of *Eucalyptus delegatensis* R. Baker and found good correlations between basic density and longitudinal (r = 0.83) dynamic elastic modulus. Hein, Silva and Brancheriau (2013) also reported a positive and significant correlation between dynamic modulus of elasticity values, obtained by longitudinal and flexural vibration tests (r = 0.97) for *Eucalyptus urophylla* × *E. grandis* trees (6-year-old) from clonal tests established in Brazil.

Tangential shrinkage was the characteristic that most correlated with the mechanical strength parameters of wood MOE BING, MOE US and MOE US Long. According to their results, mechanical properties increase as tangential shrinkage increased. It is well known that the arrangement of cellulose microfibrils in the S2 layer of the cell walls and cell wall thickness play a major role in determining the mechanical performance and shrinkage anisotropy of wood (HEIN; SILVA; BRANCHERIAU, 2013; KOLMANN; CÓTÊ, 1968; SALMÉN; BURGERT, 2009; WU et al., 2006). MFA, in combination with basic density, shows a strong relationship with modulus of elasticity and shrinkage behavior (DONALDSON, 2008; EVANS; ILIC, 2001; YANG; EVANS, 2003). Hein, Silva and Brancheriau (2013) reported negative relationships between MFA and tangential shrinkage (r = -0.33) and between

MFA and modulus of elasticity (r = -0.61) in 6-year-old *Eucalyptus urophylla* × *E. grandis* wood samples. The relationship between variation in wood tangential shrinkage and cellulose crystallite width was determined by Washusen and Evans (2001) in 11-year-old *Eucalyptus globulus*. According to their results, cellulose crystallite width was closely associated with tangential shrinkage; shrinkage increases as crystallite width increased. Consequently, the mechanical properties also will be higher. Between the radial contraction and the anisotropy coefficient, there was a significant correlation, but negative (-0.80).

These 14 components were used for the PCA analysis. Four principal components explained 83% of total variance (Table 12).

Table 12 Total variance explained by PCA on PC1, PC2, PC3 and PC4 (N = 118)

Component	Eigenvalues	% Variance	% Cumulative variance
1	5.2	37	37
2	3.0	22	59
3	2.3	16	75
4	1.1	8	83

A plot of the data in the space of the first two principal components, with the name of the corresponding parameter, can be produced, as shown in Figure 22. The PCA horizontal axis of the two first components explained 37% of the total variance, while the vertical axis, a further 22% (Figure 23). The PCA horizontal axis of the third and fourth components explained 16% of the total variance, while the vertical axis, a further 8% (Figure 23). It is observed that the first three principal components explained almost all the initial information, approximately 75% of the total variance.

Figure 23 Biplot of the (scaled) first two principal components (a) and the third and fourth principal components.

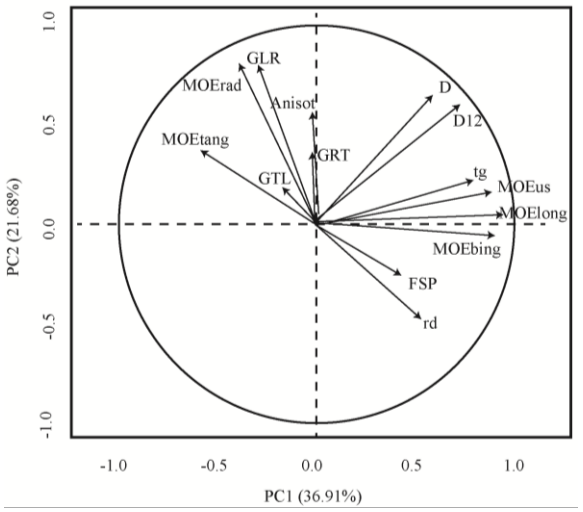

(a)

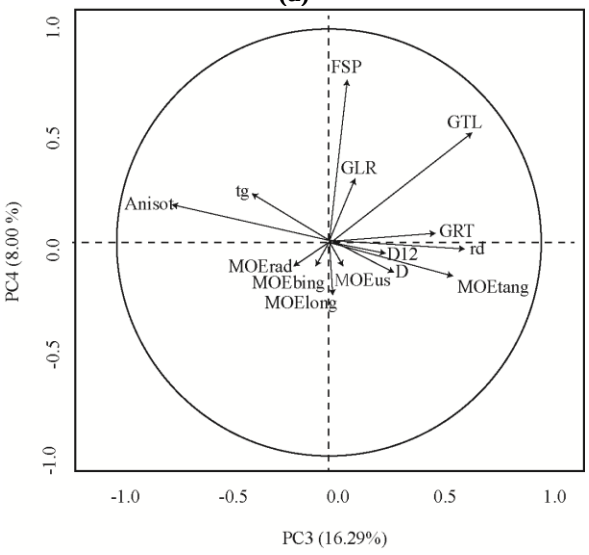

(b)

For the abbreviation of the parameters: D: Basic density, MOEbing: Modulus of elasticity in flexure by BING; MOEus: Modulus of elasticity in compression by ultrasounds (US); MOElong: Modulus of elasticity in the cubes, in the longitudinal direction; MOErad: Modulus of elasticity in compression in the cubes in the radial direction; MOEtang: Modulus of elasticity in compression in the cubes in the tangential direction; GLR, GRT and GTL: shear modulus in three directions; FSP: fiber saturation point; rd: radial shrinkage; tg: tangential shrinkage.

The multivariate statistical analysis of principal components of wood properties enables to establish, in general, which ones are best correlated with the dependent variables, identifying their order of importance. Thus, there is a wide variation among the studied physical properties of wood, corroborating the literature.

The first principal component (PC1) has the largest positive eigenvalues for apparent relative density, MOE BING, MOE US bars, MOE US Long cubes, basic density and Tg. For the second principal component (PC2), the characteristics with a higher correlation were MOE US rad and Anisot, which were the characteristics that showed the highest positive eigenvectors, and Rd, which had a negative eigenvector. On the other hand, the MOE US tang, G_{LR}, G_{TL} and G_{RT} had negative eigenvalues and the highest correlation with the third latent variable (PC3). The largest eigenvector of the fourth principal component is associated with FPS (PC4) (Table 13), a variable mainly related to the chemical composition of wood.

Normalized eigenvectors of the first four principal components obtained from the wood correlation matrix are shown in Table 13.

Table 13 Normalized eigenvectors of the first four principal components of physical and mechanical parameters of *Eucalyptus* hybrid clone wood.

	PC1	PC2	PC3	PC4
ρ12 (kg.m^{-3})	**0.85**	0.15	-0.38	-0.30
MOE BING (MPa)	**0.88**	-0.23	0.28	-0.42
MOE US (MPa)	**0.95**	-0.14	0.07	-0.39
MOE US Long (MPa)	**0.93**	-0.24	0.17	-0.28
MOE US Rad (MPa)	-0.18	**0.78**	-0.52	0.41
MOE US Tang (MPa)	-0.45	0.06	**-0.76**	0.46
G_{LR} (MPa)	-0.14	0.63	**-0.69**	0.00
G_{RT} (MPa)	0.06	-0.03	**-0.56**	0.01
G_{TL} (MPa)	-0.11	-0.15	**-0.66**	-0.36
ρ (kg.m^{-3})	**0.74**	0.14	-0.53	-0.13
FPS (%)	0.29	-0.27	0.21	**-0.91**
Rd (%)	0.42	**-0.87**	0.01	-0.35
Tg (%)	**0.82**	0.20	0.27	-0.59
Anisot	0.10	**0.90**	0.16	-0.01

4.3.2 Charcoal properties

Table 14 presents the descriptive statistics of the measured physical mechanical parameters in charcoal produced at 500 °C and 900 °C.

Table 14 Descriptive statistics of the parameters measured in charcoal carbonized at 500°C and 900°C (N = 58)

Charcoal characteristics	500°C				900°C			
	Min	Max	Average	SD	Min	Max	Average	SD
Ychar (%)	32.4	36.9	34.2	1.3	26.8	29.0	27.9	0.6
Dchar ($kg.m^{-3}$)	224	369	287	43	251	484	322	54
MOE long char (MPa)	985	1592	1247	199	2880	6153	3794	775
MOE rad char (MPa)	289	823	557	128	787	2873	1720	429
MOE tang char (MPa)	222	475	307	55	500	1629	992	236
G_{LR} char (MPa)	716	1342	1006	175	2068	3995	2769	509
G_{RT} char (MPa)	121	663	428	136	631	1967	1173	266
G_{TL} char (MPa)	117	437	255	66	499	1226	762	178

Abbreviations: Ychar: Gravimetric yield in charcoal; Dchar: Charcoal density; MOE long char: Modulus of elasticity in the longitudinal; MOE rad char: Modulus of elasticity in the radial direction; MOE tang char: Modulus of elasticity in the tangential direction; G_{LR} char: Shear modulus in the longitudinal-radial; G_{RT} char: Shear modulus in the radial-tangential direction; G_{TL} char: Shear modulus in the tangential-longitudinal direction.

The charcoal yield decreased with the increase in carbonization temperature from 500 °C to 900 °C. The charcoal yield gradually decreased with the removal of moisture and volatile compounds (CO, CO2, non-cyclic hydrocarbons, etc.), enabling the dry particles to flow more easily and to pack together more closely, as the carbonization temperature was increased (KWON et al., 2014). At temperatures above 375 °C, lignin is the key component of charcoal formation. The majority of carbohydrate polymers degraded between 300-375 °C and products from lignin conversion remain. Lignin has the highest heat of combustion, the highest charcoal

yield and also the lowest percentage of volatiles. Lignin starts to decompose at about 200 °C, but is much more stable to thermal decomposition, when compared to carbohydrate polymers (BEALL, 1972; KWON et al., 2014; SHAFIZADEH; McGINNIS, 1971). Lignin is known to increase charcoal yield due to the aromatic lignin structure being similar to graphite (ANTAL; GRØNLI, 2003). The charcoal yield decreases significantly with increase in carbonization temperatures up to 800 °C followed by a slight decrease with a further rise in temperature up to 1000 °C (KUMAR; GUPTA; SHARMA, 1992). Carbon and ash contents increase with an increase in carbonization temperature whereas volatile matter and hydrogen contents decrease (KUMAR; GUPTA; SHARMA, 1992). The *Eucalyptus* resin is expected to contribute to the charcoal yield through carbon deposition (KUMAR; GUPTA; SHARMA, 1992).

Charcoal density increased with the increase in pyrolysis temperature. These results agreed with a range of other pyrolysis studies (BLANKENHORN et al., 1978; KUMAR; VERMA; GUPTA, 1999; OLIVEIRA; GOMES; ALMEIDA, 1982). The increase in density could be due to restructuring and shrinkage of the carbon structure. Kumar and Gupta (1993) state that, at lower carbonization temperatures (up to about 500~600 °C), the loss of volatiles predominates and results in an overall opening of the structure, that is, a decrease in apparent density. However, as temperature is increased above 600 °C, condensation of carbon microcrystallites (constituted by graphitic planes in a roughly parallel arrangement) and pyrolytic carbon deposition (resulting from the cracking of hydrocarbons) take place in the pores, and enrichment of the remaining wood charcoal matrix with aromatic compounds, leading to an increase in apparent density. The true density of charcoal also increases with pyrolysis temperature, especially at temperatures higher than 450 °C (KUMAR; GUPTA, 1993; SOMERVILLE; JAHANSHAHI, 2015). True density refers to the solid carbon structure, i.e. the pore walls of charcoal particles, while apparent density includes both the solid structure and the pores within charcoal. This increase in true density is likely

to be due to restructuring of the graphitic structure at high temperatures (SOMERVILLE; JAHANSHAHI, 2015).

A variation of 372-533 $kg.m^{-3}$ in basic wood density resulted in a change of 224-369 $kg.m^{-3}$ in apparent relative density of charcoal produced at 500°C, and 251-484 $kg.m^{-3}$ in charcoal produced at 900 °C. The density of charcoal is an important control property, in order to minimize transport and handling costs, as well as to control charcoal reactivity and strength. The apparent density of charcoal for chemical characteristics ideal in high-steel furnaces can range between 220 and 270 $kg.m^{-3}$ (RAAD; MELO, 2014). For the operation of the blast furnace, a higher charcoal density indicates a higher load inside the furnace, larger load residence time within the furnace, resulting in the reduction of the specific consumption per ton of pig iron.

The values of the charcoal MOE were higher at 900 °C than at 500 °C, implying that charcoal strength increased as the carbonization temperature was increased. This result is also supported by previous studies (KUMAR; VERMA; GUPTA, 1999; MOORE et al., 1974). From a study on the mechanical properties of charcoal based on *Eucalyptus* and *Acacia* woods in relation to the carbonization temperature, Kumar, Verma and Gupta (1999) stated that the strength of charcoal decreased as the temperature was increased up to 600 °C, due to breaks in the C-H bond and to the loss of volatile compounds, and then increased in the range of 800-1200 °C, due to the decreased porosity resulting from the condensation of microcrystallites and the precipitation of pyrolytic carbon (KUMAR; VERMA; GUPTA, 1999).

SEM studies of *Acacia* and *Eucalyptus* wood charcoal, prepared under different carbonization conditions, were conducted to provide information on what happens in the transformation of wood to charcoal. The material is normally lost, as volatiles totally contribute to the formation of pores, cracks and pyrolytic carbon (KUMAR; GUPTA, 1995). Both woods exhibited similar devolatilization behavior in pore structure development, showing a decrease in pore size with an increase in

carbonization temperature. Carbonization resulted in pyrolytic carbon deposition in the resultant wood charcoal structures and caused sintering of the adjacent fibers, resulting in the formation of compacted mass (KUMAR; GUPTA, 1995). Due to the evolution of volatile matter during carbonization of wood, pitting of the vessel surface occurs which leads to the development of pores all along the walls of the vessels (KUMAR; GUPTA, 1995). Pores will always exist, since mass loss occurs without the occurrence of a contraction proportional to this loss. Carbonization treatment at different temperatures generates materials with different micropore size distributions (KWON et al., 2014). The porosity of charcoal increased linearly with pyrolysis temperature (KUMAR; GUPTA, 1993; SOMERVILLE; JAHANSHAHI, 2015). It was also found that the porosity values of slowly carbonized wood samples are lower than those of rapidly carbonized wood samples, that is, due to less carbon deposition together with cracks and void formation in rapidly carbonized samples (KUMAR; GUPTA, 1993).

Density is linked to porosity. The porosity of charcoal is closely associated with wood porosity, temperature of carbonization and the speed of carbonization (BLANKENHORN et al., 1978, OLIVEIRA; GOMES; ALMEIDA, 1982). Blankenhorn et al. (1978) indicated that, for *Prunus serotina* Ehrh., porosity increased with the increase in temperature of up to 600 °C and then decreased with temperatures of up to 900 °C. Thus, density decreased until 600 °C, and increased with the increase in temperature until 900 °C due to the occurrence of lower weight loss in relation to shrinkage. Rigidity is linked to density (amount of matter per unit of area) and to the rigidity of matter.

Kwon et al. (2014) examined the anatomy, physics and mechanics of charcoals generated from White Lauan (*Pentacmecontorta*) and Punah (*Tetrameristaglabra*) by using different carbonization temperatures and heating rates. The strength of the charcoals was found to depend on the applied process conditions and was affected predominantly by the process temperature. The samples heat-treated

at 1200 °C showed a higher strength ratio, compared with those heat-treated at 600 °C (KWON et al., 2014). This is partially explained by an unforced increase in the density of the samples during the high temperature treatment. The elastic coefficient did not show any dependence on heating rate (KWON et al., 2014).

Moutinho (2013) carbonized clones of *Eucalyptus* and *Corymbia*, 5 and 6 years-old, in a muffle furnace with a final temperature of 400 °C. The modulus of compression parallel to the fibers was on average 490 MPa; the gravimetric yield in charcoal was 52.2%; the apparent density of the charcoal was 360 $kg.m^{-3}$. Vieira (2009) observed that the acoustic modulus of elasticity of charcoal from *Eucalyptus* sp. increased with the increase of the carbonization temperature from 350 to 900 °C. He studied with two clones of *Eucalyptus* carbonized at 350 °C, 450 °C, 550 °C and 900 °C and found values respectively, of 459 MPa, 519 MPa, 671 MPa and 1027 MPa for dynamic modulus of elasticity to compression parallel to the fibers (VIEIRA, 2009).

In addition to MOE charcoal, the shear modulus can be taken as an indication of breakage/abrasion resistance of the material. The variation in the shear modulus of *Eucalyptus* wood charcoals clearly indicates that their change with carbonization temperature follows the same trend as that for MOE charcoal. The dynamic modulus and shear modulus of charcoal made at 900 °C are higher than those prepared at 500 °C, presumably due to the higher pyrolytic carbon deposition (KUMAR; GUPTA, 1997), higher apparent density (more compact nature) (KUMAR; GUPTA, 1993) and higher cell wall hardness in *Eucalyptus* charcoal (structural rearrangement of carbon). The higher pyrolytic carbon deposition, occurring as a result of cracking of hydrocarbons, in the charcoal matrix decreases its porosity (KUMAR; GUPTA, 1993) and increases the cell wall thickness/hardness, as sintering of the adjacent fibers resulting in the formation of compacted masses (KUMAR; GUPTA, 1995; KUMAR; VERMA; GUPTA, 1999). The apparent density, porosity, extent of cleavage of C-H bonds, condensation of

carbon microcrystallites, pyrolytic carbon deposition, and hardness of cell walls, play important roles in determining the mechanical strength of charcoal (KUMAR; VERMA; GUPTA, 1999).

It is also evident from Table 14 that the MOE charcoal increases with the decrease in yield, a behavior similar to that found by Kumar, Verma and Gupta (1999) for *Eucalyptus* and *Acacia* charcoal in the range between 270 and 1200°C.

Table 15 shows the correlation coefficients between the original variables of the characteristics of charcoal produced at 500 °C. This table shows that the majority of mechanical parameters were correlated with charcoal density: MOE US long char (r = 0.90), MOE US rad char (r = 0.78), G_{LR} char (r = 0.90) and G_{RT} char (r = 0.65).

Table 15 Simple Correlation of physical and mechanical properties of charcoal produced at 500°C (N = 29)

	Ychar (%)	Dchar ($kg.m^{-3}$)	MOE long char (MPa)	MOE rad char (MPa)	MOE tang char (MPa)	G_{LR} char (MPa)	G_{RT} char (MPa)
Dchar ($kg.m^{-3}$)	-0.55						
MOE long char (MPa)	-0.63	**0.90**(1)					
MOE rad char (MPa)	-0.30	**0.78**	**0.69**				
MOE tang char (MPa)	0.01	0.29	0.21	-0.09			
G_{LR} char (MPa)	-0.52	**0.90**	**0.85**	**0.72**	0.22		
G_{RT} char (MPa)	-0.38	**0.65**	0.62	**0.83**	-0.06	0.60	
G_{TL}char (MPa)	0.37	0.08	0.00	-0.22	**0.80**	0.01	-0.40

(1) Values in bold refer to significant correlations (minimum value considered 0.65)

These physical and mechanical characteristics of charcoal were subjected to a principal component analysis (PCA). Two principal components

explain 80% of the variability contained in the original eight parameters. In Table 17, it is possible to observe the values of the principal components.

Table 16 Variance explained by PCA on PC1 and PC2 for the characteristics of charcoal at 500 °C (N = 29).

Component	Eigenvalues	% Variance	% Cumulative variance
1	4.4	55	55
2	2.0	25	80

Table 17 Normalized eigenvectors of the first two principal components of the physical and mechanical parameters of charcoal produced at 500 °C.

	PC1	PC2
Ychar (%)	**-0.64**	-0.22
Dchar (kg.m^{-3})	**0.95**	-0.19
MOE long char (MPa)	**0.92**	-0.11
MOE rad char (MPa)	**0.85**	0.20
MOE tang char (MPa)	0.14	**-0.92**
G_{LR} char (MPa)	**0.91**	-0.13
G_{RT} char (MPa)	**0.80**	0.32
G_{TL} char (MPa)	-0.14	**-0.96**

The PCA horizontal axis explained 55% of the total variance, while the vertical axis, a further 25% (Figure 24).

Figure 24 Ordination diagram of eigenvectors of the two principal components obtained for charcoal parameters at 500 °C.

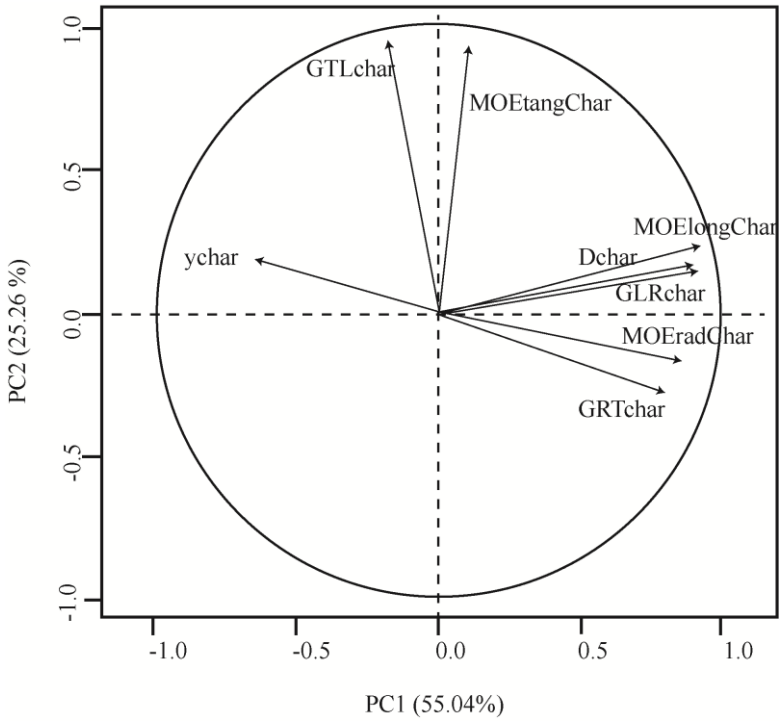

Where: ychar = gravimetric yield in charcoal; Dchar = charcoal density; MOE long char = modulus of elasticity in the longitudinal direction; MOE rad char = modulus of elasticity in the radial direction; MOE tang char = modulus of elasticity in the tangential direction; G_{TL}char = shear modulus in the tangential-longitudinal direction; G_{LR}char = shear modulus in the longitudinal-radial direction; G_{RT}char = shear modulus in the radial-tangential direction.

The analysis indicates that the mechanical and physical variability of charcoal produced at 500 °C is explained for two components. This indicates a high correlation between variables, whereas the PCA meets, in decreasing and excluding order, the characteristics common to all treatments, inferring that the correlations are explained by a maximum of two components. Moutinho (2013) found strong correlations in charcoal produced at 400 °C between its modulus of elasticity, resistance to

compression parallel to the charcoal fibers, apparent density, gravimetric charcoal yield and the radial linear degradation by PCA analysis.

Table 18 presents the simple correlations between the original variables of characteristics of charcoal produced at 900 °C. This Table shows that correlations between the characteristics of charcoal produced at 900 °C showed a low magnitude. Significant positive correlations occurred between charcoal density and MOE parameters: MOE US long char (r = 0.96) and MOE US rad char (r = 0.86).

The MOE long char at 900 °C was positively correlated with the MOE rad char (0.81). Positive correlations were also found between the G_{RT} char and MOE rad char (0.72) and G_{LR} char (0.67).

Table 18 Simple correlation of mechanical and physical properties of charcoal produced at 900 °C (N = 29).

	Ychar (%)	Dchar ($kg.m^{-3}$)	MOE long char (MPa)	MOE rad char (MPa)	MOE tang char (MPa)	G_{LR} char (MPa)	G_{RT} char (MPa)
Dchar ($kg.m^{-3}$)	-0.30						
MOE US long char (MPa)	-0.42	**0.96**[(1)]					
MOE US rad char (MPa)	-0.01	**0.83**	**0.81**				
MOE US tang char (MPa)	0.14	0.26	0.28	0.25			
G_{LR} char (MPa)	0.20	0.25	0.17	0.24	0.03		
G_{RT} char (MPa)	0.13	0.54	0.51	**0.72**	0.16	**0.67**	
G_{TL} char (MPa)	0.00	-0.03	-0.01	-0.11	0.62	0.34	0.11

[(1)] Values in bold refer to significant correlations (minimum value considered 0.65)

To evaluate the correlation between charcoal characteristics at 900°C, all the mean values were subjected to PCA. Three principal components explain 82.8% of the total variance (PC1 43.8%; PC2 22%; PC3 17%) (Table 19). Graphical representations of normalized vectors of the PCA are found in Figure 25. In Table 20, it is possible to observe the values of the principal components.

Table 19 Total variance explained by PCA on PC1, PC2 and PC3 (N = 29)

Component	Eigenvalues	% Variance	% Cumulative variance
1	3.5	44	44
2	1.8	22	66
3	1.4	17	83

Table 20 Normalized eigenvectors of the three principal components of physical and mechanical parameters of charcoal produced at 900 °C.

	PC1	PC2	PC3
Ychar (%)	0.37	-0.04	**-0.58**
Dchar ($kg.m^{-3}$)	**-0.96**	-0.13	-0.23
MOE long char (MPa)	**-0.97**	-0.15	-0.13
MOE rad char (MPa)	**-0.89**	-0.05	-0.45
MOE tang char (MPa)	-0.25	**-0.88**	-0.14
G_{LR} char (MPa)	-0.25	-0.23	**-0.84**
G_{RT} char (MPa)	-0.64	-0.13	**-0.82**
G_{TL} char (MPa)	0.04	**-0.92**	-0.21

Figure 25 Ordination diagram of eigenvectors of the two firsts principal components (a) and of the first and the third principal components (b) obtained for charcoal parameters at 900 °C.

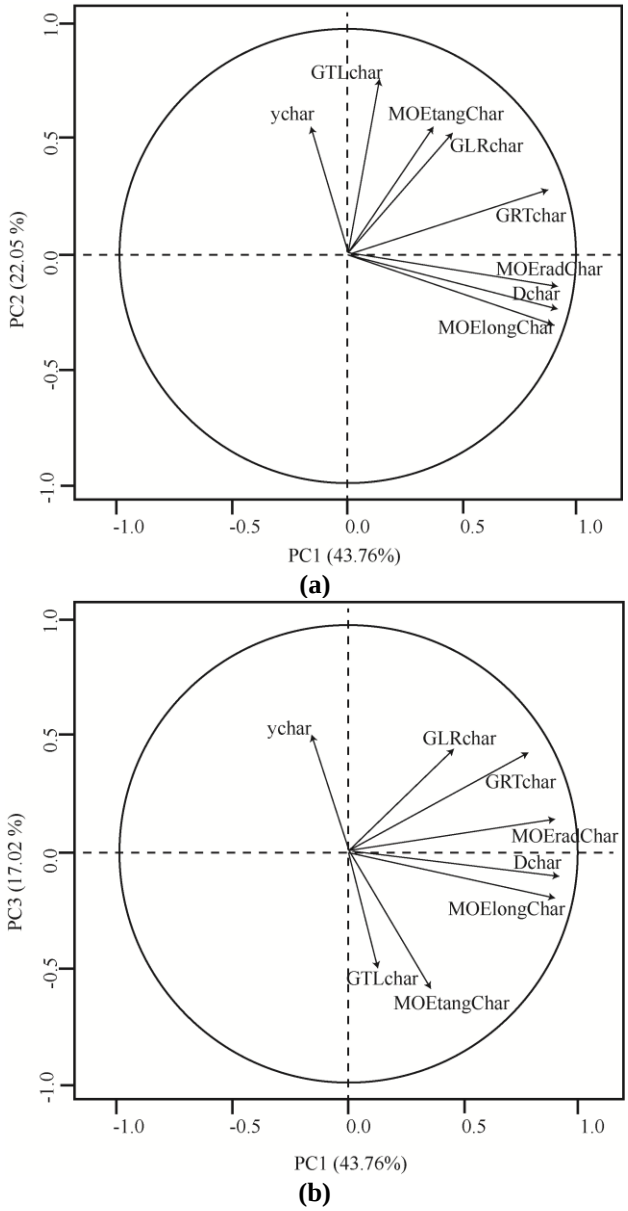

Where: ychar = gravimetric yield in charcoal; Dchar = charcoal density; MOE long char = modulus of elasticity in the longitudinal direction, MOE rad char = modulus of elasticity in the radial direction; MOE tang char = modulus of elasticity in the tangential direction; G_{TL}char = shear modulus in the tangential-longitudinal direction; G_{LR}char = shear modulus in the longitudinal-radial direction; G_{RT}char = shear modulus in the radial-tangential direction.

Charcoal at 500 °C and charcoal at 900 °C presented a different proportion of variance for PCA, with the first two principal components accounting for a large portion of data variance for charcoal at 500 °C parameters, and three first principal components accounting for a large portion of the data variance for charcoal at 900 °C parameters. Together, these two and three PCs accounted for a cumulative variance of 80% and 83% for charcoal made at 500 °C and charcoal made at 900 °C, respectively. The patterns formed by the loadings are of importance. The first principal components of both display a modulus of elasticity and charcoal density pattern. The second principal components presented a very similar spatial pattern for both charcoal made at 500 °C and charcoal made at 900 °C, with mechanical strength at the tangential direction of charcoal. The third principal component of charcoal at 900 °C accounted for 17% of total variance. The spatial pattern observed in PC3 for charcoal made at 900 °C seemed to be a better match with PC1 for charcoal made at 500 °C.

The relationships between parameters strongly correlated both in charcoals produced at 500 °C and those produced at 900 °C are presented in Figures 26, 27, 28 and 29: density of charcoal x MOE longitudinal charcoal; density of charcoal x MOE radial charcoal; MOE longitudinal charcoal x MOE radial charcoal; G_{RT} x MOE rad charcoal. The linear tendencies were clearly visible for the relations. The Figures 26, 27, 28 and 29 also show the corresponding diagrams of dispersion. Residual distributions are close to normal, being possible to distinguish two distinct points clouds relating to the results of the analysis of 500 °C and 900 °C.

Figure 26 Relationship between apparent density and charcoal MOE in the longitudinal direction according to carbonization temperature (R^2 = 0.81 for 500 °C; R^2 = 0.92 for 900 °C). N = 58.

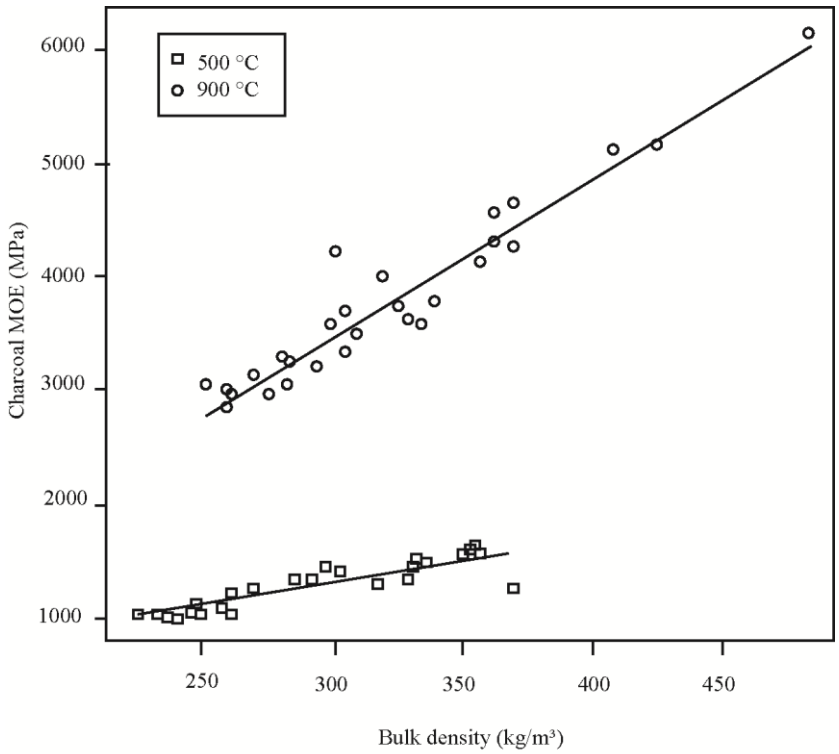

Figure 27 Relationship between apparent density and charcoal MOE in the radial direction according to carbonization temperature (R^2 = 0.60 for 500 °C; R^2 = 0.69 for 900 °C). N = 58

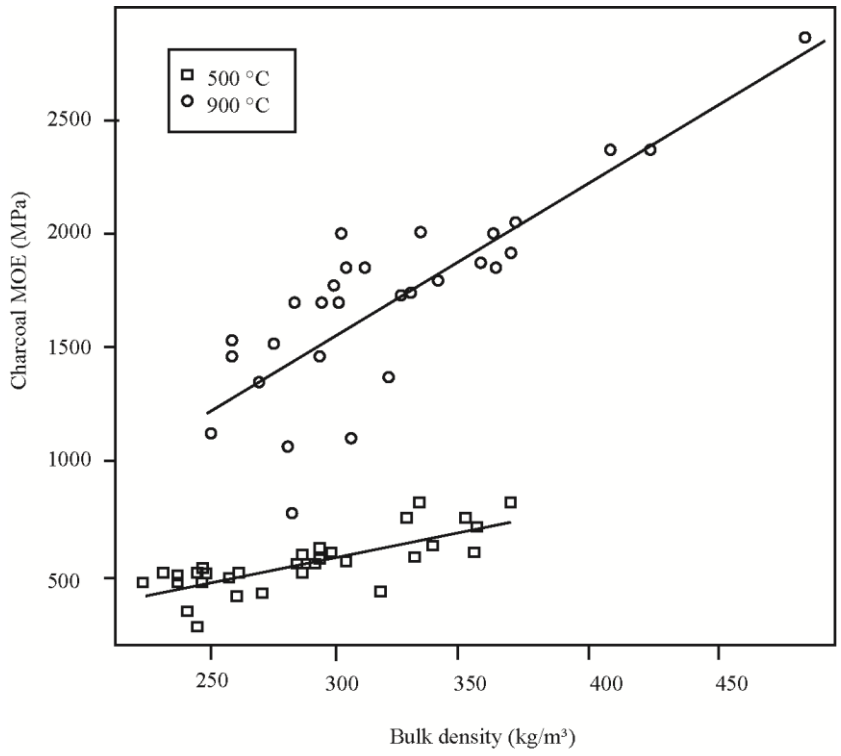

Figure 28 Relationship between longitudinal and radial charcoal MOE according to carbonization temperature (R^2 = 0.48 for 500 °C; R^2 = 0.65 for 900 °C). N = 58.

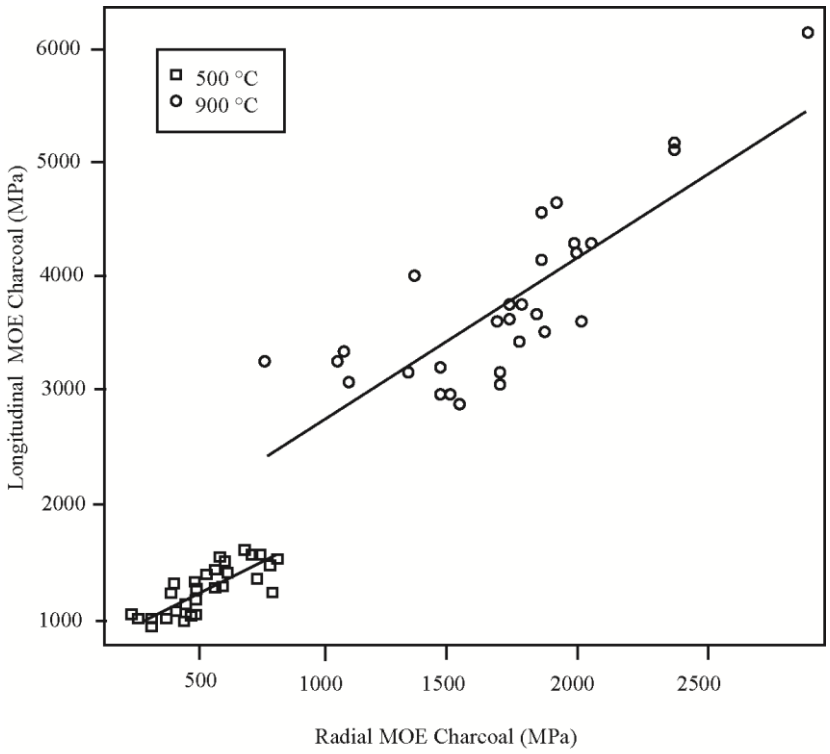

Figure 29 Relationship between G_{RT} and radial charcoal MOE according to carbonization temperature (R^2 = 0.68 for 500 °C; R^2 = 0.52 for 900 °C). N = 58.

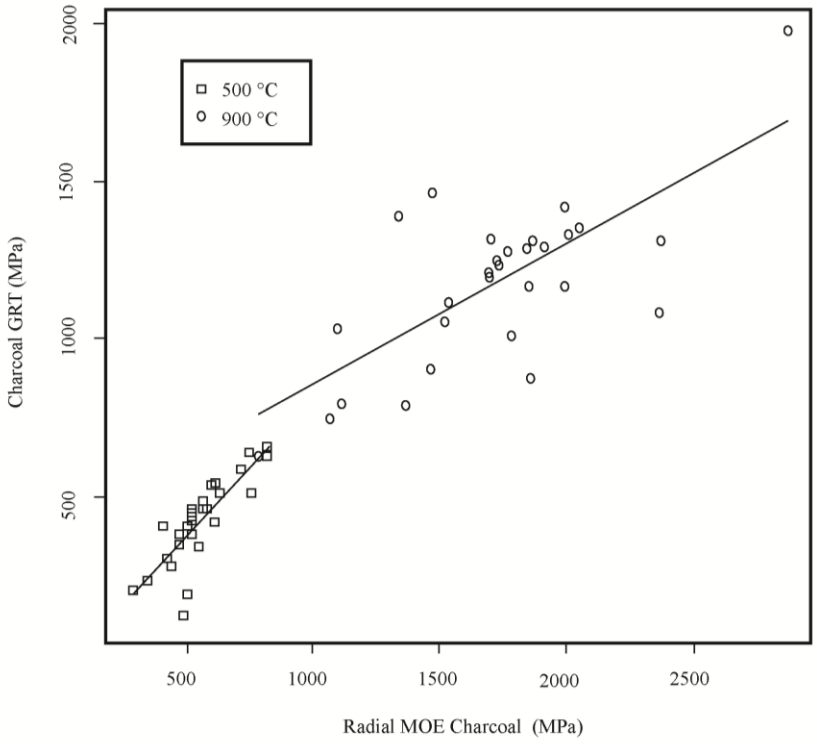

4.3.3 Link between wood and charcoal traits

A simple correlation analysis between the parameters measured in wood and charcoal allowed to highlight the links between the properties of the raw material and the product and, therefore, obtaining a set of independent predictive variables. Correlations were made, taking into account the characteristics analyzed in wood cubes and the characteristics analyzed in the same specimens after carbonization.

Table 21 represents the simple correlation matrix between 12 characteristic of wood and 8 variables obtained in charcoal at 500 °C. The high number of strong correlations observed between the properties of wood and charcoal characteristics proved the great dependence of the product in relation to its raw material (Table 21). It is possible to highlight the existing strong linear relationships between the elastic variables of charcoal and physical characteristics of wood. Many authors showed the relationship between the properties of wood and charcoal (ANTAL; GRØNLI, 2003; BRITO; BARRICHELO, 1980; CASTRO et al., 2013; MOUTINHO, 2013).

Table 21 Simple correlation of mechanical and physical properties of wood and charcoal produced at 500 °C (N = 29)

	Ychar (%)	Dchar ($kg.m^{-3}$)	MOE long char (MPa)	MOE rad char (MPa)	MOE tang char (MPa)	G_{LR} char (MPa)	G_{RT} char (MPa)	G_{TL} char (MPa)
D12 ($kg.m^{-3}$)	-0.50	**0.95**	**0.86**	**0.78**	0.24	**0.88**	0.63	0.08
MOE Long (MPa)	**-0.75** [(1)]	**0.82**	**0.85**	0.48	0.14	**0.80**	0.39	-0.03
MOE Rad (MPa)	0.36	0.14	0.03	0.53	-0.16	0.04	0.28	0.02
MOE Tang (MPa)	0.34	-0.11	-0.22	-0.31	**0.76**	-0.17	-0.32	**0.78**
G_{LR} (MPa)	0.44	0.13	-0.07	0.41	-0.18	0.11	0.21	-0.03
G_{RT} (MPa)	0.20	0.31	0.15	0.18	0.49	0.23	0.16	0.40
G_{TL} (MPa)	0.18	0.11	-0.05	0.08	0.33	0.02	0.03	0.32
D ($kg.m^{-3}$)	-0.30	**0.89**	**0.81**	**0.73**	0.40	**0.82**	0.57	0.26
FSP (%)	-0.14	0.15	0.16	0.06	-0.36	0.11	0.01	-0.27
Rd (%)	-0.33	0.31	0.29	-0.14	0.40	0.27	0.01	0.20
Tg (%)	-0.57	**0.65**	**0.73**	0.63	-0.29	0.64	0.48	-0.35
Anisot	-0.03	0.09	0.16	0.48	-0.57	0.11	0.28	-0.43

[(1)] Values in bold refer to significant correlations (minimum value considered 0.65)

Basic density was positively correlated with charcoal density (0.89), MOE US in the longitudinal (0.81) and radial (0.73) directions, and with the longitudinal-radial shear modulus (0.82) of charcoal made at 500 °C. A similar behavior occurred with apparent wood density, correlating with the same mechanical parameters of charcoal. Antal and Grønli (2003) show that charcoal density is linearly proportional to the basic wood density, with a proportionality constant of 0.82. Brito and Barrichelo (1980) also investigated the relationship between wood basic specific gravity and the charcoal apparent density of *Eucalyptus* spp. and they found a coefficient of determination of $R^2 = 0.97$. The results of the present study are in agreement with the statement of these studies.

The gravimetric charcoal yield was negatively correlated with the wood modulus of elasticity in the longitudinal direction (-0.75). The crushing strength of both *Acacia* and *Eucalyptus* charcoal were positively correlated with charcoal density and it was increased with the decrease in charcoal yield (KUMAR; VERMA; GUPTA, 1999). Some authors have shown that charcoal yield is independent of the basic density of the wood that originated it (ANTAL; GRØNLI, 2003). This statement is in accordance with this study, since charcoal yield was not correlated with the basic or apparent density of wood.

Mechanical properties of different types, but performed in the same direction, correlated to each other. MOE US in the longitudinal direction of wood and charcoal (0.85), MOE US in the longitudinal direction of wood with charcoal G_{LR} (0.80), MOE US in the tangential direction of wood with MOE US in the tangential direction of charcoal (0.76), and charcoal G_{TL} (0.78).

The morphology of charcoal will follow the basic wood shape, with the pores, channels and fibers keeping present in cases where the conditions do not affect the material (such as high heating rate, combustion, excessive moisture, dimensions of parts) (LANCELOTTI et al., 2010; OLIVEIRA; GOMES; ALMEIDA, 1982). Unlike coke, which goes through a stage of localized fusion,

charcoal does not have this reaction during carbonization which, in some cases, allows to identify the wood that gave rise to it (LANCELOTTI et al., 2010).

To evaluate the correlation between wood traits and charcoal parameters made at 500 °C and 900 °C, all the mean values were separately subjected to varimax rotated principal component. Since the mechanical and physical characteristics involved in both wood and charcoal are not independent, by applying PCA, it is possible that the first PC, which represents an important mode of variability, may also include aspects of other correlated modes (WILKS, 2006). Thus, the orthogonality constraint of regular PCA can result in the influence of several distinct physical and mechanical parameters, being represented by a single principal component. In this case, RPCA can help improve the interpretation of geographically plotted loadings by rotating the axes of a retained subset of unrotated principal components in order to achieve a degree of simple structure among variables. At 500 °C, 4 rotated principal components explain 83% of the total variance (Table 22). In Table 23, it is possible to observe the values of the rotated principal components.

Table 22 Variance explained by RPCA (varimax rotated principal component) on RPC1, RPC2, RPC3 and RPC4 for 500 ºC (N = 29).

Component	Eigenvalues	Variance (%)	Cumulative variance (%)
1	8.9	38	38
2	4.2	21	59
3	3.7	18	76
4	1.4	7	83

Table 23 Normalized eigenvectors of the four rotated principal components of physical and mechanical parameters of wood and charcoal produced at 500 °C.

	RPC1	RPC2	RPC3	RPC4
D12 ($kg.m^{-3}$)	**0.96**	0.00	0.05	0.00
MOE Long (MPa)	**0.83**	0.16	-0.28	0.51
MOE Rad (MPa)	0.18	-0.03	**0.79**	-0.56
MOE Tang (MPa)	-0.21	**-0.94**	-0.04	-0.25
G_{LR} (MPa)	0.15	0.07	0.57	**-0.87**
G_{RT} (MPa)	0.26	**-0.58**	0.11	-0.48
G_{TL} (MPa)	0.05	-0.40	-0.01	**-0.71**
D ($kg.m^{-3}$)	**0.90**	-0.23	0.10	-0.09
FSP (%)	0.12	**0.60**	-0.41	-0.09
Rd (%)	0.22	-0.19	**-0.89**	0.32
Tg (%)	**0.73**	0.60	0.17	0.18
Anisot	0.21	0.56	**0.80**	-0.15
Ychar (%)	-0.58	-0.32	0.30	**-0.64**
Dchar ($kg.m^{-3}$)	**0.98**	-0.01	-0.07	0.04
MOE long char (MPa)	**0.93**	0.11	-0.10	0.24
MOE rad char (MPa)	**0.83**	0.26	0.43	-0.18
MOE tang char (MPa)	0.20	**-0.87**	-0.38	-0.03
G_{LR} char (MPa)	**0.92**	0.05	-0.07	0.11
G_{RT} char (MPa)	**0.71**	0.26	0.27	-0.03
G_{TL} char (MPa)	-0.02	**-0.85**	-0.24	-0.23

The RPCs horizontal axis for the first component explained 37.7% of the total variance, while the vertical axis, a further 20.9%. For the third and fourth components, the RPCs horizontal axis explained 17.6% of the total variance, and the vertical axis, a further 6.7% (Figure 29). The variance represented by the rotated eigenvectors is spread uniformly. The charcoal mechanical pattern observed for RPC1 and 2 is more closely parallel to wood mechanical variables, and appears to reflect density and tangential shrinkage (Figure 29a). The other RPCs (3 and 4) appear more closely related to the loadings of wood physical parameters.

The correlations between wood parameters and charcoal characteristics at 900 °C are presented in Table 24.

Figure 30 Ordination diagram of eigenvectors of the two first rotated principal components (a) and of the third and fourth rotated principal components (b) obtained for charcoal parameters at 500 °C and wood.

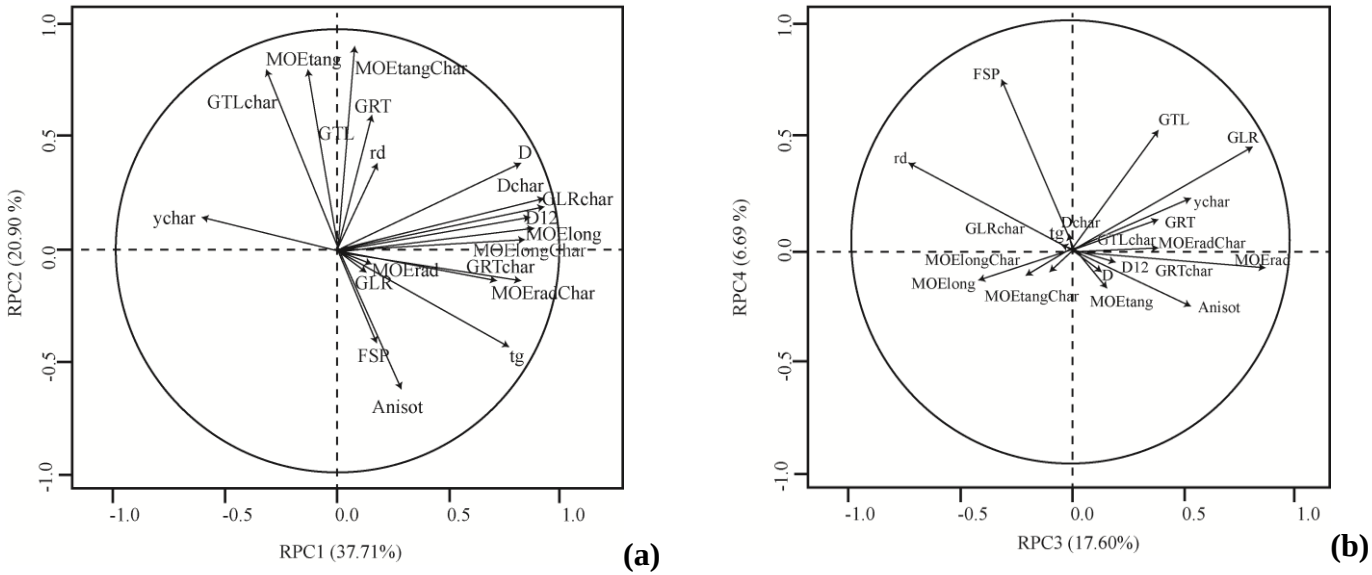

Where: D12 = apparent wood density; MOElong = wood modulus of elasticity in the longitudinal direction; MOErad = wood modulus of elasticity in the radial direction; MOEtang = wood modulus of elasticity in the tangential direction; GLR = wood londitudinal-radial shear modulus; GRT = wood radial-tangential shear modulus; GTL = wood tangential-longitudinal shear modulus; D = basic wood density; FSP = fiber saturation point; rd = wood radial contraction; tg = wood tangential contraction; Anisot = anisotropy coefficient; ychar: gravimetric yield in charcoal; Dchar = charcoal density; MOElongChar = charcoal modulus of elasticity in the longitudinal direction; MOEradChar = charcoal modulus of elasticity in the radial direction; MOEtangChar = charcoal modulus of elasticity in the tangential direction; G_{TL}char = charcoal shear modulus in the tangential-longitudinal direction; G_{LR}char = charcoal shear modulus in the longitudinal-radial direction; G_{RT}char = charcoal shear modulus in the radial-tangential direction.

Table 24 Simple correlation of mechanical and physical properties of wood and charcoal produced at 900°C (N = 29).

	Ychar (%)	Dchar ($kg.m^{-3}$)	MOE long char (MPa)	MOE rad char (MPa)	MOE tang char (MPa)	G_{LR} char (MPa)	G_{RT} char (MPa)	G_{TL} char (MPa)
D12 ($kg.m^{-3}$)	-0.12	**0.93**[(1)]	**0.87**	**0.84**	0.31	0.26	0.56	-0.08
MOE Long (MPa)	-0.57	**0.81**	**0.81**	0.47	-0.03	-0.01	0.16	-0.23
MOE Rad (MPa)	0.46	0.08	0.04	0.41	0.24	0.41	0.63	0.13
MOE Tang (MPa)	0.23	0.09	0.09	0.24	**0.75**	0.16	0.29	0.49
G_{LR} (MPa)	0.29	0.25	0.21	0.54	0.41	0.22	0.55	0.10
G_{RT} (MPa)	0.09	0.40	0.41	0.49	**0.77**	0.25	0.41	0.52
G_{TL} (MPa)	-0.25	0.50	0.56	0.49	0.42	0.02	0.35	0.19
D ($kg.m^{-3}$)	-0.04	**0.90**	**0.84**	**0.81**	0.51	0.30	0.60	0.15
FSP (%)	-0.06	0.25	0.32	0.20	-0.28	0.03	0.01	-0.28
Rd (%)	-0.40	0.28	0.34	-0.11	0.29	-0.11	-0.37	0.24
Tg (%)	-0.22	**0.66**	**0.65**	0.58	-0.32	0.10	0.34	-0.42
Anisot	0.27	0.10	0.03	0.39	-0.41	0.12	0.47	-0.41

[(1)] Values in bold refer to significant correlations (minimum value considered 0.65)

The correlations between physical and mechanical characteristics of wood and the properties evaluated both in charcoal produced at 500 °C and 900°C, showed high magnitude. Basic wood density was positively correlated with charcoal density (0.90), MOE US in the longitudinal (0.84) and radial (0.81) directions of charcoal made at 900 °C. A similar behavior occurred with apparent wood density, correlating with the same mechanical parameters of charcoal.

Mechanical properties of different types, but performed in the same direction, correlated to each other. MOE US in the longitudinal direction of wood and charcoal (0.81), MOE US in the tangential direction of wood with MOE US in the tangential direction of charcoal (0.75). At 900 °C, there is no correlation between the shear modulus of charcoal and wood properties. The gravimetric yield in charcoal was not correlated, unlike charcoal produced at 500 °C, with any property of wood.

It can be seen in Table 25 the explained and accumulated variances in each rotated principal component as well as their respective graphical representations (Figure 30) in function of rotated principal components. Four rotated principal components explain 83% of the total variance (Table 26).

Table 25 Variance explained by RPCA (varimax rotated principal component) on RPC1, RPC2, RPC3 and RPC4 for 900 °C (N = 29).

Component	Eigenvalues	Variance (%)	Cumulative variance (%)
1	7.1	36	36
2	4.6	23	59
3	3.5	18	76
4	1.3	6	83

Table 26 Normalized eigenvectors of the four principal components for physical and mechanical parameters of wood and charcoal produced at 900 °C.

	RPC1	RPC2	RPC3	RPC4
D12 (kg.m^{-3})	**0.94**(1)	0.27	0.17	0.18
MOE Long (MPa)	**0.81**	-0.21	-0.34	-0.13
MOE Rad (MPa)	0.10	0.42	**0.83**	0.52
MOE Tang (MPa)	0.08	**0.95**	0.23	0.35
G_{LR} (MPa)	0.30	0.64	**0.68**	0.24
G_{RT} (MPa)	0.39	**0.89**	0.15	0.43
G_{TL} (MPa)	0.55	**0.61**	-0.06	0.00
D (kg.m^{-3})	**0.88**	0.46	0.17	0.34
FSP (%)	0.31	**-0.39**	-0.35	-0.18
Rd (%)	0.23	0.10	**-0.90**	-0.09
Tg (%)	**0.71**	-0.50	0.05	-0.09
Anisot	0.17	-0.36	**0.80**	0.02
Ychar (%)	-0.32	0.20	**0.49**	0.26
Dchar (kg.m^{-3})	**0.98**	0.18	0.01	0.18
MOE long char (MPa)	**0.97**	0.18	-0.07	0.12
MOE rad char (MPa)	**0.87**	0.28	0.41	0.20
MOE tang char (MPa)	0.22	**0.87**	-0.07	0.32
G_{LR} char (MPa)	0.23	0.14	0.28	**0.90**
G_{RT} char (MPa)	0.59	0.27	0.61	**0.64**
G_{TL} char (MPa)	-0.08	0.60	-0.19	**0.64**

The RPCs horizontal axis for the first component explained 35.6% of the total variance, while the vertical axis, a further 23.2%. For the third and fourth rotated components, the RPCs horizontal axis explained 17.6% of the total variance, and the vertical axis, a further 6.5% (Figure 31). Like at 500 °C, the variance represented by the rotated eigenvectors is spread uniformly. The charcoal mechanical pattern observed for RPC1 and 2 is also more closely parallel to wood mechanical parameters, and appears to reflect density and

tangential shrinkage (Figure 31a). The other RPCs (3 and 4) appear more closely related to the loadings of wood physical parameters (charcoal yield gravimetric, anisotropy coefficient and radial shrinkage). The charcoal shear modulus at the two temperatures were the parameters that most oscillated between the four rotated principal components.

Both charcoal produced at 500 °C and at 900 °C presented a very similar variance when compared to the wood origin, with the first three principal components accounting for a large portion of the variance and low magnitudes of variance, starting from the 4th RPC. Together, the four RPCs of the link between the charcoal produced at 500 °C and the raw material and of the link between the charcoal produced at 900 °C and the raw material, accounted both for a cumulative variance of 83%.

A comparison of the equivalent varimax RPCs in Figures 30 and 31 indicates that a wood origin is indeed, mechanical and physically, closely related with charcoal, independently of the final carbonization temperature.

Figure 31 Ordination diagram of eigenvectors of the two first principal components (a) and of the third and fourth principal components (b) obtained for charcoal parameters at 900 °C and wood.

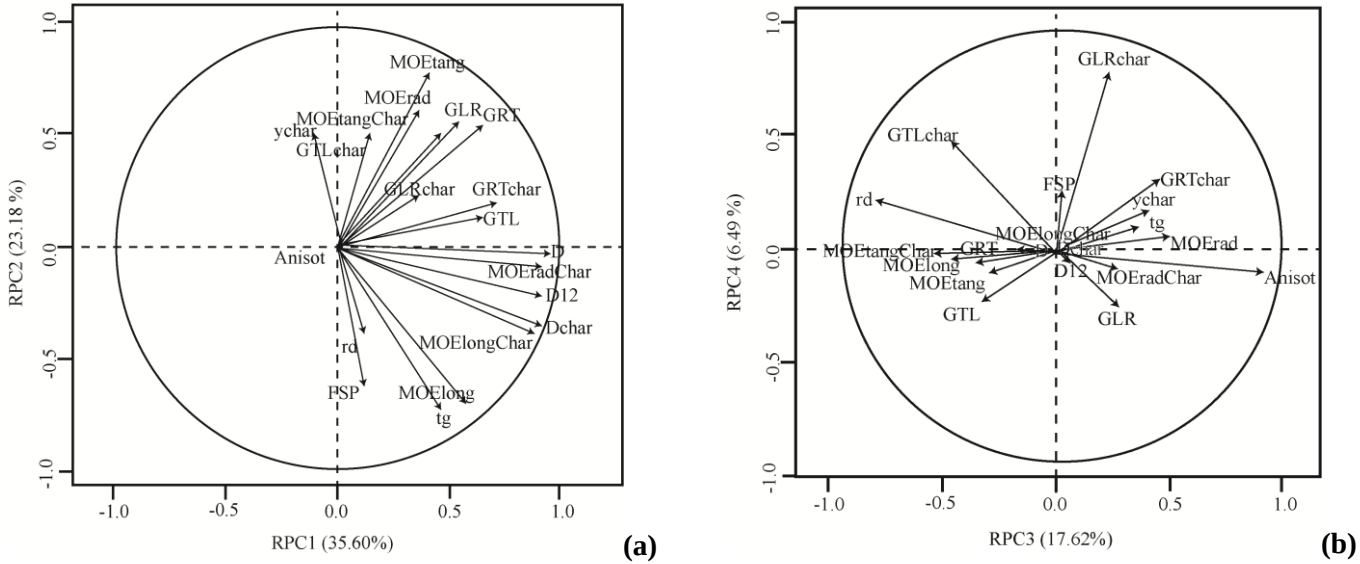

Where: D12 = apparent wood density; MOElong = wood modulus of elasticity in the longitudinal direction; MOErad = wood modulus of elasticity in the radial direction; MOEtang = wood modulus of elasticity in the tangential direction; GLR = wood londitudinal-radial shear modulus; GRT = wood radial-tangential shear modulus; GTL = wood tangential-longitudinal shear modulus; D = basic wood density; FSP = fiber saturation point; rd = wood radial contraction; tg = wood tangential contraction; Anisot = anisotropy coefficient; ychar: gravimetric yield in charcoal; Dchar = charcoal density; MOElongChar = charcoal modulus of elasticity in the longitudinal direction; MOEradChar = charcoal modulus of elasticity in the radial direction; MOEtangChar = charcoal modulus of elasticity in the tangential direction; G_{TL}char = charcoal shear modulus in the tangential-longitudinal direction; G_{LR}char = charcoal shear modulus in the longitudinal-radial direction; G_{RT}char = charcoal shear modulus in the radial-tangential direction.

4.3.4 Effect of wood properties, pyrolysis conditions and the direction of the compression force on the crushing strength of charcoal

The crushing strength determines the ability of a material to withstand the rigors of transport and can be used as an indicator of the abrasion resistance in conjunction with other properties, such as apparent density and porosity (KUMAR; VERMA; GUPTA, 1999). Crushing strength is directly linked to the maximum force (pressure) that can be applied to a piece of charcoal before complete destruction. If the crushing strength is low, the charcoal is less resistant to pressure. It is a good expression of the brittleness of charcoal.

The crushing strengths in the three directions (tangential, radial and longitudinal) of *Eucalyptus* wood charcoals produced by carbonization at temperatures of 500 °C and 900 °C are shown in Table 27.

Table 27 Average values for crushing strength of charcoal in the three sections of compression.

Crushing strength (MPa)						
	500 °C			900 °C		
	TS	RS	LS	TS	RS	LS
Min	1.1	1.1	7.8	1.8	2.4	18.9
Max	1.9	1.9	21.6	4.4	5.9	52.0
Average	1.4	1.5	11.4	2.8	3.8	30.3
SD	0.24	0.30	3.86	0.79	0.94	9.64

Abbreviation: TS: Tangential section; RS: Radial section; LS: Longitudinal section (N = 58).

The crushing strengths of charcoals showed an increase with increasing carbonization temperatures in the three directions. The comparison between averages in the three planes shows that the crushing strength values in the radial and tangential planes resemble each other at 500 °C and differ from crushing strength in magnitude in the longitudinal direction. It may be noted that the

average value of crushing strength in the radial direction of the charcoal produced at 900 °C differed considerably from the values of charcoal produced at 500 °C in the same radial plane compression, which means higher charcoal resistance with increased carbonization temperatures, even perpendicularly to the fibers. There was also an increase in crushing strength values in the tangential direction. However, the temperature effect was less pronounced than the charcoal crushing strength at radial direction.

Even though wood possesses three axes of symmetry (tangential, radial and longitudinal) for most properties, the difference is significant for actions performed parallel or perpendicular to the fibers. This is due to differences between strength and elastic properties of wood in the tangential and radial directions, which are, in general, relatively slight (WANGAARD, 1950). The increase in carbonization temperature causes a decrease in the thickness of carbon fibers. As a consequence, the charcoal is smaller than the wood source in all directions. Since the dimensional variation in the radial and tangential directions are greater than in the longitudinal direction, the effect of wood anisotropy must be intensified in charcoal. The higher absence of material (porosity) in the tangential direction ultimately results in a lower resistance in this direction (KWON; KIM; CHA, 2009).

Kumar, Verma and Gupta (1999) also observed that the heating rate influences the compression strength of the charcoals. According to the authors, the resistances of charcoals from both *Acacia* and *Eucalyptus* were higher when a heating rate of 4 °C.min^{-1} (called slow carbonization) was used, compared with a heating rate of 30 °C.min^{-1} (called rapid carbonization); both assays were performed with a final carbonization temperature of 1000 °C. In their experiment, the compressive strengths obtained by Kumar, Verma and Gupta (1999) ranged from 1.9 to 3.4 MPa and 1.2 to 1.4 MPa for the lowest and highest heating rate, respectively.

The relationships between charcoal crushing strength and wood properties, according to the coupled effects of temperature and direction of the compression force, were carried out with the analysis of covariance.

The influence of each factor measured on wood (MOE US Long, MOE US Rad, MOE US Tang, G_{LR}, G_{RT}, G_{TL}, apparent and basic density, FSP, Rd, Tg, anisotropy coefficient) with interactions was initially taken into account for the modeling (final temperatures 500 °C and 900 °C, direction of compression test, longitudinal, radial and tangential). The models were then refined using the AIC criterion in a stepwise algorithm. At the end of the procedure, only the significant variables were kept in optimal models. The results are presented in Table 28.

log(Crushing strength) ~ Apparent Density + Carbonization temperature * Compression direction

Table 28 Regression coefficients and model characteristics between charcoal crushing strength and wood properties (N = 56).

Crushing strength (MPa)							
Intercept	D12	T900	RS	TS	T900 * TS	RSE	Adjustment R^2
0.5862	0.0033	0.9939	-1.977	-2.1969	-0.3026	0.1654	0.98

RSE: Residual standard error; D12: wood apparent density; RS: Radial section; TS: Tangential section; T900: wood carbonized at temperature of 900 °C

The best predictor to estimate charcoal crushing strength was apparent density of wood (Adjusted R^2 of 0.98). The standard error of the charcoal crushing strength estimation by the apparent density of wood was 1.18 MPa associated with an average charcoal crushing strength at 900 °C of 2.8 MPa in radial direction and of 3.8 MPa in tangential direction. The model equation was: Log (Charcoal crushing strength) = 0.5862 + 0.00333 Wood Apparent Density + 0.9939 T900 – 1.977 Radial direction – 2.1969 Tangential direction – 0.3026

T900*Tangential direction. The model is easy to understand and presents precision, which is used to apparent wood density, an independent relevant variable which can be easily and precisely obtained to estimate charcoal crushing strength. In general, a selection of genetic materials based on density will result in an increase in the resistance and elasticity of charcoal.

The relationship between charcoal crushing strength and wood apparent density was presented at Figure 32. This Figure shows linear relationships between crushing strength and apparent density of wood. There are six regression lines in the model according with carbonization final temperature and direction of compression. There is an increase in crushing strength with the increase in apparent wood density, especially in the tangential direction at 900 °C. A considerable scatter can be seen in the data from this Figure, due to the variation in the direction of compression. It is possible to identify bands in which the points are concentrated, according to the radial and tangential directions, showing that the factor carbonization temperature did not significantly influence the results of crushing strength perpendicular to fibers.

Figure 32 Relationship between charcoal crushing strength and apparent density of wood (a) according to carbonization temperature and direction of compression (longitudinal, radial and tangential). N = 57.

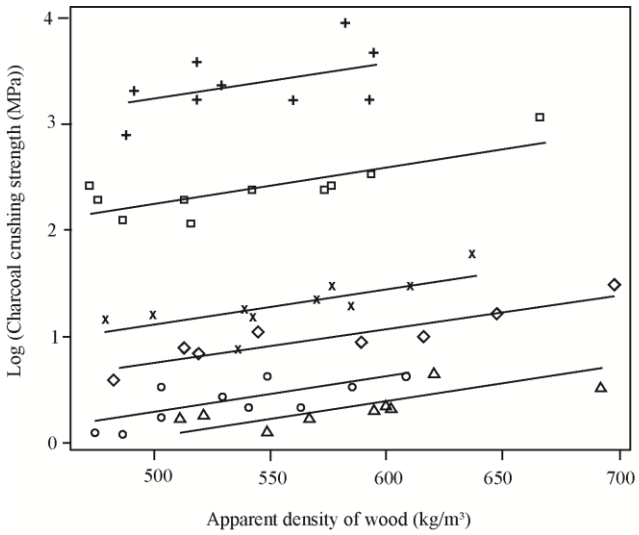

Legend and models :
(□) Longitudinal – 500 °C → Log(Charcoal Crushing strength) = 0.586229 + 0.003339 * Density ; (R^2 = 0.59)
(○) Radial – 500 °C → Log(Charcoal Crushing strength) = 0.586229 + 0.003339 * Density - 1.977265 ; (R^2 = 0.53)
(Δ) Tangential – 500 °C → Log(Charcoal Crushing strength) = 0.586229 + 0.003339 * Density - 2.196945 ; (R^2 = 0.52)
(+) Longitudinal – 900 °C → Log(Charcoal Crushing strength) = 0.586229 + 0.003339 * Density + 0.993869 ; (R^2 = 0.33)
(×) Radial – 900 °C → Log(Charcoal Crushing strength) = 0.586229 + 0.003339 * Density + (0.993869 - 1.977265 - 0.150496) ; (R^2 = 0.53)
(◇) Tangential – 900 °C → Log(Charcoal Crushing strength) = 0.586229 + 0.003339 * Density + (0.993869 - 2.196945 - 0.302602) ; (R^2 = 0.85)

Kurma, Verma and Gupta (1999) carried out compression tests on cubic-shaped samples (25 x 25 x 24 mm) issued from *Acacia* and *Eucalyptus*, carbonized in the temperature range of 270 °C - 1200 °C, in order to characterize the crushing strength. The crushing strength was determined by using a 300 kN universal testing machine. The charcoals made from both wood species showed a decrease in crushing strengths with increasing carbonization temperatures up to 600 °C, followed by a further increase. *Eucalyptus* wood yielded a charcoal stronger than those produced from *Acacia* wood under the same carbonization conditions (KUMAR; VERMA; GUPTA, 1999). Moutinho (2013) found average value of resistance to compression parallel to the fibers of charcoal of 11.1 MPa for *Eucalyptus* and *Corymbia*.

Lancelotti et al. (2010) performed mechanical tests in different South Asian tree taxa in order to understand the different response to compressive stress of wood that has been subject to a range of thermal degradations to apply on archaeological contexts. The specimens have been carbonized at three different temperatures (200 °C, 300 °C and 400 °C), under constant conditions. Afterwards, their resistance to compression has been measured on two planes, parallel (on transverse section) and perpendicular (on radial longitudinal section) to the direction of fibers. Among the species with very thick fibers that show a lower resistance to stress, all have diffuse or banded parenchyma. At the lowest temperature, all these species have resistance to stress lower than the average when compression is applied on the section transversal. When compression is applied on the radial section, the species with banded parenchyma display a resistance to stress higher than the average. This pattern, however, disappears when higher temperatures are applied.

It is possible to identify the fibrous structure by scanning electron microscopy of various charcoals. This type of structure will cause different mechanical properties in longitudinal and cross section (anisotropy), as well as in

composite materials or metals formed in one direction. The initial wood structure is maintained even at temperatures above 1000 °C, clearly seen in the cross section (KUMAR; GUPTA, 1995). Therefore, one way to control the properties of charcoal is controlling wood quality prior to the carbonization process.

4.4 Characterization of the mechanical behavior of charcoal beds in uniaxial compression

Charcoal bed compression assays were based on the breakage of an amount of a charcoal sample with controlled size through a predetermined compressive load (12000 N) and subsequent analysis of size distribution of the sample. The effects of assay temperature, particle size and charcoal production temperature on the behavior of charcoal beds were analyzed. Selecting two particle size ranges, 10 mm and 20 mm, and two carbonization temperatures, 500 °C and 900 °C, experiments were carried out by changing the bed temperature at the time of compression, 20 °C and 300 °C, to assess its influence on the results. For the analysis and comparison of assay data with different particle sizes, the percentage of assay particle size distribution is created, defined by Equation 8, which aims to assess the mechanical strength of charcoal after compression.

$$\%dist = \frac{mrange}{mtotal}\ x\ 100 \tag{8}$$

Where: dist% is the percentage of particle size distribution; mrange is the mass of the particle size range; mtotal is the total mass tested.

There are precedents of bed compression assays with iron ore pellets. Gustafsson et al. (2013) observed the friction between iron ore pellets and

between iron ore pellets with the steel tube used to compression experiments. The authors found that the residual frictional stress is approximately 2.5% of the maximum stress, which means little effect on the results, and was neglected in their study. Following the compression tests, Gustafsson et al. (2013) performed the analysis of the fracture index, counting the bulk of broken pellets divided by the total mass of pellets. Thus, the authors determined that confined compression test is a viable experiment to determine the properties and fracture data of iron ore bed pellets.

Figures 33 and 34 show pie charts displaying the relative percentages of the different fragment size of charcoal beds under cold (20 °C) and hot (300 °C) compression. The dimension of fragments seems to be correlated with wood carbonization temperature. Charcoal produced at 900 °C, for instance, maintains a very high proportion of fragments >8 mm throughout the entire experiment, independently of compression temperature and particle size, whilst charcoal at 500 °C generally shows a higher level of brittleness with, on average, less fragments in the >8 mm category independently of assay conditions (Figures 33 and 34). In addition, samples exposed to the highest compression temperature generally show less fragments in the >8mm category. At the highest particle size (20 mm), all these charcoal beds have resistance to stress higher than the other particle size (10 mm). There is a larger amount of particles close to the original size (>8 mm category) or fine (<1.6 mm).

Figure 33 Pie charts displaying the relative percentages of the different fragment sizes of cold compressed charcoal beds (20 °C). **a** Charcoal at 500 °C and particle size 10 mm; **b** Charcoal at 500 °C and particle size 20 mm; **c** Charcoal at 900 °C and particle size 10 mm; **d** Charcoal at 900 °C and particle size 20 mm.

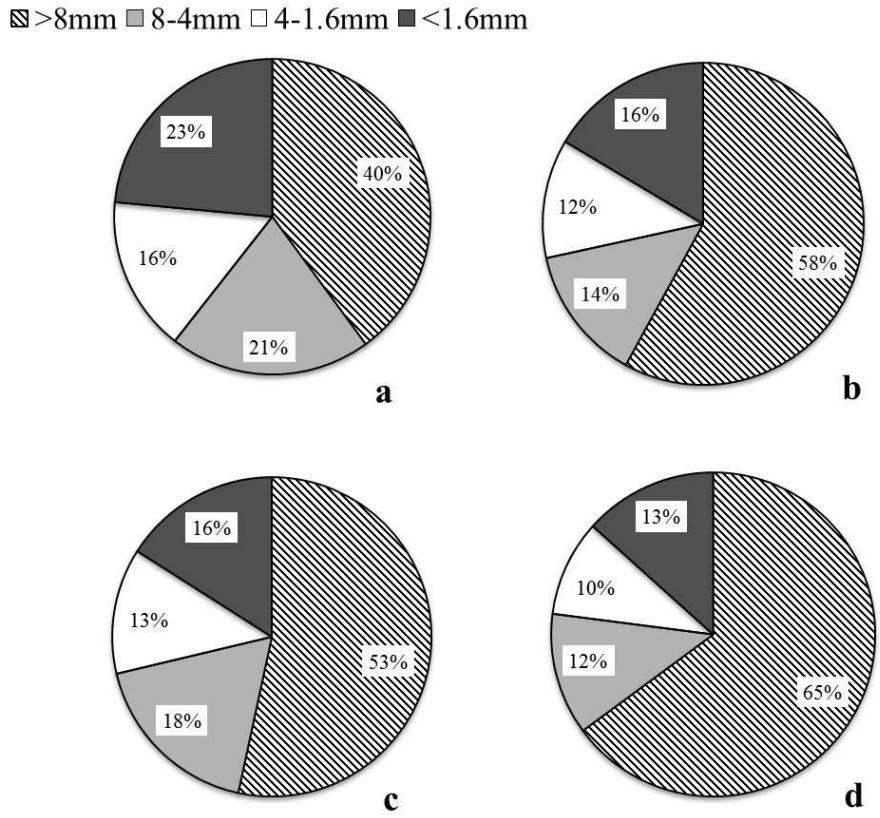

Figure 34 Pie charts displaying the relative percentages of the different fragment sizes of hot compressed charcoal beds (300 °C). **a** Charcoal at 500 °C and particle size 10 mm; **b** Charcoal at 500 °C and particle size 20 mm; **c** Charcoal at 900 °C and particle size 10 mm; **d** Charcoal at 900 °C and particle size 20 mm.

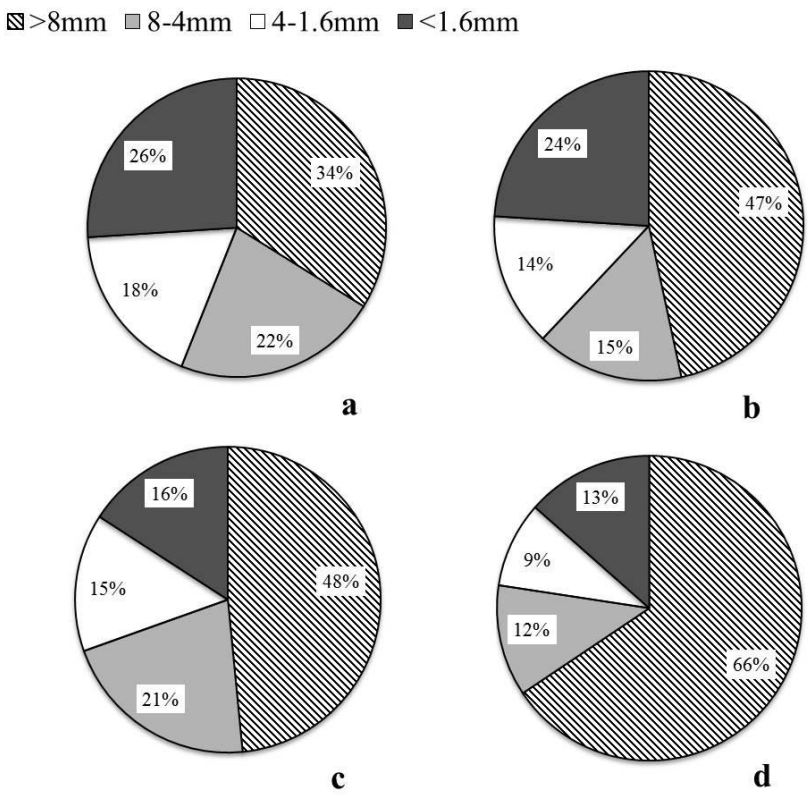

The generation of fines is strongly influenced by mechanical strength and must not be greater than 15%, recorded after the removal of the carbonization oven, passing through a 9.52 mm screen (RAAD; MELO, 2014). On the other hand, the maximum size of charcoal can not exceed 200 mm, in order not to cause problems in furnace loading. The mechanical properties of charcoal can range as a function of particle size. The difference in size may affect charcoal distribution in

the bed, leading to different results. The furnace operates in countercurrent mode, with hot gases upwards and load downwards. Fragmentation resistance at the time of charcoal handling is the most important factor to maintain a constant load permeability to gas circulation, which is essential to ensure the regular operation of the furnace. A fragile charcoal can also break under the weight of the load and cause obstructions, as well as care in handling during production, storage and charcoal ovening. A higher fine generation hinders the contact gas/metal load, through the formation of preferential paths within the furnace, making ore reduction more difficult. Charcoal fines generated in the beneficiation process, generally lower than 10 mm, can be directed to the fine injection process, or marketed. Current technology allows injection through tuyeres in the range from 100 to 200 kg of charcoal dust per ton of pig iron (RAAD; MELO, 2014).

The power indicator decreases when the carbonized temperature increases, with energy being more affected than this one (Table 29). The energy indicator evolves markedly with granulometry. A high value of particle size will stiffen the response as more energy is needed to crack the particles. It appears that fracture of charcoal beds demands less energy at high temperatures.

Table 29 Average values for properties of the charcoal beds: 8 treatments: 2 temperature carbonization, 2 particle size, 2 temperature of test (N = 13).

Carbonization temperature (°C)	Particle size (mm)	Test temperature (°C)	Power ($J.s^{-1}$)	Energy (N.m)
500	10	20	17.5	108.3
	20		17.9	125.5
900	10		19.2	98.5
	20		20.4	108.6
500	10	300	15.6	86.2
	20		17.0	112.3
900	10		17.9	71.1
	20		20.5	74.8

Figure 35 illustrates the load/displacement relationship (only one diagram is presented here as an example of the type of relation that occurs). It can be noticed that, at the beginning, the curve presents a gradual rise after the initial contact, which corresponds to setting up the compression, then a rapid, constant and straight rise of the stress until 12000 N, which corresponds to the end of the test. It is also observed that the curve tended to present the same behavior if the test were continued until complete compaction of charcoal bed, since the crushing strength of the entire sample (complete destruction), common in assays with individual samples, was not reached.

The further load intensification affects the fibers, compacting them. In general, more than one failure happens at the same time. Although not enough replicates were made for a prediction test, some general patterns can be extrapolated from the data. A positive correlation exists between higher temperature and lower resistance. Indeed, the maximum fragility occurs in those samples that were carbonized at 500 °C, with a particle size of 10 mm. Brittleness is not correlated with the compression temperature, with no difference between the assays (Table 30).

Figure 35 Resistance to stress: exemplifying load/displacement diagram of charcoal beds. Bed formed by charcoal carbonized at 900 °C, particle size of 10 mm and compressed at 20 °C. This graphic shows a typical stress/strain curve with a power-shaped line of direct correlation between the two variables.

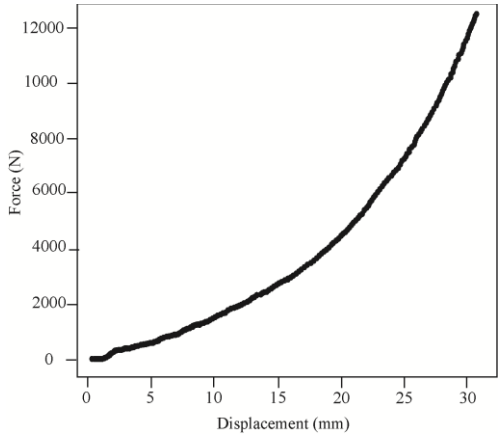

The results of the simple correlations obtained for the evaluated potency, energy and particle size ranges for charcoal beds are shown in Table 30.

Table 30 Simple correlation of the properties evaluated in charcoal beds.

	Power	Energy	sup8mm	sup4mm	sup1.6mm
Energy	0.07				
sup8mm	0.60	0.18			
sup4mm	-0.47	-0.36	**-0.91**[(1)]		
sup1.6mm	-0.60	-0.22	**-0.99**	**0.92**	
sup0mm	-0.62	0.00	**-0.93**	**0.70**	**0.89**

[(1)] Values in bold refer to significant correlations (minimum value considered 0.65)

There is a significant negative correlation between the particle size range of top charcoal at 8 mm and other lower particle size ranges (greater than 4 mm, at 1.6 mm and 0 mm). Positive correlations between the particle size range of top charcoal at 4 mm and top charcoal at 1.6 mm and 0 mm, and between top charcoal at 1.6 mm and greater than 0 mm corroborate this result, since it leads to the conclusion that higher percentages of charcoal retained in larger mesh sieves at the same compression force produce a lower percentage of smaller particle sizes and/or fine charcoals. The process of fragmentation described by Chabal (1988) states that charcoal tends to fragment in a few big and many small pieces. This means that the mass and number of fragments are correlated and the relative proportion of different fragment sizes is constant for all species.

In Figure 36, the experimental curve of particle size <1.6 mm / particle size> 8 mm gives a trendline with a determination coefficient $R^2 = 0.98$, that is close to a straight line.

Figure 36 Correlation between particle size (N = 13).

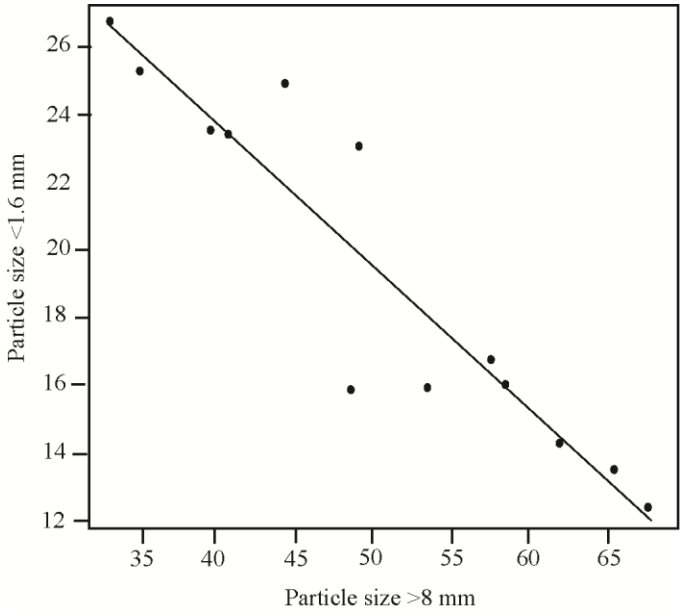

Table 31 shows total variance explained by PCA on PC1 and PC2. The principal components PC1 and PC2 together, explain 87% of the variance. The first principal component explained 69% of the total variance and can be interpreted as an average between the variables with a higher coefficient in the linear combination.

In Table 32, it is possible to observe the values of the normalized eigenvectors of the principal components of charcoal bed assays. The analysis indicates that the variability of charcoal beds in relation to energy, potency and particle size ranges can be explained by two factors, and the second component consists only of the factor energy (Table 32).

Table 31 Total variance explained by PCA on PC1 and PC2 (N= 13).

Component	Eigenvalues	Variance (%)	Cumulative variance %)
1	4.1	69	69
2	1.1	18	87

Table 32 Normalized eigenvectors of the two principal components of charcoal bed assays (N = 13).

	PC1	PC2
Power	**0.72**	0.10
Energy	0.13	**0.96**
sup8mm	**0.99**	0.39
sup4mm	**-0.88**	-0.59
sup1.6mm	**-0.98**	-0.43
sup0mm	**-0.94**	-0.15

A plot of the data in the space with the first two principal components with the name of the corresponding parameter can be produced, as shown in Figure 37.

Figure 37 Graphical analysis of the properties determined in charcoal beds; variables factor map PCA.

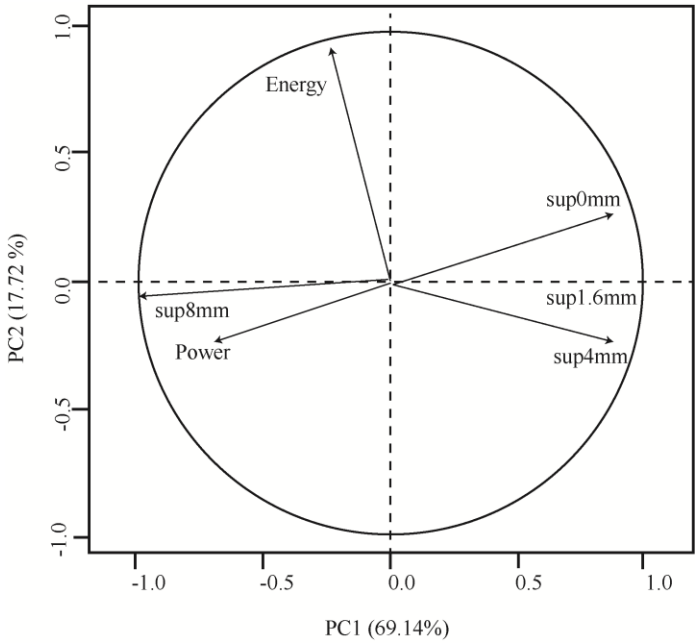

In Figure 38, the score plot of PCA is observed for assays of charcoal beds produced at final carbonization temperatures of 500 °C and 900 °C, particle sizes of 10 mm to 20 mm and assay temperatures of 20 °C and 300 °C. From this analysis, grouping and separation of charcoal beds were possible. The PCA indicated four groups, identified by different carbonization temperatures (circled in red) and particle sizes (circled in blue). The beds consisting of charcoals produced at different temperatures clearly stood out, forming two separate groups in the PCA. However, the temperature effect of charcoal beds is not significant, since temperature is not a cumulative effect. If the compression temperature were increased to 1000 °C, for example, the time between the reduction in charcoals produced at 500 °C and 900 °C would tend to be very close and the behavior of both carbonization temperatures would tend to be very similar.

Figure 38 Individual factor map (PCA) of 13 charcoal bed assays.

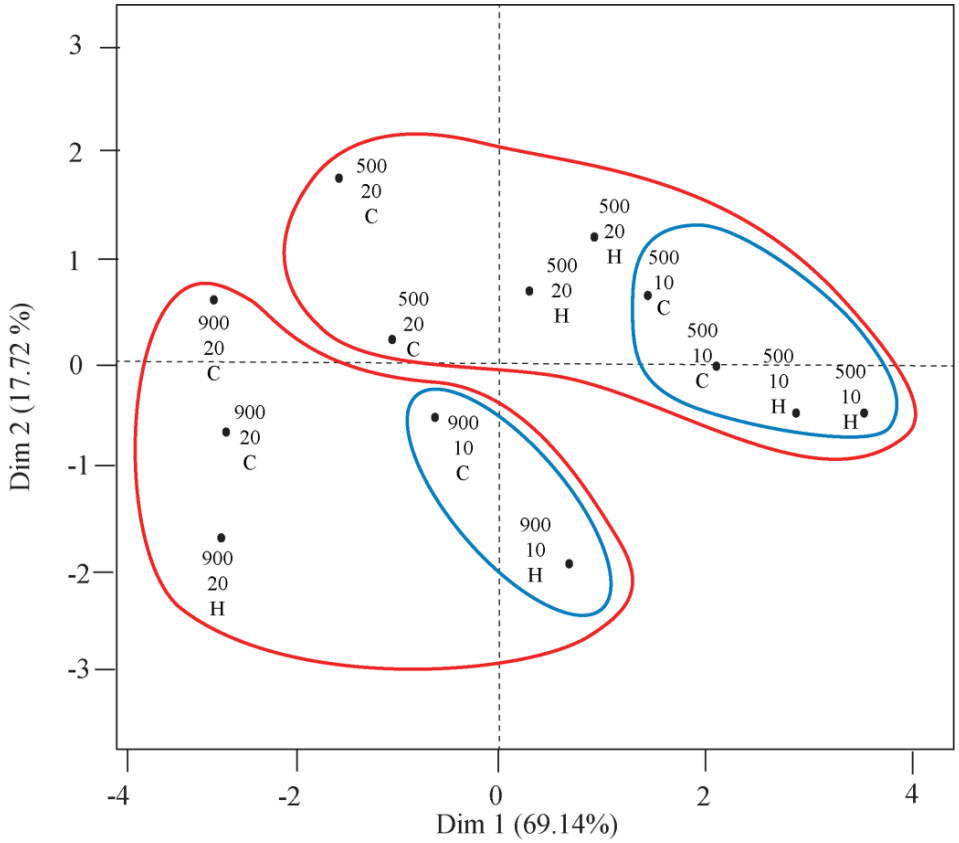

For the abbreviation: 500 = 500 °C, 900 = 900°C: charcoal carbonization temperatures; C = Cold (20°C), H = Hot (300°C): compression temperatures; 10 = 10 mm, 20 = 20 mm: particle sizes used in the assays

Kumar, Verma and Gupta (1999) studied the relationship between an impact strength index, the charcoal used in assays and carbonization temperature. The shatter index is used as an indication of resistance of material to breakage/abrasion on being dropped from a height. It was observed that smaller and granular forms have a lower impact strength than larger samples prepared in cubic forms. The authors attributed this fact to the difference in their cross-sectional area and the distribution of load on their surfaces. In comparison to cubic samples, lumps have smaller cross-sectional areas and irregular shape,

and hence the load applied gets concentrated into certain small regions. The result is, thus, more breakage in lumpy samples. In the case of cubes, the load applied is distributed over the large cross-sectional area, and hence, less breakage occurs (KUMAR; VERMA; GUPTA, 1999). The impact strength of *Acacia* and *Eucalyptus* charcoal decrease with the increase in carbonization temperature up to 600 ºC is followed by an increase thereafter (KUMAR; VERMA; GUPTA, 1999). The increase in compressive strength would also lead to an increase in impact strength (KUMAR; VERMA; GUPTA, 1999).

5 CONCLUSIONS

The pertinence of the sampling location was a question during the study; this was solved by a statistical analysis, allowing to group locations with similar properties. Wood properties were lower near the pith. The radial variation observed for wood properties (density and MOE) was explained by the transition from juvenile to mature wood. Radial position and carbonization temperature had significant effects on charcoal density and mechanical properties of charcoal. The charcoal MOE increased with the final pyrolysis temperature; however, this effect was less pronounced for charcoal density. Furthermore, the charcoal MOE and density were found to be higher near the bark, but a high carbonization temperature seemed to soften this effect of radial position.

The relationships among wood properties were investigated. There were strong linear relationships between wood density, MOE and tangential shrinkage. Tangential shrinkage was the characteristic that most correlated with the mechanical strength parameters of wood.

In relation to effects of pyrolysis conditions on charcoal properties, the mechanical and physical properties (crushing strength, MOE, shear modulus and density) of *Eucalyptus* wood charcoals have been found to be influenced by carbonization temperature. The charcoal MOE and shear modulus increased with the final pyrolysis temperature, but the temperature effect was less significant for density.

Wood properties are strongly correlated with those of charcoal, mainly wood apparent and basic density. The origin wood is indeed closely related with charcoal, independently of the final carbonization temperature. The gravimetric yield in charcoal was not correlated with any property of wood, unlike charcoal produced at 500 °C, in which the gravimetric charcoal yield was negatively correlated with the wood modulus of elasticity in the longitudinal direction.

The crushing strengths of charcoals showed an increase with the increasing carbonization temperature in the three directions. The comparison between averages in the three planes shows that crushing strength values in the radial and tangential planes resemble each other at 500 °C and differ in magnitude of crushing strength in the longitudinal direction. However, it may be noted that the average crushing strength value in the radial direction of the charcoal produced at 900 °C differed considerably from the values of charcoal produced at 500 °C in the same radial plane compression, which means higher charcoal resistance with increased carbonization temperature, even perpendicularly to the fibers. There was also an increase in crushing strength values in the tangential direction; however, the temperature effect was less pronounced for the charcoal crushing strength in this direction. The final carbonization temperature increased about three times the value of crushing strength performed parallel to the fibers (11 MPa to 30 MPa). The best predictor to estimate crushing strength of charcoal was wood density.

Knowledge about the bulk behavior and fracture data for charcoal is of great importance for improving material transportation and handling systems and to increase product quality. The charcoal bed compression approach has the potential to provide information to gauge the strength of charcoal. The effects of assay temperature, particle size and charcoal production temperature on the behavior of charcoal beds were analyzed. The PCA indicated four groups, identified by different carbonization temperatures and particle sizes: 500 °C and 10 mm, 500 °C and 20 mm, 900 °C and 10 mm, 900 °C and 20 mm. The temperature effect of assay charcoal beds is not significant, since temperature is not a cumulative effect. If the compression temperature were increased to 1000 °C, for example, the time between the reduction in charcoals produced at 500 °C and 900 °C would tend to be very close and the behavior of both carbonization temperatures would tend to be very similar.

For the analysis and comparison of assay data with different particle sizes, the percentage of assay particle size distribution was created. The dimension of fragments seems to be correlated with wood carbonization temperature. Charcoal produced at 900 °C, for instance, maintains a very high proportion of fragments >8 mm throughout the entire experiment, independently of compression temperature and particle size, whilst charcoal at 500 °C generally shows a higher level of brittleness with, on average, less fragments in the >8 mm category, independently of assay conditions. In addition, samples exposed to the highest compression temperature generally show less fragments in the >8 mm category, except for the treatment at 900 °C and 20 mm. There is a larger amount of particles close to the original size (>8 mm category) or fine (<1.6 mm).

6 FINAL CONSIDERATIONS

The steel industry has a great interest in techniques that improve and help to increase the use of charcoal as a thermo reducer. Mechanically, charcoal is considered to be brittle. The main limitation of charcoal, as a replacement for coke, is its low compression strength for supporting the load in a blast furnace. Here, the carbonization process temperature parameter was examined, as well as correlations between wood mechanical and physical properties and charcoal samples from *Eucalyptus* plantations. *Eucalyptus* plantations have successfully met the demand for raw material with the quality required by the bioenergy industry. Historically in Brazil, the wood of native forests was the main raw material used to make charcoal. However, a combination between stricter environmental rules and the improvement in inspection have currently increased the use of wood from planted forests, mainly *Eucalyptus*, for the production of charcoal of industrial use. The main species of the genus *Eucalyptus* planted for use as bioenergy in Brazil are *Eucalyptus camaldulensis*, *E. saligna*, *E. tereticornis*, *E. grandis*, *E. urophylla* and their hybrids and, currently, the hybrids *Corymbia citriodora* and *C. torelliana* are being cultured with the purpose of high productivity and high density. The Brazilian success is a mixture of investments in technology and natural conditions. The findings have shown that charcoal mechanical properties are under strong carbonization temperature control, indicating that the improvement in charcoal mechanical properties is possible through an improvement in the carbonization process. Thereby, careful controls of raw material and pyrolysis conditions are required to produce charcoal with sufficient properties to replace coke in blast furnaces. Taking into account the final pyrolysis temperature, wood density is an important property which allows to control charcoal density, rigidity and strength. However, because of an unfavorable correlation between charcoal

gravimetric yield and wood modulus of elasticity, taking into account the positive relationship between the modulus of elasticity of charcoal and wood, the selection for increasing stiffness will result in a reduction in volume production. Forest managers and wood producers will have to strike a balance between overall wood and carbonization parameters. Indeed, slight reductions in charcoal gravimetric yield may be of little consequence, when considering the mechanic gains in metallurgical charcoal. Initiating the replacement of the current models for more efficient processes brick kilns, with co-product recovery and lower CO_2 emissions, may be the first step in dealing with the unfavorable charcoal mechanical resistance.

REFERENCES

ASSOCIAÇÃO BRASILEIRA DE NORMAS TÉCNICAS. **NBR 8740**: Carvão vegetal - Determinação do índice de quebra e abrasão - Método de ensaio. Rio de Janeiro, 1985. 4 p.

AMERICAN SOCIETY FOR TESTING AND MATERIALS. **ASTM D143-94**: standard test methods for small clear specimens of timber. West Conshohocken, 2009.

AMERICAN SOCIETY FOR TESTING AND MATERIALS . **ASTM D2395- 07**: standard test methods for specific gravity of wood and wood-based materials. West Conshohocken, 2007.

ANDRADE, A. M.; DELLA LUCIA, R. Avaliação da higroscopicidade do carvão vegetal e dos seus efeitos na resistência ao esmagamento. **Floresta e Ambiente**, Seropédica, v. 2, p. 19–26, 1995.

ANDRADE, C. R. **Espectroscopia no Infravermelho Próximo para predizer propriedades da madeira e do carvão de plantio clonal de *Eucalyptus* sp.** 2009. 107 p. Dissertação (Mestrado em Ciência e Tecnologia da Madeira) - Universidade Federal de Lavras, Lavras, 2009.

ANTAL, M. J. et al. High-yield biomass charcoal. **Energy & Fuels**, Washington, v. 10, n. 3, p. 652-658, 1996.

ANTAL, M. J.; GRØNLI, M. The art, science, and technology of charcoal production. **Industrial & Engineering Chemistry Research**, Washington, v. 42, n. 8, p. 1619-1640, 2003.

ANTAL, M. J.; MOK, W. S. L. Review of methods for improving the yield of charcoal from biomass. **Energy & Fuels**, Washington, v. 4, n. 3, p. 221-225, 1990.

ASSIS, P. S.; MARTINS, W. B.; VIEIRA, C. B. Avanços na injeção de carvão pulverizado para a sua aplicação em altos-fornos. **Rem: Revista Escola de Minas**, Ouro Preto, v. 56, n. 4, p. 281-285, 2003.

ASSOCIAÇÃO BRASILEIRA DE NORMAS TÉCNICAS. **NBR 7402**: Carvão vegetal - Determinação granulométrica. Rio de Janeiro, 1982. 3 p.

ASSOCIAÇÃO BRASILEIRA DE NORMAS TÉCNICAS. **NBR 7416**: Carvão vegetal - Determinação do índice de quebra. Rio de Janeiro, 1984. 9 p.

ASTLEY, R. J.; STOL, K. A.; HARRINGTON, J. J. Modeling the elastic properties of softwood – Part II: the cellular microstructure. **Holz als Roh-und Werkstoff**, Berlin, v. 56, n. 1, p. 43-50, 1998.

BABICH, A.; SENK, D.; FERNANDEZ, M. Charcoal behaviour by its injection into the modern blast furnace. **ISIJ international**, Tokyo, v. 50, n. 1, p. 81-88, 2010.

BAILEYS, R. T.; BLANKENHORN, P. R. Calorific and porosity development in carbonized wood. **Wood Science,** Madison, v. 15, n. 1, p. 19-28, 1982.

BARNETT, J. R.; BONHAM, V. A. Cellulose microfibril angle in the cell wall of wood fibres. **Biological Reviews**, Cambridge, v. 79, p. 461-472, 2004.

BARTKOWIAK, M.; ZAKRZEWSKI, R. Thermal degradation of lignins isolated from wood. **Journal of Thermal Analysis and Calorimetry**, Dordrecht, v. 77, n. 1, p. 295-304, 2004.

BEALL, F. C.; BLANKENHORN, P. R.; MOORE, G. R. Carbonized wood-physical properties and use as an SEM preparation. **Wood Science**, Madison, v. 6, p. 212-19, 1974.

BEALL, F. C. Introduction to thermal analysis in the combustion of wood. **Wood Science**, Madison, v. 5, n. 2, p. 102-108, 1972.

BENDTSEN, B. A. Properties of wood from improved and intensively managed trees. **Forest Products Journal**, Madison, v. 28, n. 10, p. 69-72, 1978

BERNDNT, H. Improving comparability of ultrasonic measurements on wood. In: SYMPOSIUM NONDESTRUCTIVE TESTING OF WOOD, 13., 2002, Berkeley. **Proceedings...** Berkeley : [s. n.], 2002. p. 173–177.

BLANKENHORN, P. R. et al. Porosity and pore size distribution of Black Cherry carbonized in an inert atmosphere. **Wood Science**, Madison, v. 11, n. 1, p. 23-29, 1978.

BLANKENHORN, P. R.; JENKINS, G. M.; KLINE, D. E. Dynamic mechanical properties and microstructure of some carbonized hardwoods. **Wood and Fiber,** Lawrence, v. 4, n. 3, p. 212-224, 1972.

BLANKENHORN, P. R.; KLINE, D. E.; BEALL, F. C. Dynamic mechanical behavior of carbonized black cherry wood (*Prunus serotina* ehrh.). **Carbon**, Elmsford, v. 11, n. 6, p. 603-611, 1973.

BRIANE, D.; DOAT, J. Guide technique de la carbonization. La fabrication du charbon de bois. Aix-en-Provence: EDISUD, 1985. 180 p.

BRIDGWATER, A. V. Review of fast pyrolysis of biomass and product upgrading. **Biomass and Bioenergy**, Oxford, v. 38, p. 68-94, 2012.

BRITO, J. O.; BARRICHELO, L. E. G. Correlações entre características físicas e químicas da madeira e a produção de carvão: 2. densidade da madeira x densidade do carvão. **IPEF**, Piracicaba, n. 20, p. 121-126, 1980.

BRITO, J. O. Princípios de produção e utilização do carvão vegetal de madeira. **Documentos Florestais**, Oxford, v. 9, p. 1-19, 1990.

BROWN, T. et al. R**educing CO_2 emissions from heavy industry**: a review of technologies and considerations for policy makers. London: Grantham Institute Briefing, 2012. (Paper, 7).

CASTRO, A. F. N. M. et al. Análise multivariada para seleção de clones de eucalipto destinados à produção de carvão vegetal. **Pesquisa Agropecuária Brasileira**, Brasília, v. 48, n. 6, p. 627-635, 2013.

CHABAL, L. L'etude palaeoecologique des sites protohistorique a partir des charbons de bois: la question de l'unite' de meseuredenombrement des fragments ou pesees. In: HACKENS, T. ; MUNAUT, A. V. ; TILL, C. (Ed.). **Wood and archaeology**. Strasbourg : Conseil de l'Europe, 1988. p. 189–205. (Acts of the European Symposium held at Louvain-la Neuve, October 1987).

CHATTERJEE, A. **Hot metal production by smelting reduction of iron oxide.** New Delhi: PHI Learning Pvt, 2010.

CHEREMISINOFF, P. N. **Biomass**: applications, technology, and production. New York : M. Dekker, 1980.

CHRZAZVEZ, J. et al. Impact of post-depositional processes on charcoal fragmentation and archaeobotanical implications: Experimental approach combining charcoal analysis and biomechanics. **Journal of Archaeological Science**, New York, v. 44, p. 30-42, 2014.

COUTINHO, A. R.; FERRAZ, E. S. B. Determinação da friabilidade do carvão vegetal em função do diâmetro das árvores e temperatura de carbonização. **IPEF**, Piracicaba, n. 38, p. 33-37, 1988.

COUTO, A. M. et al. Qualidade do carvão vegetal de *Eucalyptus* e *Corymbia* produzido em diferentes temperaturas finais de carbonização. **Scientia Forestalis**, Piracicaba, v. 43, n. 108, p. 817-831, 2015.

CRUZ, C. R.; LIMA, J. T.; MUNIZ, G. I. B. Variações dentro das árvores e entre clones das propriedades físicas e mecânicas da madeira de híbridos de *Eucalyptus*. **Scientia Forestalis**, Piracicaba, n. 64, p. 33-47, 2003.

DEMIRBAŞ, A. Carbonization ranking of selected biomass for charcoal, liquid and gaseous products. **Energy Conversion and Management**, Oxford, v. 42, n. 10, p. 1229-1238, 2001.

DIBLASI, C. et al. Product distribution from pyrolysis of wood and agricultural residues. **Industrial & Engineering Chemistry Research**, Washington, v. 38, p. 2216–2224, 1999.

DOAT, J.; PETROFF, G. La carbonisation des bois tropicaux: essais de laboratoire et perspectives industrielles. **Revue Bois et Forêts des Tropiques**, Paris, v. 159, p. 55-72, 1975.

DONALDSON, L. Microfibril angle: measurement, variation and relationships - a review. **IAWA Journal**, Utrecht, v. 29, n. 4, p. 345-386, 2008.

EMMERICH, F. G. et al. Applications of a granular model and percolation theory to the electrical resistivity of heat treated endocarp of babassu nut. **Carbon**, Elmsford, v. 25, n. 3, p. 417-424, 1987.

EVANS, R.; ILIC, J. Rapid prediction of wood stiffness from microfibril angle and density. **Forest Products Journal**, Madison, v. 51, n. 3, p. 53, 2001.

EVANS II, J. W.; SENFT, J. F.; GREEN, D. W. Juvenile wood effect in red alder: analysis of physical and mechanical data to delineate juvenile and mature wood zones. **Forest Products Journal**, Madison, v. 50, n. 7/8, p. 75, 2000.

FERRARI, P. E.; REZENDE, M. C. Carbono Polimérico: processamento e aplicação. **Polímeros: Ciência e Tecnologia**, São Carlos, v. 8, n. 4, p. 22-30, 1998.

GALVÃO, A. P. M.; LANKOWSKY, I. P. **Secagem racional da madeira.** São Paulo: Nobel, 1985. 111 p.

GAUR, S.; REED, T. B. **An atlas of thermal data for biomass and other fuels**. Golden: National Renewable Energy Laboratory (NREL), 1995.

GLASS, S. V.; ZELINKA, S. L. Moisture relations and physical properties of wood. In: FOREST PRODUCTS LABORATORY. **Wood handbook**: wood as an engineering material. Madison: FPL, 2010. cap. 4, p. 1-20.

GOMES, P. A.; OLIVEIRA, J. B. Teoria da carbonização da madeira. In: _____. **Uso da madeira para fins energéticos**. Belo Horizonte: CETEC, 1980. v. 1, p. 27-42.

GONÇALVES, R.; TRINCA, A. J.; PELLIS, B. P. Elastic constants of wood determined by ultrasound using three geometries of specimens. **Wood Science and Technology**, New York, v. 48, n. 2, p. 269-287, 2014.

GRØNLI, M. G. **A theoretical and experimental study of the thermal degradation of biomass.** 1996. 115 p. Thesis (PhD) - The Norwegian University of Science and Technology, Trondheim, 1996.

GUITARD, D. **Mécaniques du matériau bois et composites.** Toulouse : CEPADUES, 1987. 238 p.

GUPTA, R. C. Woodchar as a sustainable reductant for ironmaking in the 21st century. **Mineral Processing and Extractive Metallurgy Review**, London, v. 24, n. 3/4, p. 203-231, 2003.

GUSTAFSSON, G. et al. Determination of bulk properties and fracture data for iron ore pellets using instrumented confined compression experiments. **Powder Technology**, Lausanne, v. 241, p. 19-27, 2013.

HAINES, D. W.; LEBAN, J. M.; HERBE, C. Determination of Young's modulus for spruce, fir and isotropic materials by the resonance flexure method with comparisons to static flexure and other dynamic methods. **Wood Science and Technology**, New York, v. 30, n. 4, p. 253-263, 1996.

HEIN, P. R. G. et al. Resonance of scantlings indicates the stiffness even of small specimens of *Eucalyptus* from plantations. **Wood Science and Technology**, New York, v. 46, n. 4, p. 621-635, 2012.

HEIN, P. R. G.; SILVA, J. R. M.; BRANCHERIAU, L. Correlations among microfibril angle, density, modulus of elasticity, modulus of rupture and shrinkage in 6-year-old *Eucalyptus urophylla*× *E. grandis*. **Maderas. Ciencia y Tecnología**, Concepcion, v. 15, n. 2, p. 171-182, 2013.

HELLE, H. et al. Optimisation study of ironmaking using biomass. **Ironmaking & Steelmaking**, London, v. 37, n. 8, p. 590-598, 2010.

HELLE, H.; HELLE, M.; SAXÉN, H. Nonlinear optimization of steel production using traditional and novel blast furnace operation strategies. **Chemical Engineering Science**, New York, v. 66, n. 24, p. 6470-6481, 2011.

ILIC, J. Relationship among the dynamic and static elastic properties of air-dry *Eucalyptus delegatensis* R. Baker. **Holz als Roh-und Werkstoff**, Berlin, v. 59, n. 3, p. 169-175, 2001.

JENKINS, G. M.; KAWAMURA, K. **Polymeric carbons-carbon fibre, glass and char.** Cambridge: Cambridge University, 1976.

JUVILLAR, J. B. O carvoejamento da madeira e seus reflexos na qualidade do carvão: qualidade da madeira. **IPEF**, Piracicaba, n. 64, p. 1-6, 1979.

KAISER, H. F. The varimax criterion for analytic rotation in factor analysis. **Psychometrika**, Williamsburg, v. 23, p. 187-200, 1985.

KHEZAMI, L. et al. Production and characterisation of activated carbon from wood components in powder: cellulose, lignin, xylan. **Powder Technology**, Lausanne, v. 157, n. 1, p. 48-56, 2005.

KIM, N. H.; HANNA, R. B. Morphological characteristics of Quercus variabilis charcoal prepared at different temperatures. **Wood Science and Technology**, New York, v. 40, n. 5, p. 392-401, 2006.

KLAR, M. **The technology of wood distillation.** London: Chapman & Hall, 1925.

KOLLMANN, F. R.; CÔTÉ, W. A. **Principles of wood science and technology.** Berlin: Springer-Verlag, 1968. 592 p.

KRZESIŃSKA, M.; ZACHARIASZ, J. Correlation between the carbonization temperature and the physical parameters of porous carbons derived from *Yucca flaccida*. **Journal of Physics**, Moscou, v. 79, n. 1, p. 1-5, 2007.

KUMAR, M.; GUPTA, R. C. Influence of carbonization conditions on physical properties of *Acacia* and *Eucalyptus* wood chars. **Transactions of the Indian Institute of Metals**, Heidelberg, v. 46, n. 6, p. 345-352, 1993.

KUMAR, M.; GUPTA, R. C. Scanning electron microscopic study of *Acacia* and *Eucalyptus* wood chars. **Journal of Materials Science**, Norwell, v. 30, n. 2, p. 544-551, 1995.

KUMAR, M.; GUPTA, R. C.; SHARMA, T. Effects of carbonisation conditions on the yield and chemical composition of *Acacia* and *Eucalyptus* wood chars. **Biomass and Bioenergy**, Oxford, v. 3, n. 6, p. 411-417, 1992.

KUMAR, M.; VERMA, B. B.; GUPTA, R. C. Mechanical properties of *Acacia* and *Eucalyptus* wood chars. **Energy Sources**, New York, v. 21, n. 8, p. 675-685, 1999.

KWON, S. M.; KIM, N. H.; CHA, D. S. An investigation on the transition characteristics of the wood cell walls during carbonization. **Wood Science and Technology**, New York, v. 43, n. 5/6, p. 487-498, 2009.

KWON, G. J. et al. Tailoring the characteristics of carbonized wood charcoal by using different heating rates. **Journal of the Korean Physical Society**, Seoul, v. 64, n. 10, p. 1474-1478, 2014.

LANCELOTTI, C. et al. Temperature, compression and fragmentation: an experimental analysis to assess the impact of taphonomic processes on charcoal preservation. **Archaeological and Anthropological Sciences**, Heidelberg, v. 2, n. 4, p. 307-320, 2010.

LOBO, A. O. et al. Caracterização de materiais carbonosos por espectroscopia Raman. **Revista Brasileira de Aplicações de Vácuo**, Rio de Janeiro, v. 24, n. 2, p. 98-103, 2005.

LULLIN, A. **Recherches sur les temperatures d'inflammation du bois et sur les enduits ignifuges**. 1925. 36 p. Thèse (Docteur es Sciences techniques) - l'Ecole Polytechnique Fédérale, Zurich, 1925.

MANABE, T. et al. Effect of carbonization temperature on the physicochemical structure of wood charcoal. **Transactions-Materials Research Society of Japan**, Yokohama, v. 32, n. 4, p. 1035-1038, 2007.

MANLY, B. F. J. **Multivariate statistical methods**: primer. London : Chapman and Hall, 1986.

MANYÀ, J. J. et al. Biochar from slow pyrolysis of two-phase olive mill waste: effect of pressure and peak temperature on its potential stability. **Energy & Fuels**, Washington, v. 28, n. 5, p. 3271-3280, 2014.

MCBEATH, A. V. et al. Determination of the aromaticity and the degree of aromatic condensation of a thermosequence of wood charcoal using NMR. **Organic Geochemistry**, Oxford, v. 42, n. 10, p. 1194-1202, 2011.

MCGINNES, E. A.; KANDEEL, S. A.; SZOPA, P. S. Some structural changes observed in the transformation of wood into charcoal. **Wood and Fiber**, Laurence, v. 3, n. 2, 1971.

MEYERS, H.; JENNINGS, R. F. Charcoal ironmaking - a technical and economic review of Brazilian experience. **Seaisi Quarterly**, Singapore, v. 8, n. 3, p. 38-80, 1979.

MIKSIC, A. **Étude des propriétés mécaniques et acoustiques d'un milieu granulaire sous chargements cycliques**. 2008. 173 p. Thesis (PhD in Physique) - Université Paris-Est, Paris, 2008.

MOORE, G. R. et al. Some physical properties of birch carbonized in a nitrogen atmosphere. **Wood and Fiber**, Laurence, v. 6, n. 3, p. 193–199, 1974.

MOREIRA, W. S. **Relações entre propriedades fisico-mecânicas e características anatômicas e químicas da madeira**. 1999. 119 p. Tese (Doutorado em Ciências Florestais) - Universidade Federal de Viçosa, Viçosa, MG, 1999.

MOUTINHO, V. H. P. **Influência da variabilidade dimensional e da densidade da madeira de *Eucalyptus* sp. and *Corymbia* sp. na qualidade do carvão**. 2013. 164 p. Tese (Doutorado em Recursos Florestais) - Escola Superior de Agricultura "Luiz de Queiroz", Piracicaba, 2013.

NISGOSKI, S. et al. Influence of carbonization temperature on the anatomical characteristics of *Ocotea porosa* (Nees & Mart. Ex Nees) L. Barroso. **Wood Science and Technology**, New York, v. 48, n. 2, p. 301-309, 2014.

NORGATE, T.; LANGBERG, D. Environmental and economic aspects of charcoal use in steelmaking. **ISIJ international**, Tokyo, v. 49, n. 4, p. 587-595, 2009.

NUMAZAWA, S. **Contribution à l'étude de la pyrolyse lente sous pression du bois. Détermination des paramètres optima du procédé et caractéristiques des produits obtenus**. 230 p. Thesis (Phd in Génie des Procedes Industriels) - Université de Technologie de Compiègne, Compiègne, 2000.

OCARIS, E. R. Y. C**aracterização por espectroscopia Raman do endocarpo de babaçu tratado termicamente.** 2014. 88 p. Dissertação (Mestrado em Ciências Físicas) - Universidade Federal do Espírito Santo, Vitória, 2014.

OLIVEIRA, J. B.; GOMES, P. A.; ALMEIDA, M. R. Estudos preliminares de normalização de testes de controle de qualidade do carvão vegetal. In: _____. **Carvão vegetal**: destilação, carvoejamento, propriedades e controle de qualidade. Belo Horizonte: CETEC, 1982. v. 6, p. 8-38.

OLIVEIRA, L. T.; ALMEIDA, M. R. Avaliação de carvão vegetal. In: **_____**. **Uso da madeira para fins energéticos**. Belo Horizonte: CETEC, 1980. v. 1, p. 42-53.

PANSHIN, A. J.; ZEEUW, C. **Textbook of wood technology**. 4th ed. New York: McGraw-Hill Book Co, 1980. 772 p.

PEEL, M. C.; FINLAYSON, B. L.; MCMAHON, T. A. Updated world map of the Köppen-Geiger climate classification. **Hydrology and Earth System Sciences**, Berlin, v. 11, p. 1633-1644, 2007.

PATRICK, J. W.; STACEY, A. E. The strength of industrial coke s: Further studie s of the influence of additive s in a coke oven charge on the tensile strength of coke. **Fuel**, London, v. 57, p. 258-2 64, 1978.

PEREIRA, B. L. C. et al. Estudo da degradação térmica da madeira de *Eucalyptus* através de termogravimetria e calorimetria. **Revista Árvore**, Viçosa, MG, v. 37, n. 3, p. 567-576, 2013.

PEREIRA, B. L. C. et al. Quality of wood and charcoal from *Eucalyptus* clones for ironmaster use. **International Journal of Forestry Research**, London, v. 1, p. 1-8, 2012.

PEREIRA, J. C. D. et al. **Características da madeira de algumas espécies de *Eucalyptus* plantadas no Brasil.** Colombo: Embrapa Florestas, 2000. 113 p. (Documentos, 38).

PRIOR, J.; ALVIN, K. L. Structural changes on charring woods of *Dichrostachys* and *Salix* from southern Africa: the effect of moisture content. **IAWA Journal**, Ultrecht, v. 7, n. 3, p. 243-250, 1986.

RAAD, T. J.; MELO, V. F. **Mapeamento de ações institucionais para sustentabilidade da produção de ferro-gusa a partir de carvão vegetal**. Brasília: CGEE, 2014. 26 p.

RAGAN, S.; GRINT, A.; MARSH, H. Strength in me tallurgical coke , correlations of microstrength indices, industrial drum te st indice s and ultrasonic ve locity measure - ments. **Fuel**, London, v. 60, p. 646-647, 1981.

RAMOS, L. M. A. et al. Variação radial dos caracteres anatômicos da madeira de *Eucalyptus grandis* W. Hill Ex Maiden e idade de transição entre lenho juvenil e adulto. **Scientia Forestalis**, Piracicaba, v. 39, n. 92, p. 411-418, 2011.

RAVEENDRAN, K. ; GANESH, A. ; KHILAR, K. Influence of mineral matter on biomass pyrolysis characteristics. **Fuel**, London, v. 74, p. 1812–1822, 1995.

RAYLEIGH, J. W. S. **The theory of the sound**. New York: [s. n.], 1877. (Edition of 1945).

R DEVELOPMENT CORE TEAM. **R**: a language and environment for statistical computing. Vienna: R Foundation for Statistical Computing, 2015. Available on: <http://www.R-project.org>. Accessed on: 10 June 2015.

RECORD, S. J. **The mechanical properties of wood**. New York: J. Wiley & Sons, 1914.

RICHARD, J. R.; ANTAL, M. J. Thermogravimetric studies of charcoal formation from cellulose at elevated pressures. In : BRIDGWATER, A. V. **Advances in thermochemical biomass conversion**. Dordrecht: Springer Science & Business Media, 1994. v. 2, p. 784-792.

ROUSSET, P. et al. Pressure effect on the quality of *Eucalyptus* wood charcoal for the steel industry: a statistical analysis approach. **Fuel Processing Technology**, Amsterdam, v. 92, n. 10, p. 1890-1897, 2011.

SALMÉN, L.; BURGERT, I. Cell wall features with regard to mechanical performance. A review COST Action E35 2004–2008: wood machining-micromechanics and fracture. **Holzforschung**, Berlin, v. 63, n. 2, p. 121-129, 2009.

SHAFIZADEH, F.; MCGINNIS, G. D. Chemical composition and thermal analysis of cottonwood. **Carbohydrate Research**, Amsterdam, v. 16, n. 2, p. 273-277, 1971.

SILVA, D. A.; TRUGILHO, P. F. Comportamento dimensional da madeira de cerne e alburno utilizando-se a metodologia de análise de imagem submetida a diferentes temperaturas. **Revista Cerne**, Lavras, v. 9, n. 1, p. 56-65, 2003.

SINDICATO DA INDÚSTRIA DE FERRO NO ESTADO DE MINAS GERAIS. **Estatísticas para a produção de ferro-gusa (2014)**. Available on: <http://www.sindifer.com.br). Accessed on: 10 Jan. 2016.

SINHA, N. C. et al. Abrasion characteristics of coals. **Fuel**, London, v. 61, p. 1285-1286, 1982.

SOARES, V. C. **Comportamento térmico, químico e físico da madeira e do carvão de *Eucalyptus urophylla* x *Eucalyptus grandis* em diferentes idades**. 2011. 109 p. Tese (Mestrado em Ciência e Tecnologia da Madeira) - Universidade Federal de Lavras, Lavras, 2011.

SUN, H. et al. Multiple controls on the chemical and physical structure of biochars. **Industrial & Engineering Chemistry Research**, Washington, v. 51, n. 9, p. 3587-3597, 2012.

SUOPAJÄRVI, H.; PONGRÁCZ, E.; FABRITIUS, T. The potential of using biomass-based reducing agents in the blast furnace: a review of thermochemical conversion technologies and assessments related to sustainability. **Renewable and Sustainable Energy Reviews**, Golden, v. 25, p. 511-528, 2013.

SYRED, C. et al. A clean, efficient system for producing Charcoal, heat and power (CHaP). **Fuel**, London, v. 85, n. 10, p. 1566-1578, 2006.

TOBIESEN F. A., SVENDSEN H. F. and MEJDELL T. Modeling of blast furnace CO_2 capture using amine absorbents". **Industrial & Engineering Chemistry Research**, Washington, v. 46, p. 7811-7819, 2007.

TRUGILHO, P. F. et al. Aplicação da análise de correlação canônica na identificação de índices de qualidade da madeira de eucalipto para a produção de carvão vegetal. **Revista Árvore**, Viçosa, MG, v. 21, n. 2, p. 259–267, 1997.

TRUGILHO, P. F. et al. Avaliação de clones de *Eucalyptus* para a produção de carvão vegetal. **Revista Cerne**, Lavras, v. 7, n. 2, p. 104-114, 2001.

TRUGILHO, P. F. Densidade básica e estimativa de massa seca e de lignina na madeira em espécies de *Eucalyptus*. **Ciência e Agrotecnologia**, Lavras, v. 33, n. 5, p. 1228-1239, 2009

TRUGILHO, P. F.; LIMA, J. T.; MENDES, L. M. Influência da idade nas características físico-químicas e anatômicas da madeira de *Eucalyptus saligna*. **Revista Cerne**, Lavras, v. 2, n. 1, p. 15, 1996.

TRUGILHO, P. F.; SILVA, D. A. Influência da temperatura final de carbonização nas características físicas e químicas do carvão vegetal de jatobá (*Himenea courbaril* L). **Scientia Agraria**, Curitiba, v. 2, n. 1/2, p. 45-53, 2001.

TSAI, C. Y. et al. Corre lation of microstrength and industrial drum strength indice s of me tallurgical cokes. **Fuel,** London, v. 63, p. 866-868, 1984.

TSUPARI, E. et al. Post-combustion capture of CO_2 at an integrated steel mill – Part II: economic feasibility. **International Journal of Greenhouse Gas Control**, Cheltenham, v. 16, p. 278-286, 2013.

UEDA, S.; ARIYAMA, T. Evaluation of biomass injection into blast furnace for reducing CO_2 emission. In: INTERNATIONAL CONFERENCE ON PROCESS DEVELOPMENT IN IRON AND STEELMAKING, 3., 2008, Luleå. **Proceedings…** Luleå: [s. n.], 2008. v. 2, p. 217-226.

VELDEN, M. V. et al. Fundamentals, kinetics and endothermicity of the biomass pyrolysis reaction. **Renewable Energy**, Oxford, v. 35, n. 1, p. 232-242, 2010.

VIEIRA, R. S. **Propriedades mecânicas da madeira de clones de *Eucalyptus* e carvão produzido entre 350°C e 900°C.** 2009. 97 p. Tese (Doutorado em Ciência e Tecnologia da Madeira) - Universidade Federal de Lavras, Lavras, 2009.

WANGAARD, F. F. **The mechanical properties of wood**. New York: J. Wiley, 1950. 377 p.

WASHUSEN, R.; EVANS, R. Prediction of wood tangential shrinkage from cellulose crystallite width and density in one 11-year-old tree of *Eucalyptus globulus* Labill. **Australian Forestry**, Queen Victoria, v. 64, n. 2, p. 123-126, 2001.

WENZL, H. F. J. **The chemical technology of wood.** New York: Academic, 1970.

WILKS, D. S. **Statistical methods in the atmospheric sciences**. 2nd ed. Amsterdam: Academic, 2006. 648 p.

WU, W. et al. Chemical characterization of rice straw-derived biochar for soil amendment. **Biomass and Bioenergy**, Oxford, v. 47, p. 268-276, 2012.

WU, Y. Q. et al. Relationships of anatomical characteristics versus shrinkage and collapse properties in plantation-grown eucalypt wood from China. **Journal of Wood Science**, London, v. 52, n. 3, p. 187-194, 2006.

XIE, X. **Production and characterization of carbon structures derived from wood.** 2008. 92 p. Thesis (Ph.D) - The University of Maine, Maine, 2008.

YANG, J. L.; EVANS, R. Prediction of MOE of *Eucalyptus* wood from microfibril angle and density. **Holz als Roh- und Werkstoff**, Berlin, v. 61, p. 449-452, 2003.

ZINK-SHARP, A. The mechanical properties of wood. In : BARNETT, J. R.; JERONIMIDIS, G. **Wood quality and its biological basis**. Boca Raton : CRC, 2009. p. 187-209.